THE ROLE OF SURFACE CHEMISTRY AND WETTABILITY OF MICROTEXTURED TITANIUM SURFACES IN OSTEOBLAST DIFFERENTIATION

A Dissertation
Presented to
The Academic Faculty

by

JUNG HWA PARK

In Partial Fulfillment
of the Requirements for the Degree
Doctor of Philosophy in the
School of Materials Science and Engineering

Georgia Institute of Technology
August, 2012

THE ROLE OF SURFACE CHEMISTRY AND WETTABILITY OF MICROTEXTURED TITANIUM SURFACES IN OSTEOBLAST DIFFERENTIATION

Approved by:

Dr. Barbara D. Boyan, Advisor
Department of Biomedical Engineering
Georgia Institute of Technology

Dr. Zvi Schwartz
Department of Biomedical Engineering
Georgia Institute of Technology

Dr. Rina Tannenbaum, Co-advisor
Department of Biomedical Engineering
University of Alabama at Birmingham

Dr. David Bucknall
School of Materials Science & Engineering
Georgia Institute of Technology

Dr. Karl Jacob
School of Materials Science & Engineering
Georgia Institute of Technology

Dr. Mark R. Prausnitz
School of Chemical & Biomolecular Engineering
Georgia Institute of Technology

Date Approved: month date 2012

ACKNOWLEDGEMENTS

I would like to thank my advisor Dr. Barbara D. Boyan for giving me the opportunity to work with her, and providing me research guidance. Dr. Boyan has been an outstanding mentor to me, and I have matured as a scientific researcher. I would like to thank my co-advisor Dr. Rina Tannenbaum who has pushed me to understand the science and always demanded more from me. I am thankful for Dr. Zvi Schwartz who has been a strong influence about my research and instrumental to me being able to work hard and understand the big picture.

I would also like to thank my thesis committee members, Dr. Karl Jacob, Dr. Mark R. Prausnitz, and Dr. David Bucknall have provided many fruitful discussions about my work, which has helped shape this dissertation and improve the quality of the research.

I would also like to thank to Dr. Rene Olivares-Navarrete who provided many insightful discussions about cell behaviors and materials science. The members of the Boyan laboratory: Sharon Hyzy, Jiaxuan Chen, Reyhaan Chaudhri, Christopher Lee, Jiaxuan Chen, Khairat El-Baradie, Chris Hermann, Rolando Gittens, Maryam Doroudi, Shirae Leslie, Srishti Bhutani, Qingfen Pan, Erin Hewitt, James Wade, Alice Cheng, Min Lai, Janina Sedlaczek, Xiaokun Wang, Maribel Baker, Chelsea Britt, Megan Merritt, Ethan Lotz, Ms. Brentis Henderson, and Nicole Beach without their help, I am not able to survival my Ph.D. program. A special note of thanks goes to Sharon Hyzy who has helped me over the years. She was very helpful in providing an extra set of hands for numerous experiments and assays.

I would to acknowledge my parents and my husband for their support and patient during past 5 years. Finally, I am so lucky to have an amazing son, Sean Lee. He didn't any complain when he had to come to the lab with me for feeding cells or having a meeting with Dr. Schwartz during the weekend. I would not be here without his endless love, support, encouragement, and patience.

TABLE OF CONTENTS

LIST OF TABLES

LIST OF FIGURES

LIST OF SYMBOLS AND ABBREVIATIONS

Ra	surface profile average roughness
Sa	surface area average roughness
AC	autoclave
AFM	atomic force microscopy
CHI	chitosan
CLSM	confocal laser microscopy
CP	cleaning procedure
EO	ethylene oxide
GI	gamma irradiation
OCN	osteocalcin
OP	oxygen plasma
OPG	osteoprotegrin
PGA	poly(L-glutamic acid)
PLL	poly(L-lysine)
PT	pretreated titanium
PTFE	polytetrafluoroethylene
SEM	scanning electron microscopy
SLA	sand-blast/acid-etched
TCPS	tissue culture polystyrene
UV	ultraviolet
XPS	x-ray photoelectron microscopy

SUMMARY

Titanium has been widely used as an implant material due to the excellent biocompatibility and corrosion resistance of its oxide surface. The integration of implants with host tissue is governed by biomaterial surface properties, suggesting that they play an important role in regulating cellular response.

All biomaterials must undergo cleaning and sterilization after manufacturing and before clinical use. However, surface characterization is often performed on materials before this final processing and little consideration is given to how these steps may affect biological response. A novel cleaning method to remove organic contaminants from used titanium surfaces was developed to characterize how these steps, in combination with several common sterilization techniques including autoclave, gamma irradiation, oxygen plasma, and ultraviolet light, affect surface properties and cell response. The results indicate that re-cleaned and re-sterilized titanium implant surfaces cannot be considered the same as the original surfaces in terms of surface properties and cell responses. Therefore, the re-use of titanium implants after re-sterilization may not result in the same tissue responses as found with never-before-implanted specimens.

Microtextured and hydrophilic titanium surfaces enhance osteoblast differentiation and increase bone-to-implant contact *in vivo*. However, material surface properties are inter-connected directly and indirectly, so it is difficult to investigate the effect of a specific surface property such as surface chemistry on cell response without changing other parameters. Therefore, in this dissertation, we developed novel polyelectrolyte thin films on microtextured titanium surfaces to modify the chemistry

without altering micron scale roughness and examined cell response. Titanium substrata used in this study were pretreated (PT, Sa = 0.37 μm) and sand-blasted/acid-etched (SLA, Sa = 2.54 μm) titanium surfaces. Three different polyelectrolytes were used, including chitosan, poly(L-glutamic acid), and poly(L-lysine). Enhanced surface wettability was achieved using the polyelectrolyte thin films without modifying surface microtexture. The study showed that surface chemistry, rather than wettability, was the dominant regulatory parameter on smooth surfaces; whereas, surface roughness was the dominant regulatory parameter on microtextured surfaces.

In order to focus more on surface wettability with a specific chemistry, a surface wettability gradient was prepared with a novel coating method. Increased surface wettability was correlated with decreased cell number while increasing osteocalcin and osteoprotegerin production levels, indicating a more mature osteoblast phenotype. Expression of integrins, which are transmembrane receptors linking the cytoskeleton to the extracellular matrix, was also sensitive to surface wettability. The results enhance the understanding of how different levels of surface wettability on rough surfaces can directly regulate osteoblast response. Taken together, this research provides fundamental information about the effect of surface chemistry, including wettability, chemical composition, and charge density, on the impact of titanium biomaterials on osteoblast maturation.

CHAPTER 1

SPECIFIC AIMS

Biomaterial surface energy, chemical composition, charge, wettability and roughness all play an important role in determining the degree of the direct bone-to-implant interface, termed osseointegration (1). Previous studies have shown that osteoblasts, bone formation cells, proliferate less and become more differentiated on rough titanium surfaces (2-6). Osteoblasts generate an osteogenic microenvironment, secreting more prostaglandin E_2 (PGE_2) and transforming growth factor-β1 (TGF-β1) to promote osteoblastic maturation on rough titanium surfaces (3, 7, 8). Surface chemistry, which is influenced by surface energy, wettability, and composition, is another factor that determines osteoblast phenotype and regulates osteoblast maturation (9). Increased surface energy is desirable for bone implants due to enhanced interaction between the implant surface and the biological environment (10). The extent of bone formation *in vivo* is also increased with increasing water wettability of implants (11).

The physiological role of implant surface chemistry is important in determining the success of implant osseointegration because of molecular rearrangements, surface reactions, contamination, and release of toxic or biologically active ions that are determined by the starting chemistry. However, the role of surface chemistry on osteoblast response is not fully studied. Therefore, the ***overall goal*** of this dissertation is to understand how the surface chemistry, including wettability, chemical composition, and charge density, of titanium biomaterials impacts osteoblast maturation (*in vitro*). This study focuses on the ***general hypothesis*** that modifications of surface chemistry of

titanium surfaces with sterilization or polyelectrolyte coating on titanium surfaces regulate osteoblast response.

Specific aim 1: to determine the effect of cleaning and sterilization of titanium surfaces on osteoblast phenotype. The working hypothesis is that titanium surface properties are sensitive to cleaning and sterilization methods, resulting in modified surface properties that affect osteoblast phenotype. To test this hypothesis, we used two cleaning procedures developed in our laboratory and four different sterilization methods, including autoclave, gamma irradiation, oxygen plasma, and ultraviolet light, to clean and sterilize used titanium surfaces. We used biochemical assays to determine the effects of re-cleaned and re-sterilized titanium surfaces on osteoblast proliferation and differentiation *in vitro.*

Specific aim 2: to determine how surface wettability controlled by different polyelectrolyte thin films on titanium surfaces affects on osteoblast phenotype. The hypothesis is that increased surface wettability by coating polyelectrolyte thin films on microtextured titanium surfaces enhances osteoblast differentiation. To examine this hypothesis, we used three different polyelectrolytes, including chitosan, poly(L-glutamic acid), and poly(L-lysine), and optimized coating processes, including pH and ionic strength. We used biochemical assays to determine the effects of enhanced wettability of titanium surfaces on osteoblast proliferation and differentiation *in vitro.*

Specific aim 3: to control surface wettability with chitosan on microtextured titanium surfaces and to determine how surface wettability affects osteoblast phenotype. The hypothesis is that osteoblast differentiation is regulated as surface wettability gradient dependent. To test this hypothesis, we developed surface wettability gradient by oxygen plasma treatment followed by aging, and then coated chitosan on

microtextured titanium surfaces. We used biochemical assays to determine the effects of surface wettability on osteoblast proliferation and differentiation in an *in vitro* model.

CHAPTER 2

BACKGROUND

OSSEOINTEGRATION

Osseointegration, first described by Branemark, refers to "a direct bone-to-implant interface without interposition of non-bone tissue" (1). The degree of osseointegration is determined by how cells and tissues respond to implanted materials and, consequently, influences clinical outcome. Enhancing osseointegration is important especially in patients who have unhealthy bone (12). Several components can contribute to osseointegration: biological factors, patient health conditions, and implanted material properties. Biological factors, including cell number, activity of osteogenic cells and osteoclasts, balance of local factors acting on bone formation and remodeling, bone cell proliferation rate, and vascularization of the implant surface affect osseointegration (13). The health condition of patients is also an important factor in osseointegration (12, 14). The primary interaction between biological tissues and implanted materials takes place at the outermost surface of biomaterials, through the regulation of water, ions, and adsorption of proteins that influence integrin expression and cell responses (9, 15). Hence, surface properties, including surface chemical composition, energy, charge density, topography, roughness, and sterilizations all either directly or indirectly influence osseointegration (13, 16-19). Among aforementioned components for osseointegraion, this study focuses on the biomaterial surface properties.

BONE COMPOSITION, STRUCTURE, AND REMODELING

Bone is a natural, composite material made of organic and inorganic components. Bone consists of an organic matrix, a mineral phase, and water. The organic matrix is composed of collagen and non-collagenous proteins such as osteopontin, osteonectin, and bone sialoprotein among others. The mineral phase of bone is primarily composed of calcium and phosphate in the form of carbonate-substituted hydroxyapatite. Small amounts of carbonate and some inorganic impurities such as magnesium, potassium, fluoride, and citrate are found in the mineral section (20).

Bone structure consists of three different complex scale structures, including macro (cortical and trabecular bone), micro- (lamellae and osteons), and nano- (collagen, noncollagenous proteins, and inorganic minerals) in Figure 2.1 (21, 22).

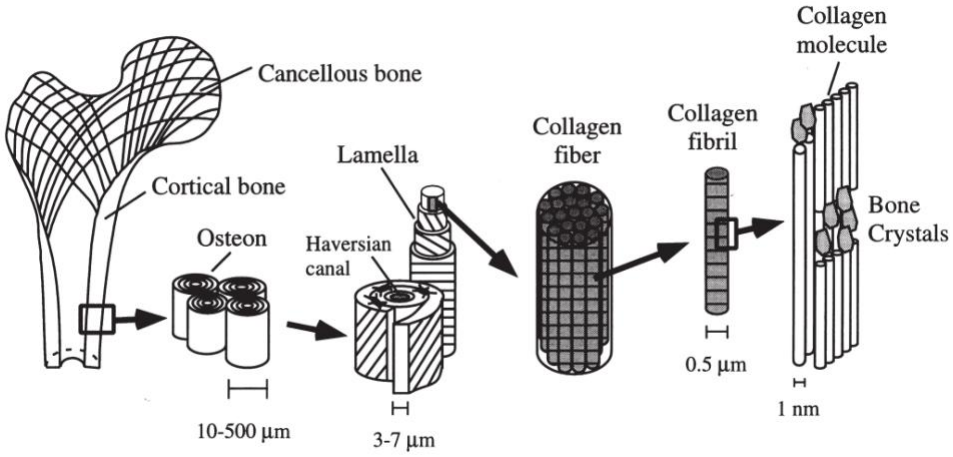

Figure 2.1. Illustration of the hierarchical structure of bone from the macroscale to the nanoscale (22).

Cortical bone, also known as compact bone, is found in the outer layer of all bones and the diaphysis of long bones. Cortical bone consists of distinct osteons, which consist of vascular channels circumferentially surrounded by lamellar bone. Lamellae

consist of well-aligned collagen fibers (3~7 μm thickness). Collagen fibrils are made of collagen molecules and bone crystals which are hydroxyapatite crystals formed in nanoscale sheets. Trabecular bone, also known as cancellous bone, is mainly found in the metaphyses and epiphyses of long bones as well as in the vertebrae. Trabecular bone has a highly porous, three-dimensional structure that gives it a lower density and much larger surface area than cortical bone. Therefore, trabecular bone is subject to a much greater rate of bone turnover. The complex bone structure at different size scales makes it an extremely efficient structure in terms of mechanical strength (22-24).

Bone is a living tissue in which old bone is continually replaced by new bone (22). Bone matrix formation by osteoblasts and resorption by osteoclasts are coordinated by specific remodeling events (Figure 2.2).

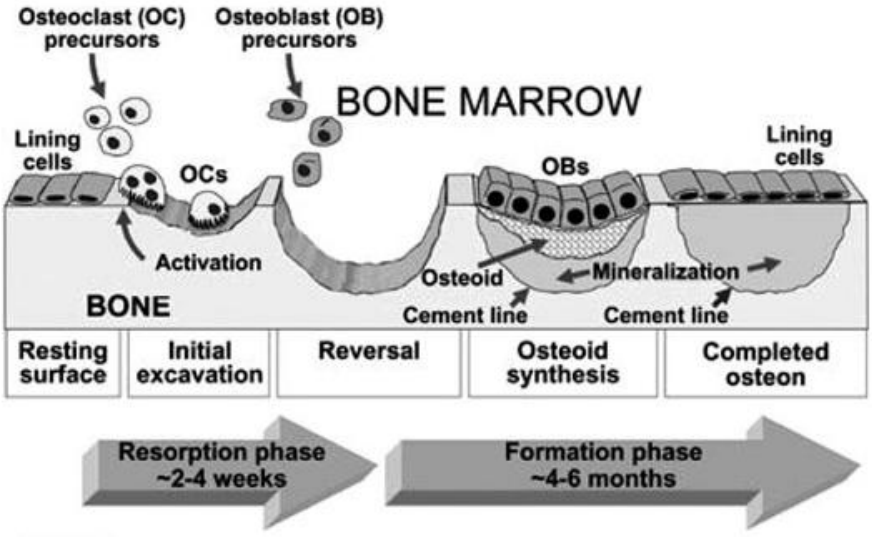

Figure 2.2. Illustration of the bone remodeling process: bone resorption by osteoclast and new bone formation by osteoblasts (25).

Osteoblasts found along the bone surfaces synthesize bone matrix through production, maturation, and mineralization of the osteoid. Osteoprogenitor cells differentiate via a series of transition steps. First, the cells increase production of collagen

type I, which is the major protein of the bone extracellular matrix. Second, alkaline phosphatase activity, an early marker of osteoblast differentiation, is increased. Third, subsequent production of non-collageneous bone matrix proteins such as osteopontin, bone sialoprotein, and osteonectin, finally osteocalcin, a late marker of osteoblast differentiation (10).

Osteocalcin, also known as bone gamma-carboxyglutamic acid (Gla) protein (BGP), is the most abundant non-collagenous protein in the organic matrix of bone and dentin (26, 27). Osteocalcin is synthesized by osteoblasts and mainly accumulated in the extracellular matrix of bone (27). Osteocalcin binds with high affinity to hydroxyapatite, which indicates that its function is the formation of mineralized bone matrix (28). Osteocalcin levels and function can be affected by various bone metabolism disorders; therefore, osteocalcin is often used in the clinical assessment of bone disease through screening the closely coupled bone formation and resorption processes. More importantly, osteocalcin is used widely as a marker of osteoblast maturation because osteocalcin synthesized by osteoblasts has been recognized as the most osteoblast-specific gene, particularly in late-stage osteoblast differentiation (29).

Osteoclasts are bone resorbing cells with multiple nuclei and homogenous cytoplasm that remove bone tissue by dissolving the mineralized matrix with secreted acid. Osteoclasts can tightly cover the bone surface with their ruffled borders and dissolve hydroxyapatite crystals and bone matrix. After bone resorption by osteoclasts, different micron and submicron scale surface morphology is left on the bone surface (20). These naturally generated different length scale roughness characteristics can provide an important indication to modify surface roughness.

INTERFACE BETWEEN BONE AND SURFACE

The bone-material interface is spontaneously formed between the outermost implanted material surface and surrounding bone when biomaterials are placed in a defect site. The first interaction at the interface is the adsorption of proteins, lipids, and ions from serum or blood (30). In vitro studies have shown that the surface topography and surface energy can affect the selective adsorption of proteins such as albumin, fibronectin, and vitronectin onto the surfaces. Moreover, fast blood clot stabilization on the implant surface, followed by vascularization are necessary events that lead to fast bone integration (31). Cells contact the material surface through the conditioned layers formed on implanted surfaces rather than by directly interacting with the actual materials (32). Cells interact with the extracellular matrix through binding of integrin receptors to proteins such as collagen and fibronectin. Conditioned protein layers recruit cells from surrounding tissue. Cellular attachment takes place first, followed by cellular adhesion. Three types of proteins are involved such as extracellular matrix proteins, cell membrane proteins (integrins), and cytoskeletal proteins. The extracellular matrix not only connects cells together in tissues, but also guides their movement during the healing process. The integrins cluster together into focal contacts after ligand binding. Cytoskeletal proteins and complex signaling molecules, including cytoskeletal rearranging proteins, and focal adhesion kinase are activated. These signaling pathways can regulate many cellular functions such as cell adhesion, motility, shape, growth, and differentiation (33).

Integrins are heterodimeric glycoproteins consisting of a pair of α and β subunits (34). Integrin expression can change with the stage of the osteoblast development (35). Since integrins bind specifically to extracellular matrix proteins through specific binding

sites on the extracellular matrix proteins, the adhesion of cells to matrix through binding of integrin receptors can deliver information between the extracellular matrix and cell (15). The expression of osteoblast specific genes can be modulated by different material surface properties. For instance, rougher titanium surfaces lead to higher α2β1 expression and lower α5β1 expression (35). This indicates that the initial interactions on the interface can regulate integrin expression depending on surface chemistry, energy, roughness, and topography (36-38). However, the firm conclusion, as to how and which surface property can primarily or secondarily impact the interaction has not yet been found. Therefore, to understand and optimize of specific material surface properties are important to enhance osseointegration through controlling integrin expression and thus osteoblast differentiation.

TITANIUM AS IMPLANT MATERIALS

Pure titanium and titanium alloy are most commonly used as orthopaedic and dental implant applications. The mechanical properties of titanium, including its high strength, fatigue resistance, and low elastic modulus with low density, are similar to native bone as shown in Table 1 (3, 21, 39). Titanium has a thin oxide layer of a few nanometers (2 ~ 6 nm) when in air or aqueous solution (40). This formed passivating layer can contribute to enhanced biocompatibility and corrosion resistance of titanium implants (39). The titanium oxide layer can have several different oxidation states such as TiO_2, Ti_2O_3, and TiO. The most stable oxidation state is titanium dioxide (TiO_2) (41). The structure of the titanium oxide layer can have an amorphous or a crystal structure depending on the oxidation environment. At room temperature, titanium oxide layers are

mostly amorphous, which has been confirmed by X-ray diffraction analysis (41). When the temperature increases, the titanium oxide layers have a different long-range order such as rutile, anatase, or brookite (42).

Table 1. Materials properties for orthopaedic and dental implant applications.

Material	Elastic Modulus (Gpa)	Tensile Strength (MPa)	Advantages	Disadvantages
commercially pure Titanium	110	400	Biocompatibility Corrosion resistance	Fatigue & wear resistance
Titanium alloy (Ti-6Al-4V)	124	940	Biocompatibility Corrosion resistance Fatigue resistance	Wear resistance
Stainless Steel	193	540	Cost, avaiability	Biocompatibility Corrsion
CoCr	214	480	Wear & Corrosion resistance Fatigue strength	Biocompatibility Stress shielding
PMMA	3	35 ~ 35	Rapid fixation	Fatigue & cracking
Bone	10 ~ 30	70 ~ 150	_	_

TITANIUM SURFACE PROPERTY AND MODIFICATION

Surface Roughness

Surface roughness enhances osteoblast differentiation and affects growth factor production by increasing the physical contact area, which provides increased primary mechanical stability (43). Morphological modifications have been extensively applied with successful clinical outcomes (3, 8, 32). The degree of roughness is grouped with different scales such as micron-, submicron-, and nanoscale.

Micron scale roughness is positively correlated to enhance osteoblast differentiation when compared with polished smooth surfaces *in vitro* (44). Many

fabrication methods have been used to produce micron scale roughness such as blasting the surface with hard ceramic particles including alumina (Al_2O_3), titania (TiO_2), and calcium phosphate (45). Titanium plasma-spraying (TPS) is another way to produce micron scale roughness on surfaces (Ra = 4 μm). An i*n vivo* study demonstrated that micron scale surface roughness induced by TPS showed much faster and stable bone formation on the interface between bone and the implant surface than when a smooth surface implant was used (46).

Submicron scale roughness of titanium surfaces produced by acid-etching (Ra = 700 nm) or porous anodization (Ra = 400 nm) plays a major role in increasing osteocalcin levels by osteoblasts compared to smooth (Ra = 60 nm) surfaces. Interestingly, osteocalcin levels were higher on acid-etched surfaces than porous anodized surfaces (47). Although both acid-etching and porous anodized surfaces had submicron scale roughness, different osteocalcin levels suggest that osteoblasts are sensitive to an imbalanced force induced by distinguishable surface shapes. Acid-etched surfaces showed a spiked and sharp curvature all over the surface with an irregular or asymmetric pattern which means un-evenly distributed forces. Porous anodized surfaces had more smooth area between pores and relatively even distribution of pores on the surfaces (47-49).

Nano scale features, with dimensions of less than 100 nm, constitute an important scale with which to influence cell response through protein adsorption and integrin binding (50-52). Nano scale features on implanted materials can influence cells to respond in a favorable manner through minimizing the adaptation time with the new environment. Cell proliferation and differentiation have been shown to increase on silicon

wafers with nano scale features (51). The effect of nano scale surface topography on osteoblast differentiation can be found with alumina and titania characterized with nanophase grain sizes. The amount of calcium-containing mineral produced by osteoblasts grown on nanophase substrates was higher than on substrates with conventional grain size (> 100 nm) (53).

Hybrid micron-/submicron scale surface roughness was obtained using the following method: sandblasting of mechanically polished titanium surfaces (micronscale) and superimposing of submicron scale (1~3 μm) features by acid etching in a hot mixtures of H_2SO_4/HCl (54). The surface morphology of these surfaces can be described by irregularly shaped craters with an unclear boundary of pits. Osteocalcin production levels by osteoblasts on hybrid micron-/submicron scale rough surfaces were higher than on surfaces with only either micron- or submicron scale roughness alone (4, 55, 56).

The effect of the combined different roughness scales on osteocalcin production levels by osteoblasts was examined with a micron-nano-hybrid titanium topography produced by the combination of acid-etching (micronscale pit) and TiO_2 sputter deposition (nanoscale). This method of adding nanoscale nodule features on surfaces was desired because it resembles the morphology of calcium-binding proteins (10 ~ 50 nm), including osteocalcin molecules. These superimposed nanoscale nodule features in micron-pit surfaces regulate osteoblast differentiation while inhibiting fibroblast functions (57).

Three different scales (micron-/submicron-/nanoscale) were combined on titanium surfaces and evaluated for the effect of complex surface topography on osteoblast differentiation (42). Osteocalcin production levels on micron-/submicron-/nano

scale surfaces were higher than on micron-/submicron scale surfaces. This suggests that nano scale features play an important role in enhancing osteoblast differentiation. However, nano scale features alone cannot give substrates enough roughness to influence osteoblast differentiation. Therefore, a desirable surface roughness for faster healing times and stronger osseointegration *in vivo* must be acquired by the combination of complex roughness including different scale. Mimicking osteoclast resorption pits on bone wafers after cleaning by enzymes and secreted acid supports the use of complex different scale reoughness (58-61).

Surface Chemistry

Besides the surface roughness of the substrate, surface chemical composition, charge and wettability have been modified to improve osseointegration through modulating interface reactivity at the biomolecular levels (62). Most proteins are amphiphilic and partially soluble in an aqueous condition. In order to lower energy, protein adsorption is governed by entropic forces. The conformation, unfolding rate, and the degree of biological functionality of proteins are determined by the surrounding aqueous environment (63). In addition, protein adsorption is determined by surface wettability induced by different functional groups, polarity, or chemical composition. Depending on the affinity between proteins and surfaces, adsorbed proteins can change the conformation on the surface caused by denaturation of the protein. Consequently, proteins can impact the cell's surface receptors followed by cellular response. The adsorption of proteins on surfaces and following reactions are highly complex and occur rapidly within milliseconds (32). The sequence of events and details underlying protein absorption on the surface is not completely understood and controversial.

Cell attachment, adhesion, and migration can be regulated by different surface charges (64, 65). For instance, the negatively-charged, large, linear glycosaminoglycan (D-N-acetylglucosamine-β-d-glucuronic acid), hyaluronan, have been used to induce strong attachment of cells to positively charged surfaces (66). In contrast, when positively charged resins were covering the surfaces, trabecular bone formation was reduced (67). New bone formation was observed on negatively charged surfaces (68). Due to the conflicting results in previous research, an in-depth study must be conducted to elucidate the role of surface charges on cell response.

Osteoblast differentiation is sensitive to surface chemical composition. Osteocalcin levels produced by osteoblasts increase on titanium with an oxide layer compared to tissue culture polystyrene and titanium alloy (Ti-6Al-4V) surfaces (69-71). *In vivo* studies show that higher bone-to-implant contact and push out failure load is found with hydroxyapatite coated titanium surfaces than with titanium plasma-spraying surfaces (46, 72).

Depending on the affinity of water molecules on surfaces, surfaces can have hydrophilic (good water wettablility) and hydrophobic (poor water wettablility) properties. Surfaces with higher energy bonds water molecules through hydrogen bonding with adhesive forces that are characterized as hydrophilic surfaces. Hydrophobic surfaces repel and minimize contact areas with water molecules (63). Highly hydrophilic surfaces can reduce the gap between the surrounding tissue and biomaterial surface and help to organize the peri-implant clot *in vivo* (9, 10, 62, 73). Hydrophobic surfaces support protein adsorption, but blood coagulation takes longer than on hydrophilic surfaces. In an *in vitro* study, osteocalcin levels on superhydrophilic surfaces increased

compared on hydrophobic surfaces (4). In an *in vivo* study, superhydrophilic with micron-/submicronscale rough surfaces obtained higher bone-to-implant contact and removal torque from bone than hydrophobic micron-/submicronscale rough surface (9, 62, 74). These results indicate that excellent initial wettability with micron-/submicronscale roughness can induce more differentiation of osteoblasts *in vitro* and enhanced bone-to-implant contact area with increasing removal torque *in vivo* (4). However, the role of surface chemistry, including wettability, on osteoblast cell response is not completely understood.

Cells are more proliferative through coupling specific proteins and reorganizing other biomolecules (34). Many surface chemical modification methods have been used for achieving better bone formation: coating bioactive ceramic, protein/peptide, coating polyelectrolyte thin films, glow discharge treatment, and printing biomolecules on surfaces, which can all influence a specific cell response. In order to minimize the nonspecific adsorption of protein on implant surfaces, several immobilizing techniques have been used by conjugating platelet-derived or insulin-like growth factors, fibronectin, and collagen with polymers composed of carboxyl activated derivatives (75).

Polyelectrolyte Thin Films

Polyelectrolyte thin film coating on substrates as "bottom-up" nanomodification has been used to modify surface chemistry and wettability. A polyelectrolyte is a macromolecular species that upon being placed in water or any other ionizing solvent dissociates into a highly charged polymeric molecule (76). Different surface charge species and densities can be easily implanted on the surface, and the number of layers is built by tailoring different charges (Figure 2.3). The surface affinity and stability of the

polyelectrolyte is highly dependent upon many parameters including system solvent quality, pH of solution, surface charge, surface charge density, polyelectrolyte charge, and polyelectrolyte charge density because the driving force for the surface adsorption of polyelectrolytes is electrostatic interaction (77). Depending on the degree of ionization in an aqueous solution, polyelectrolytes are grouped as strong or weak polyelectrolytes. A weak polyelectrolyte is characterized as partially ionized in a pH-dependent manner (78). For example, strong acid groups like sulphate, sulphonic and phosphate remain negatively charged over the whole ambient pH range. Strong basic groups, including the amines and alkylamines, remain essentially positive over that range (79).

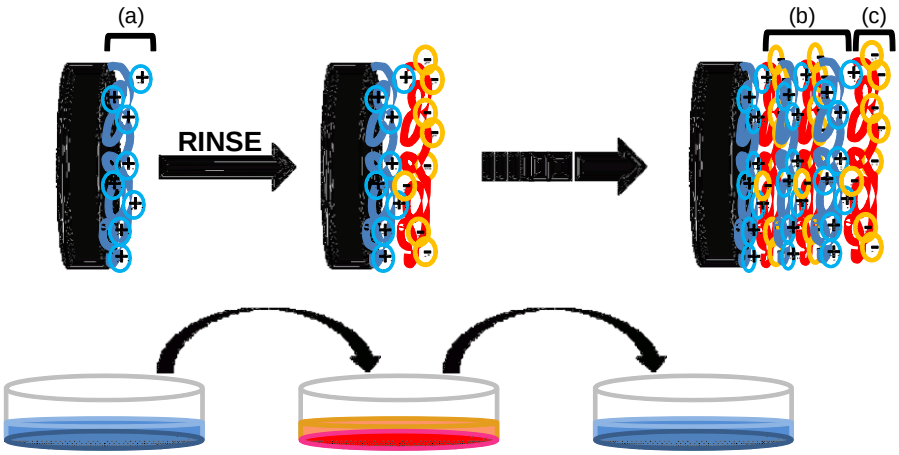

Figure 2.3: Illustration of polyelectrolyte multilayer foaming on substrates. Section (a) is the first adsorbed layer on the substrate, section (b) is the bulk layer, and section (c) is the top layer, which is the dominant contributor to the chemical properties of the surface (80).

Three weak polyelectrolytes - chitosan, poly(L-lysine), and poly(L-glutamic acid) - were used in this study (Figure 2.4). Polyelectrolytes have several features similar to proteins and biological tissues such as low toxicity, hydrophilicity, ability to bind with oppositely charged molecules, and phase separation due to ionic nature. These properties make polyelectrolytes attractive candidates for biomedical use (81). Surface modification

with polyelectrolyte thin films can be applied in a number of important fields, including thin films for promoting or inhibiting specific biological molecules and cells, protecting substrates from chemical or thermal degradation, or preventing contact damage among other uses (81, 82).

Chitosan is a polysaccharide based biomaterial that consists of linear chains of β-(1,4)-D-glucosamine (deacetylated unit) and N-acetyl-D-glucosamine (acetylated unit). Chitosan is a hydrophilic polysaccharide and is soluble in dilute aqueous organic acid solutions. In solution, the 2-amino group is protonated, thus providing the polycationic nature of chitosan molecules in solution. Chitosan is one of a few natural cationic polyelectrolytes and has been used as a biomaterial for medical applications including bone, cartilage, nerve, skin, wound healing, hemostatic, artificial kidney membranes, contact lenses, dermatology, and drug delivery (83-85). Synthetic polyelectrolytes, poly(L-lysine) and poly(L-glutamic acid), offer several advantages including reproducibility and controlled mechanical properties as biomaterial applications. Poly(L-lysine), known as being immunogenic, (86) is a commonly used polycation for coating negatively charged surfaces such as alginate beads for cell encapsulation (87). Multilayers consisting of poly(L-lysine) and poly(L-glutamic acid) have showed to enhance adhesion of osteoblasts, chondrocytes, myoblasts, and smooth muscle cells to surfaces (88).

The advantage of coating polyelectrolyte thin films is that charged polymer chains can reach any crevices, pores or cracks on a substrate and coat them without clogging their opening (89). Therefore, surface chemistry can be modified without altering surface roughness.

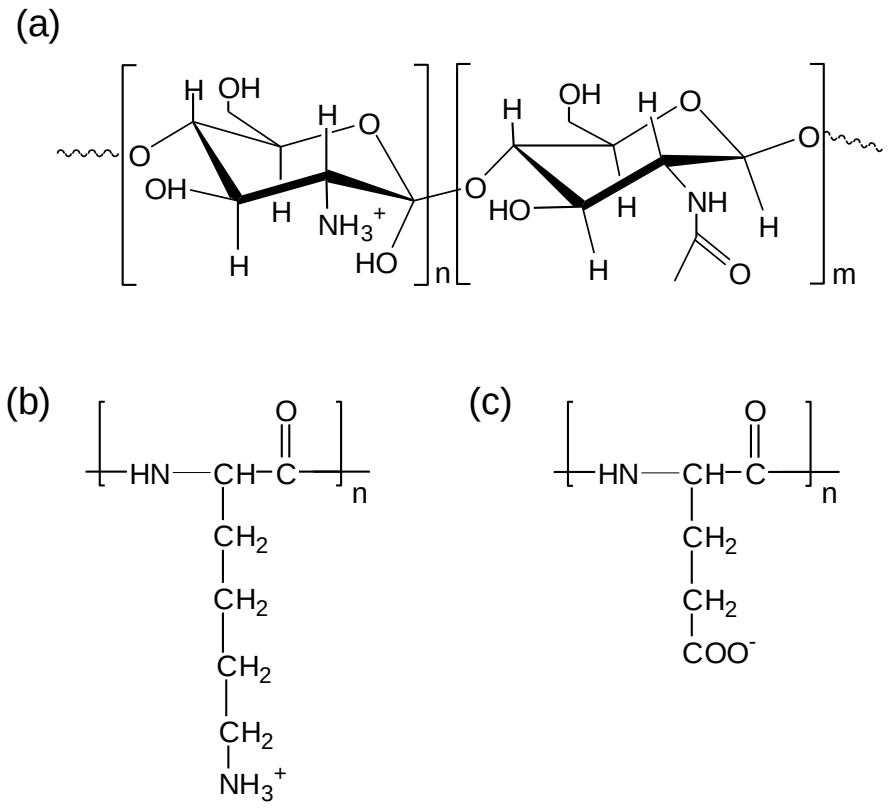

Figure 2.4. Chemical structure of the polyelectrolytes used for the surface modification of Titanium implant surface: (a) Chitosan (CHI), (b) Poly(L-lysine) (PLL), and (c) Poly(L-glutamic acid) (PGA).

Sterilization

Sterilization is an essential step for medical devices and surgical instruments. Failed sterilization of implantable medical devices can introduce microorganisms and pathogens, lead to infection, and transmit diseases. If bacteria are able to colonize an implant surface, the resulting biofilm can lead to implant failure (90).

Sterilization is a process in which all forms of microbial life, including endospores, are destroyed or eliminated by physical or chemical methods through the irreversible coagulation and denaturation of enzymes and structural proteins (91). Many different sterilization methods have been used including steam or dry-heat, hydrogen peroxide, ethylene oxide, ionizing radiation (gamma radiation), oxygen plasma,

ultraviolet, microwave, ozone, formaldehyde steam, gaseous chloride dioxide and so on. Appropriate sterilization methods depend on the nature of the material and final applications (40).

In order to enhance the effectiveness of sterilization, organic and inorganic foreign materials from substrates have to be removed by using water, detergents, or proper organic solvents (40). This process is called cleaning. Sterilization is done on biomaterials before implantation, and surface properties can be modified with sterilization methods (92). For example, steam sterilization can make the surface more hydrophobic due to deposition of hydrocarbons during the process. Cleaning is done first followed by sterilization. Therefore, sterilization might be considered as the last step of surface modification (Figure 2.5) (93-96). In this study, we investigated how different cleaning and sterilization methods can affect cellular response.

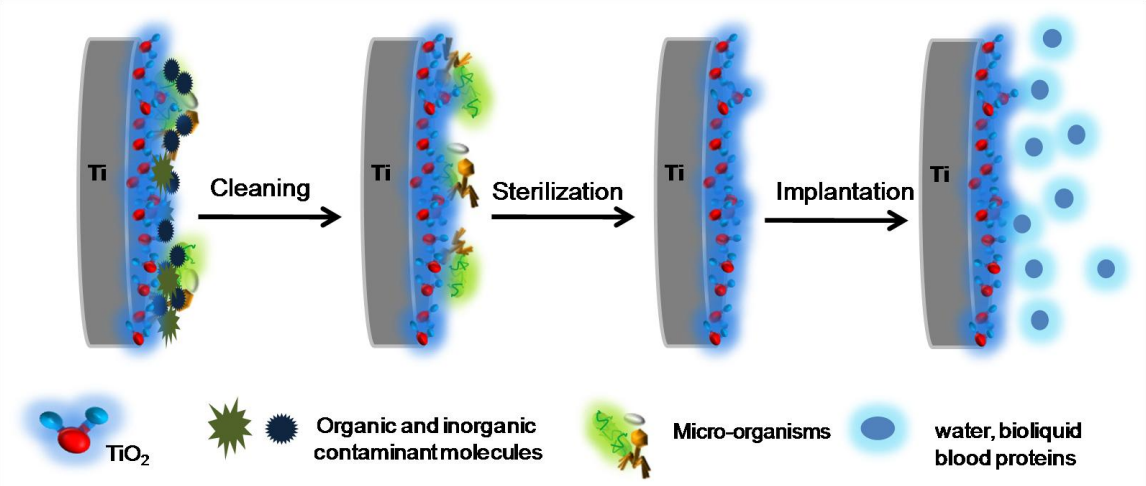

Figure 2.5. Illustration of events at the titanium surface during cleaning, sterilization, and implantation (40).

CHAPTER 3

EFFECT OF CLEANING AND STERILIZATION ON TITANIUM IMPLANT SURFACE PROPERTIES AND CELLULAR RESPONSE

INTRODUCTION

Titanium has been widely used as an implant material due to the biocompatibility and excellent corrosion resistance of its thin titanium oxide layer (1). In order to enhance osseointegration of dental and orthopaedic implants, many surface modification strategies have been pursued, focusing on the important role of the biomaterial surface properties (1, 9, 30). Since the biomaterial device has to be sterile before implanting in the body, the sterilization process is considered as the last step of the surface modification (95). Depending on the biomedical device or material, secondary cleaning or sterilization may be done in a clinical setting. Therefore, it is possible for biomaterials to undergo several uncounted cleaning and sterilization steps in an uncontrolled manner. In situations where implant devices are approved for re-use, cleaning and sterilization are key steps in the reconditioning of the implant to its initial state, but may also contribute to modification from initial surface properties (97).

Cleaning and sterilization can be distinguished in terms of function. The purpose of cleaning is to remove or reduce visible soils including blood, protein and debris on the surface of substrata. Sterilization serves to eliminate or stop reproduction of microorganisms including bacteria, spores, and fungi (98). Usually, cleaning is done first, followed by sterilization. Figure 2.5 illustrates the processing of biomaterials from cleaning to implantation.

There are many different sterilization methods available, each with different modes of action. Depending on material properties, the methods used for a particular device have to be carefully selected. In this study, autoclaving (AC), gamma irradiation (GI), oxygen plasma (OP), and ultraviolet (UV) were used to sterilize titanium. Autoclaving (AC) is a physical method of sterilization, which exposes the living organisms to unsustainable conditions of temperature, pressure, and time (121℃, 18 psi, 20 minutes). However, depending on the material density, volume, and size, the effectiveness of the autoclave may vary (99). Chemical methods such as OP can also be used. In this method, an ionized gas bombards the substratum surface and promotes the formation of free radicals under vacuum. Active species like polar groups break down and strip the surface layer. The thickness of the removed layer and the new surface properties can be modified by the type of gas, supplied gas purity, applied gas pressure, and sample position (100-102). UV is also used for surface sterilization. The shortest wavelength region with the highest energy intensity, 280 nm ~ 100 nm, is used to eliminate bacteria by inducing formation of thymine dimers, inhibiting DNA replication (99, 103). GI is used to sterilize biomaterials and medical equipment because ionized high energy is strong enough to promote DNA damage without releasing toxic residues. Due to good penetration depth, GI is useful for densely packed products and pre-packed materials.

GI is an appropriate sterilization method for heat sensitive devices or materials because the temperature of the materials does not noticeably increase during or after the process. In AC, the material temperature increases due to applied steam heat. Also, the AC chamber must remain closed until the heat cools to room temperature and any

moisture dries. Therefore, AC is not recommended for heat sensitive biomaterials. (104, 105). Although ethylene oxide (EO) sterilization method is often used for cellulose based biomaterials and plastic products, we did not use it in this study because it can leave toxic residues on device surface (106) which could negatively impact the cells growing on the titanium surface. Dry heat sterilization has a long history compared to other methods. However steam heat sterilization is more efficient in terms of heat transfer. Therefore, in this study, autoclaving was used instead of using both dry and steam heat sterilization methods.

It is well understood that the biological, chemical and mechanical properties of biomaterials are susceptible to change by diverse sterilization methods (104, 107-110). However, the contribution of the outermost molecular layer of an implant to its *in vivo* function is less well established. This layer plays an important role in determining the surface properties including surface energy, chemistry, and wettability. These properties directly affect the interactions with surrounding host tissue *in vitro* and *in vivo* (3, 7, 9, 30, 32, 55). Cleaning and sterilization can cause changes in the surface properties of biomaterials (97, 98, 105, 108, 111), but how these changes alter biological response is less well understood.

Because physical and chemical properties of materials are sensitive to small variations in their surface chemical composition and morphology (112, 113), two contrasting types of titanium implant surfaces were used: (1) PT, consisting of titanium surfaces that were pretreated with a prepickling step, and (2) SLA, consisting of titanium surfaces that were sandblasted followed by acid etching. Prior to exposure to cell culture, these two types of surfaces differ in their micron- and submicron scale combined surface

roughness, a property that has been recognized as important in the enhancement of peri-implant bone formation (4). The purpose of the present study was to assess the effects of commonly used sterilization methods on the surface properties of titanium and to correlate these changes with cell responses associated with osteoblastic differentiation. We also examined how cleaning contaminated titanium substrata prepared by exposing to biological cell growth and extracellular matrix production alters the surface and cell response following re-sterilization.

MATERIALS AND METHODS

Materials

Gamma irradiation-sterilized titanium disks 1 mm thick and 15 mm in diameter were donated by Institut Straumann AG (Basel, Switzerland). Prior to gamma irradiation, the disks had been treated so as to exhibit two different surface structures: pretreated surface (PT, Ra = 0.4 μm) and sandblasted/acid-etched surface (SLA, Ra = 3.4 μm). Pretreated surfaces are prepared by washing in acetone and then processing through 2% ammonium fluoride/2% hydrofluoric acid/10% nitric acid solution at 55℃ for seconds, they but have not yet been modified by the sand blasting and acid etching process used to generate the SLA surface. PT and SLA surface characterization prior to cell culture has been described previously (54). Reagent grade acetone, isopropanol, and ethanol were purchased from Sigma-Aldrich (St. Louis, MO).

Disk Cleaning and Sterilization

In order to demonstrate if cleaning protocols used in this study effectively remove organic contaminants on titanium surfaces, bio-contaminated PT and SLA surfaces were

prepared as follows: control Ti disks were placed in full media with cells and cultured for 5-7 days as described previously (21). Confluent cell monolayers were removed by two sequential trypsin digestions based on previous observations showing this removes all cells on the surface, but it does not remove extracellular matrix adhered to the disk. Contaminated titanium disks were cleaned by sonication in 2% Micro-90® detergent (International Product Corporation, Burlington, NJ) in distilled, ultrapure water for 2x15 min followed by two 15 min rinses in ultrapure water (Figure 3.1). Samples were rinsed in sequential ultrasonic baths of reagent grade acetone, isopropanol, and ethanol. Two different cleaning regimens were performed, varying the rinse time in each solvent: two 15 min rinses (CP2); or three 30 min rinses (CP3). After cleaning, disks were rinsed with ultrapure water three times for 10 min in a sonicated bath.

Cleaned disks were packed self-sealed sterilization pouches (Cardinal Health, Dublin, OH) and sterilized by gamma irradiation or autoclaving. For ultraviolet light sterilization the disks were exposed to UV overnight in a chamber and then packaged in sterile pouches. Cleaned individual titanium disks were treated with oxygen plasma under a sterile hood and packed in sterile pouches for further experiments. The detailed conditions of each sterilization method was as follows autoclaving for 20 min at 121℃ and 18 psi (2540E, Tuttnauer Autoclave, NY, USA); gamma irradiation at 25kGy over-night; oxygen plasma for 2 min per side (PDC-32G, Harrick Plasma, NY, USA); or ultraviolet light for 90 min at 254 nm (CL-1000 Ultraviolet Crosslinker, VUP). Gamma irradiated PT and SLA disks as supplied from the manufacturer were used as the primarily cleaned and sterilized controls. Surfaces cleaned and sterilized as described above are denoted as follows with respect to their substratum-cleaning protocol-

sterilization method. For example, the PT-CP2-GI represents a bio-contaminated used PT surface that was cleaned with cleaning protocol (CP2, two sequential 15 minute rinses) and then sterilized with gamma irradiation (GI).

The surface chemical composition of titanium disks before and after cleaning and sterilization was determined by x-ray photoelectron spectroscopy (XPS) (ESCA-SSX 100, Service Physics, Bend, OR). The XPS analysis chamber was evacuated to a pressure of 10^{-8} Torr or lower before collecting XPS spectra. This system was equipped with a monochromatic Al Kα x-ray source ($h\nu$ = 1486.6 eV photons) at a 55^{o} takeoff angle. General survey spectra were obtained using an x-ray spot size of 800 µm. The C1s binding energy of the aliphatic C-C bond at 284.6 eV was used as an internal reference. XPS results were evaluated using the ESCA 2005G software package provided by Service Physics, Inc. Three measurements were made on each of two separate surfaces per group.

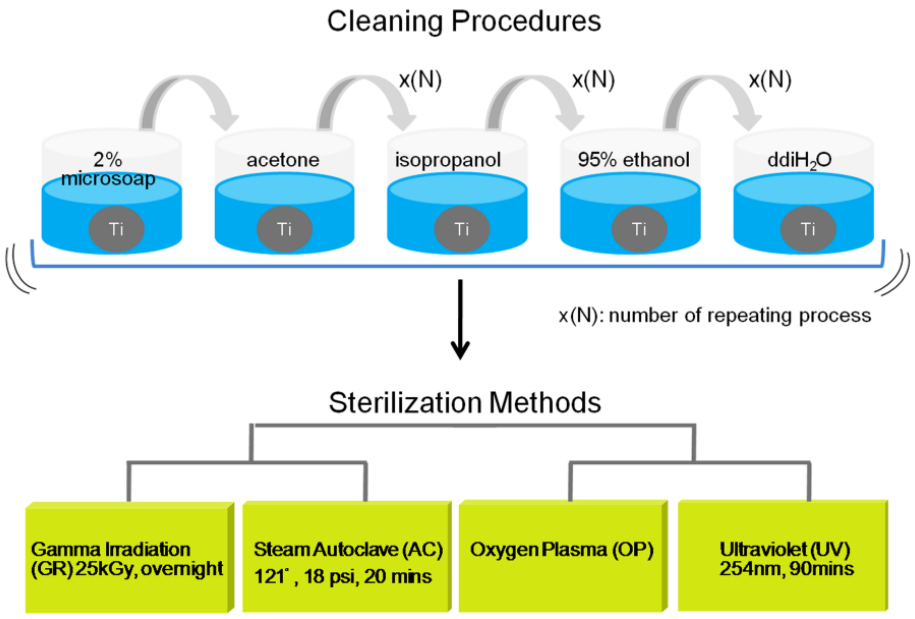

Figure 3.1. Cleaning procedures (CP) and sterilization methods used in this study.

Surface Characterization

Oxygen plasma (OP) can make surfaces very active. OP-sterilized surfaces have a high affinity for the adsorption of molecules onto the surface, including contaminants (114). Therefore, precise control of the time between OP sterilization and implantation is critical in minimizing recontamination of the surface. To demonstrate this, the contact angle was measured as a function of time after OP sterilization. The contact angle of titanium disks before and after secondary cleaning and sterilization was determined by a Ramé-Hart goniometer (Model 250-F1, Mountain Lakes, NJ). Images were analyzed with the DROPimage CA software package (Ramé-Hart Instrument Co.). The ultrapure water droplet volume (2 µL) was precisely controlled with a syringe scale. All measurements were performed in a cleanroom. Three measurements were made on two separate surfaces per group (i.e., a group being a particular cleaning and sterilization protocol).

The two-dimensional surface roughness of titanium disks before and after secondary cleaning and sterilization was measured using a KLA-Tencor P-15 contact profilometer (KLA Tencor, CA, USA) equipped with a 2 µm diamond-tracing stylus tip and 90° point angle. Twelve random areas per specimen (n=6) were measured over a scan length of 500 µm to obtain the arithmetic mean roughness (Ra, µm). All analyses were performed in a cleanroom.

The surface morphology of titanium disks before and after secondary cleaning and sterilization was examined by scanning electron microscopy (SEM) using an Ultra 60 field emission (FE) microscope (Carl Zeiss SMT Ltd., Cambridge, UK). Samples were not over-coated; images were recorded using a 5 kV accelerating voltage. Two separate surfaces per group were examined (n=2).

Cell Response

Cell responses to primary and secondarily cleaned and sterilized surfaces were performed using human osteoblast-like MG63 cells (American Type Culture Collection, Manassas, VA). Cells were plated at a density of 10,000 cells/cm^2 on either tissue culture polystyrene (TCPS) or titanium surfaces and cultured in Dulbecco's modification of Eagle's medium (Cellgro® , Mediatech Inc., Manassas, VA) supplemented with 10% fetal bovine serum (Hyclone, Waltham, MA) and 1% penicillin-streptomycin (Invitrogen, Carlsbad, CA) at 37℃, 5% CO_2, and 100% humidity. Cells were grown until confluence was achieved on TCPS. At confluence, fresh media were added to all cells and the cells were further incubated for 24 hours. After incubation, cell number was counted in all cultures and conditioned media were collected. To collect all cells on the rough Ti surfaces, cells were released by two sequential 10 min incubations in 0.25% trypsin-EDTA. Cells were counted using Z1 Particle Counter (Beckman Coulter, Fullerton, CA). Cellular alkaline phosphatase specific activity was measured by determining *p*-nitrophenol (*p*NP) release from *p*-nitrophenylphosphate (*p*NPP) at pH 10.2 in the cell lysate and normalized to total protein content (Macro BCA Protein Assay kit, Pierce). Osteocalcin (OCN) levels in the conditioned media were determined by radioimmunoassay (Human Osteocalcin RIA Kit, Biomedical Technologies, Stoughton, MA). Osteoprotegerin (OPG) was determined by enzyme-linked immunosorbent assay (ELISA) kit (Osteoprotegerin DuoSet, R&D System, Minneapolis, MN). Immunoassay results were normalized to total cell number.

Statistical Analysis

Data were analyzed using a one-way analysis of variance (ANOVA) for all surfaces. If there was a statistical difference noted, Bonferroni's modification of Student's t-test for multiple comparisons was used. $P < 0.05$ was considered significant. The presented data are from one of two repeated experiments, both with comparable results. In each experiment, there were 6 individual samples or cultures per variable, which provided sufficient power (n=6) to allow statistically significant differences to be detected. Thus, we did not have to combine samples from multiple experiments and can present actual values rather than treated/control ratios.

RESULTS

Effect of Secondary Cleaning on Titanium Surfaces

Both CP2 and CP3 protocols effectively cleaned and removed small organic molecules (C and N) from the contaminated titanium surfaces. SEM images of contaminated PT and SLA surfaces prior to cleaning showed unidentified materials (Figure 3.2A). However, visible surface deposits were removed after cleaning with both CP2 (Fig. 2A) and CP3 (data not shown). XPS analysis confirmed the presence of carbon (C), oxygen (O), titanium (Ti), and nitrogen (N) on both contaminated and secondarily cleaned titanium surfaces (Figure 3.2B & 2C). Traces of sulfur (0.8 %) were detected on contaminated PT surfaces, but not on contaminated SLA surfaces (Table 2). XPS analysis indicated that the outermost surface of contaminated PT and SLA substrata was composed mainly of molecules C, O, N, and Ti. However, after cleaning the amounts of C and N were markedly reduced and the percentages of Ti and O on the surface were increased.

The water contact angle of the PT-CP2 and PT-CP3 surfaces increased compared to the contact angle of the contaminated PT surfaces before cleaning (Figure 3.2D). However, only the SLA-CP3 surface exhibited an increase in water contact angle as compared to the contaminated SLA surfaces prior to cleaning. Contaminated (before cleaning) PT and SLA surfaces had a roughness of 0.4 µm and 3.9 µm, respectively. After cleaning, there was no difference in roughness, regardless of the cleaning protocol used (Figure 3.2E).

Table 2. XPS chemical component analysis on used PT and SLA before and after cleaning. B.C. is before cleaning (contaminated titanium disks), CP2 is two time cleaning protocol, and CP3 is three time cleaning protocol.

Atom	Cleaning					
	PT			SLA		
	B.C.	CP2	CP3	B.C.	CP2	CP3
C	44.6	16.3	20.5	69.9	13.6	19.3
O	31.1	38.7	39.7	22.3	39.6	37.9
Ti	18.4	43.9	38.8	1.1	45.5	42.4
N	5.1	1.0	0.9	6.7	1.3	0.8
S	0.8					

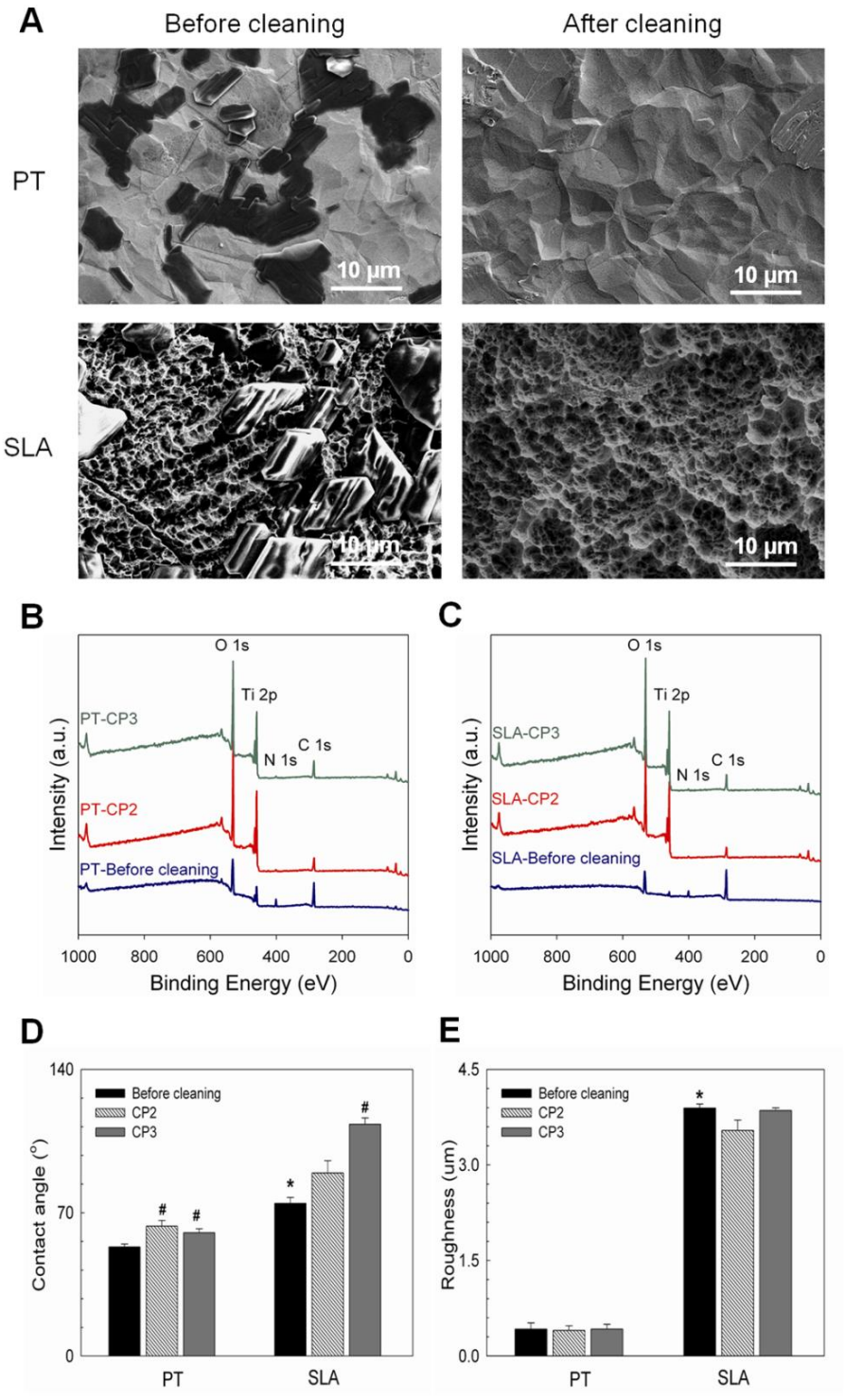

Figure 3.2. Effect of cleaning procedures on surface properties of used PT and SLA disks. Surface properties of PT and SLA surfaces before and after cleaning with CP2 were examined using SEM (A), XPS low resolution spectra (B, C), water contact angle (n=2) (D) and surface roughness (n=6) (E). *, $p < 0.05$, PT vs. SLA; #, $p < 0.05$, vs. Before cleaning.

Effect of Sterilization on Surface Properties

Surface chemistry: Low resolution XPS spectra revealed the presence of C, O, Ti, and N atoms on control PT and SLA surfaces and surface chemical composition fluctuated depending on the different cleaning and sterilization methods used (Figure 3.3). The chemical composition of the PT-CP(2 or 3)-GI and SLA-CP(2 or 3)-GI surfaces showed a similar distribution of elemental concentration as control PT and SLA (GI sterilized Ti disks) surfaces. A higher percentage of C was detected on the AC sterilized PT and SLA surfaces and SLA-CP(2 or 3)-UV surfaces compared to control substrates and other methods used. Increased O concentration with decreased C concentration on the PT-CP(2 or 3)-OP and SLA-CP2-OP surfaces was detected by XPS analysis. Silicon (Si) was detected only on the SLA-CP3-OP surface. The percentage of N was increased on the SLA-CP(2 or 3)-UV surface. However, N was not detected on the PT-CP2-UV surface.

Surface wettability: The PT-CP(2 or 3)-AC and SLA-CP(2 or 3)-AC surfaces exhibited an increase in water contact angle in comparison to control PT and SLA surfaces (Figure 3.4A & 4B). Other sterilization methods including OP, GI, or UV resulted in a decrease in contact angle on both PT and SLA surfaces in comparison to control and AC-sterilized surfaces. The PT-CP(2 or 3)-OP and SLA-CP(2 or 3)-OP surfaces had the best water wettability among all surfaces. Surface wettability was sensitive to storage time after OP (Figure 3.4C). There was a 63% increase in water contact angle within 30 min after processing. There was a further increase in contact angle at 6 h, 8 h, and 24 h.

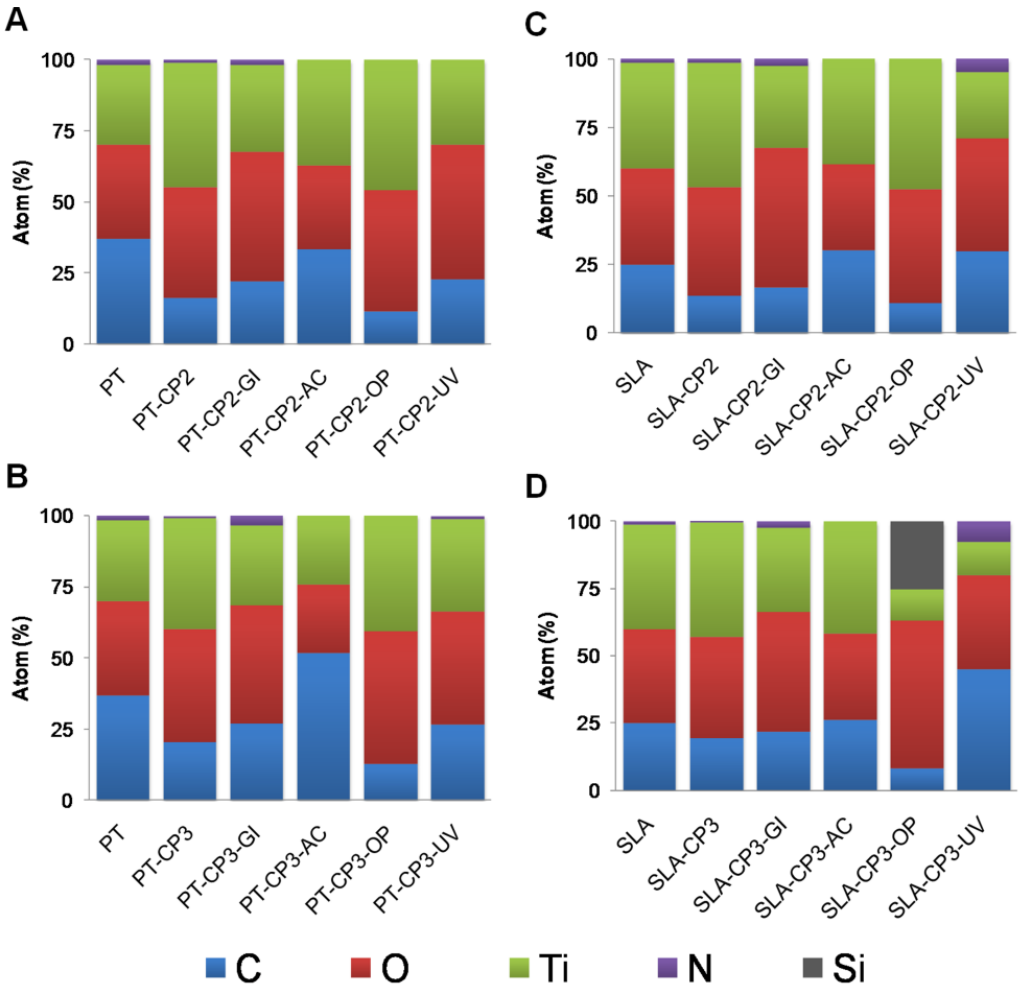

Figure 3.3. Effect of sterilization method on surface chemical composition of cleaned PT and SLA surfaces (n=2). Atomic percentages (%) of components on the surface after sterilization were obtained by XPS for the PT-CP2 (A), the PT-CP3 (B), the SLA-CP2 (C), the SLA-CP3 (D). PT and SLA are new, unused and sterilized with gamma irradiation surfaces. Before cleaning (B.C.); autoclave (AC); gamma irradiation (GI); oxygen plasma (OP);and Ultraviolet (UV)

Surface roughness: Contact profilometry showed that unused PT surfaces (Ra = 0.4 µm) were relatively smoother than SLA surfaces (Ra = 3.4 µm) (Figure 3.5A & 5B). None of the sterilization methods altered the roughness of the PT surface. SLA surface roughness was modified with AC, OP, and UV sterilization. Autoclaved SLA surfaces had lower Ra values than any of the other treated SLA surfaces, while OP-treated SLA surface roughness was much rougher than that of the unused control SLA surface. The SLA surface roughness increased after UV sterilization. This suggests surface deposition of steam-borne contaminants during autoclaving, versus oxidative stripping away of such a priori contaminants in the plasma device.

Surface morphology: SEM confirmed that control PT and SLA surfaces had different surface morphologies (Figure 3.6A). Whereas control PT was relatively smooth, SLA had micronmeter scale craters and submicronmeter scale pits. After secondary cleaning and sterilization, the surface morphology of PT surfaces (Figure 3.6B) was similar to that of the control surfaces. However, irregular scratch marks were observed on all secondarily cleaned and sterilized PT surfaces. Similarly, a larger number and bigger size cracks were observed on secondarily cleaned and sterilized SLA surfaces. No differences were detected as a function of sterilization method.

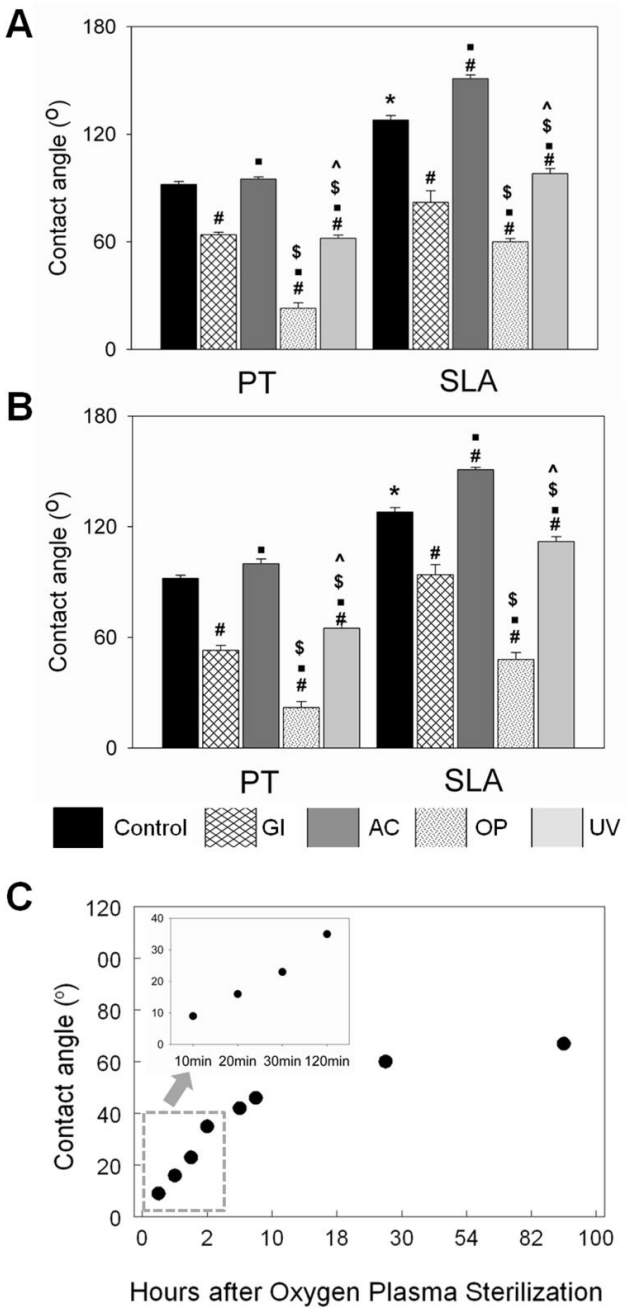

Figure 3.4. Effect of sterilization method on water contact angle of cleaned PT and SLA surfaces. Contact angle was measured on PT and SLA disks after cleaning with CP2 (A) and CP3 (B). Control surfaces are new, unused PT and SLA surfaces. (C) PT-CP3 surfaces were sterilized with oxygen plasma and contact angle was measured as a function of hours after oxygen plasma. *, $p<0.05$, PT vs. SLA control surface; #, $p<0.05$, vs. control, ▪, $p<0.05$, vs. CP, $, $p<0.05$, vs. GI, ^, $p<0.05$, vs. AC, &, $p<0.05$ vs. OP.. Cleaning protocol (CP); autoclave (AC); gamma irradiation (GI); oxygen plasma (OP); and Ultraviolet (UV)

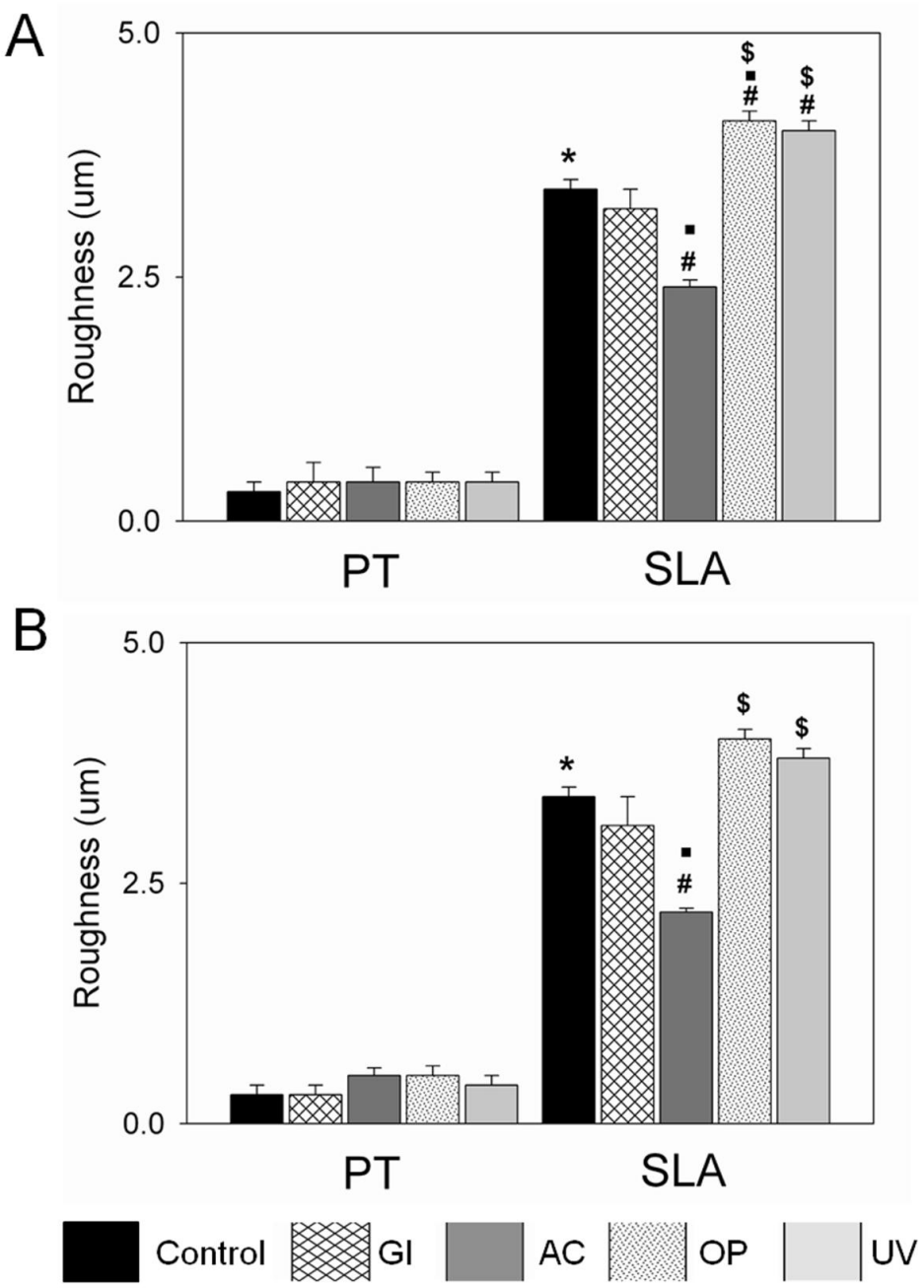

Figure 3.5. Effect of sterilization method on roughness of cleaned PT and SLA surfaces. Surface roughness of PT and SLA surfaces was measured after cleaning with CP2 (A) or CP3 (B). Control surfaces are new, unused PT and SLA surfaces. *, $p<0.05$, PT vs. SLA control surface; #, $p<0.05$, vs. control, ▪, $p<0.05$, vs. CP, $, $p<0.05$, vs. GI, ^, $p<0.05$, vs. AC, &, $p<0.05$ vs. OP. Cleaning protocol (CP); autoclave (AC); gamma irradiation (GI); oxygen plasma (OP); and Ultraviolet (UV)

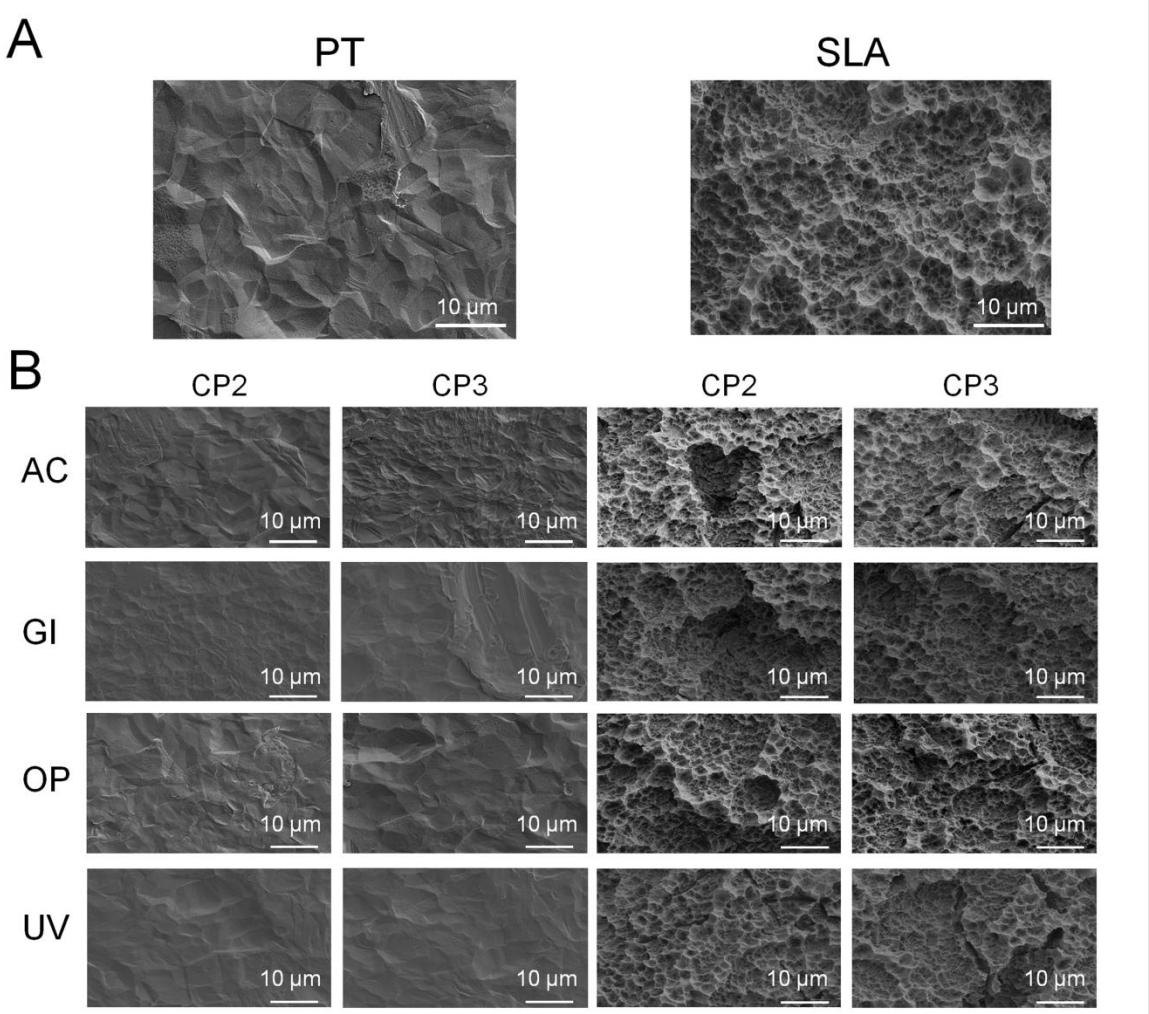

Figure 3.6. Surface morphology of PT and SLA surfaces. (A) SEM images of new PT (left) and SLA (right) surfaces. (B) SEM images of PT and SLA surfaces after cleaning (CP2 or CP3) and sterilization. Autoclave (AC); Gamma irradiation (GI); Oxygen plasma (OP); Ultraviolet (UV)

Effect of Sterilization on MG63 Cell Response

Responses of the MG63 cells were sensitive to the secondary cleaning and sterilization protocols. Cell number was lower on unused SLA than on TCPS or PT surfaces (Figure 3.7A). Similarly, cell numbers on SLA-CP2-GI were lower than on PT-CP2-GI (Figure 3.7B). However, cell number on SLA-CP3-GI and PT-CP3-GI surfaces was not different (Figure 3.7C). Cell number on PT-CP2-GI was higher than on PT secondarily sterilized with other methods (Figure 3.7B). The SLA-CP3-UV surfaces had more cells than control and SLA re-sterilized with GI, AC, and OP (Figure 3.7C).

Alkaline phosphatase specific activity, osteocalcin, and osteoprotegerin levels were higher on control SLA than on TCPS or control PT surfaces as shown in Figure 3.8A, 8D, and 8G, respectively. Similarly, alkaline phosphatase specific activity on the PT-CP2-GI surface was lower than on the SLA-CP2-GI surface (Figure 3.8B). In contrast, enzyme activity was higher on the PT-CP3-GI surface than on the SLA-CP3-GI surface (Figure 3.8C). Enzyme activity on PT surfaces secondarily sterilized with AC, OP, or UV was comparable to activity on SLA surface cleaned and sterilized using the same protocols.

Osteocalcin was greater in the conditioned media of cells grown on control SLA compared to control PT or TCPS (Figure 3.8D). Sterilization methods altered osteocalcin levels in cultures grown on cleaned PT and SLA surface. Osteoblasts grown on SLA-CP2-GI had higher levels of osteocalcin in their media than were seen when the cells were cultured on PT-CP2-GI surface (Figure 3.8E). No difference was observed between PT-CP3-GI and SLA-CP3-GI surfaces. Osteocalcin production on PT-CP2-AC was greater than on PT-CP2-GI, whereas no differences were observed among PT-CP2-OP,

PT-CP2-UV, control and GI treated surfaces. Osteocalcin levels were lower on SLA-CP3-UV compared to SLA-CP3-OP (Figure 3.8E & 8F).

Osteoblasts grown on PT-CP2-AC, OP, or UV surfaces had higher levels of osteoprotegerin in their conditioned media by sterilization methods on PT-CP3 surfaces (Figure 3.I8). Significantly more osteoprotegerin was produced on SLA-CP3-OP when compared to SLA-CP3-GI, SLA-CP3-AC, and SLA-CP3-UV (Figure 3.8I). The lowest osteoprotegerin production levels were found in cultures grown on SLA-CP3-UV.

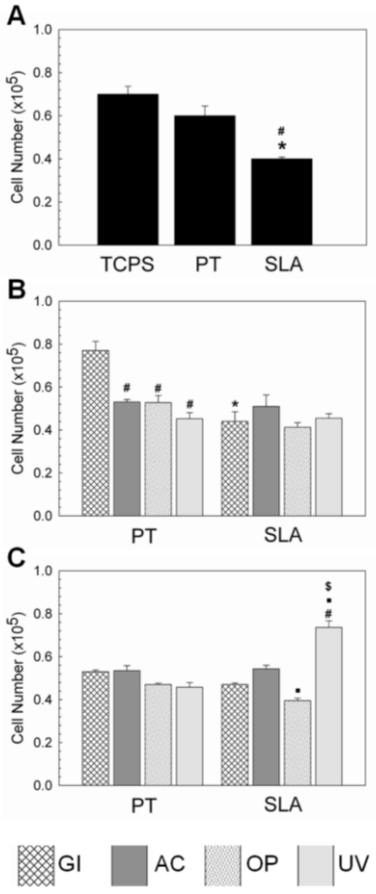

Figure 3.7. Effect of sterilization method of PT and SLA on MG63 cell number. MG63 cells were cultured on TCPS, PT and SLA surfaces and grown to confluence. At confluence, cell number on (A) new, unused, and sterilized with gamma irradiation PT and SLA surfaces,*, $p<0.05$ Ti vs. TCPS; #, $p<0.05$ SLA vs. PT, (B) cleaned with CP2 and then sterilized, and (C) cleaned with CP3 and sterilized. *, $p<0.05$, PT vs. SLA; #, $p<0.05$, vs. GI, ·, $p<0.05$, vs. AC; $, $p<0.05$, vs. OP.

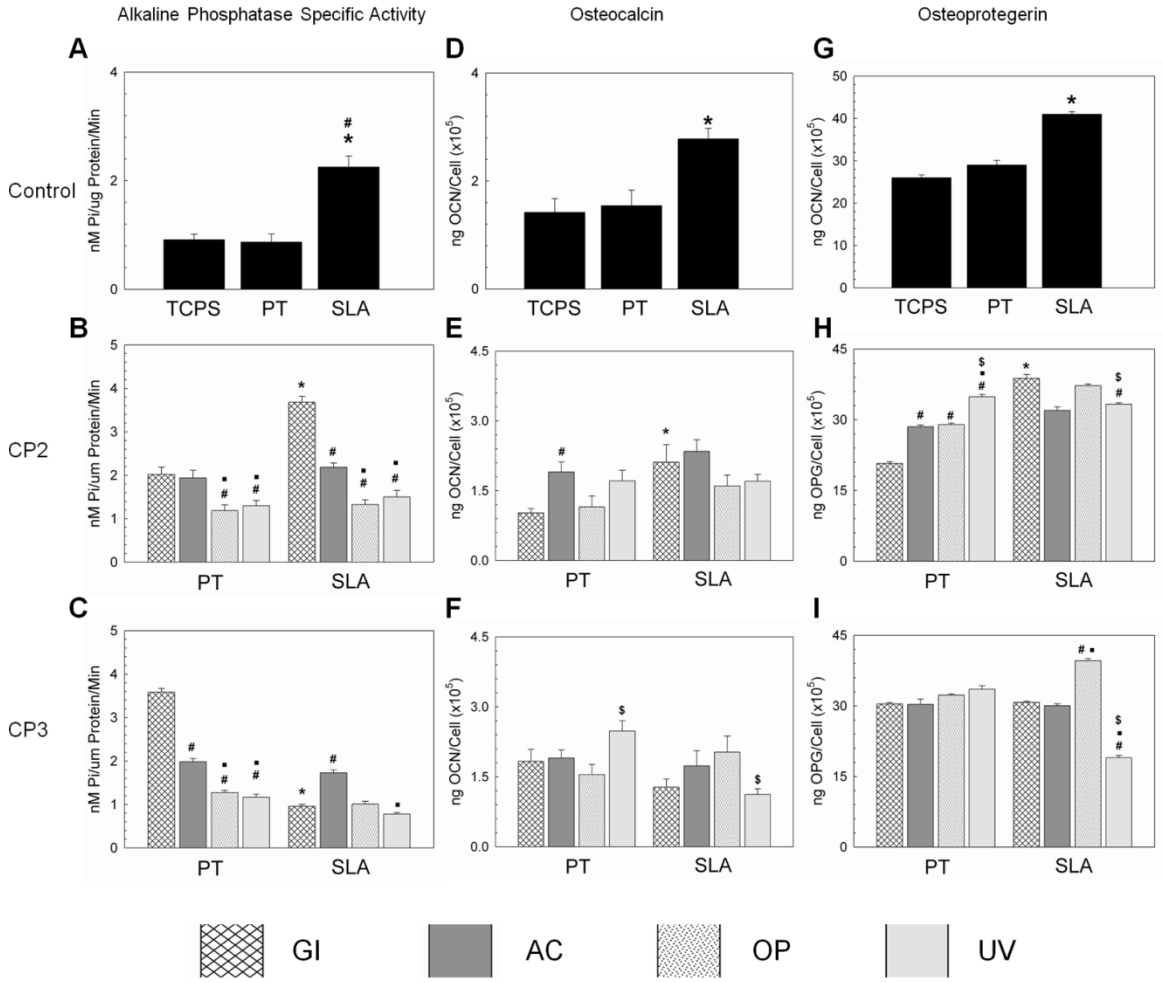

Figure 3.8. Effect of PT and SLA surface treated with different sterilization methods on MG63 cells. MG63 cells were plated on TCPS, PT and SLA surfaces and grown to confluence. At confluence, alkaline phosphatase (ALP) specific activity, osteocalcin (OCN), and osteoprotegerin (OPG) for new surface (A), (D), and (G), respectively. *, $p<0.05$ Ti vs. TCPS; #, $p<0.05$ SLA vs. PT. Alkaline phosphatase specific activity with CP2 and CP3 is (B) and (C), respectively. Osteocalcin with CP2 and CP3 is (E) and (F), respectively. Osteoprotegerin with CP2 and CP3 is (H) and (I), respectively. *, $p<0.05$, PT vs. SLA; #, $p<0.05$, vs. GI, ▪, $p<0.05$, vs. AC; $, $p<0.05$, vs. OP. Inserted red and blue dotted lines indicate PT and SLA control surfaces, respectively.

DISCUSSION

Titanium implant surface properties such as surface chemistry, wettability, and morphology have been shown to affect osteoblast proliferation, extracellular matrix production, local factor production, and stimulation of an osteogenic microenvironment (9, 73, 99). Therefore, understanding how the sterilization process affects these surface properties is important for clinical outcome. There is no general agreement, yet, on what the most desirable starting surface properties should be for clinically placed dental implants or for orthopaedic endoprostheses. The effect of sterilization on surface properties has not been well studied, but may affect responses of implants both *in vitro* and *in vivo*.

Although implants are intended for single use clinically, they may be re-used under some circumstances. Moreover, investigators developing new surfaces or investigating biological responses to biomaterials may consider their re-use to conserve resources. Thus, an understanding of how cleaning can alter surface properties and how this might affect changes due to sterilization is important.

In the present study, we developed two cleaning protocols, CP2 and CP3, to clean bio-contaminated PT and SLA surfaces. Surface roughness was not changed by the two protocols. However, increased water contact angle values showed increased surface hydrophobicity of secondarily cleaned surfaces was due to chemical differences in the outermost surface layer. XPS analysis also indicated that the chemical composition of the secondarily cleaned surfaces was altered after cleaning, even though both cleaning protocols were effective at removing organic contaminants based on XPS analysis.

However, the CP3 protocol resulted in a greater contact angle on the rougher SLA surfaces, indicating that it was less effective on the more complex topography.

Surface preparation outcomes were also affected by not only cleaning but also the sterilization method used. Others have shown that autoclaved titanium surfaces might be coated with N, F, Mg, Si, and Cl (39), although these contaminants were not observed on the autoclaved PT and SLA surfaces in this study.

All of the secondarily sterilized surfaces had adventitious carbon-based contaminants, but the amounts differed as a function of cleaning protocol and sterilization method. The presumed source of the most abundant carbon species on the surfaces was molecules that were adsorbed at the surface/air interface (112). PT and SLA surfaces were directly treated with OP in a glass chamber. OP was under vacuum conditions, and AC was performed under pressure (18 psi). The other two sterilization methods were done at atmospheric pressure (14.7 psi). Molecule adsorption can be influenced by these factors. Moreover, molecules can be re-deposited or bounced from the surface during sterilization. This was particularly the case for the autoclaved surfaces (96, 109, 111), and may have contributed to the increase in hydrophobicity.

Detecting Si only on the SLA-CP3-OP surfaces is interesting finding in this study. It is hard to explain this phenomenon other than the possibility of Si coming from the glass chamber, as noted previously (91, 94, 95). Operational conditions such as plasma treatment time, gas pressure, and the purity of gas do affect the rate and amount of deposition of SiO_2 on the surfaces. Beneficially, OP sterilization best decreased surface carbon content and hydrophobicity of the PT and SLA surfaces.

Differences in surface wettability may also be due to the reduction of titanium in the oxide layer, i.e., the transition from the more stable and less polar Ti^{4+} state to the Ti^{3+} state (99, 115). Machnee et al. reported that the oxide layer thickness was not modified significantly by surface treatments such as cleaning, sterilization in an autoclave, or radiofrequency glow discharge (116). Although there was no statistical difference in oxide layer thickness observed, the surfaces do not necessarily have similar oxidation states. In contrast, other researchers have found that surface oxide layer thickness and composition varies with the sterilization processes used, including sterilization in an autoclave (39, 93, 111). The temperature and pressure during AC can affect the oxidation states and the oxide layer thickness on the surface. Not only the processing conditions but also defects in the grain boundaries of the metal structure may contribute to modification of the oxide layer (39, 115). In addition, sterilization methods have been shown to alter mechanical properties and cellular response (17, 93). OP treatment can increase the Ti^{3+} concentration on the surface and improve surface hydrophilicity on PT and SLA, as exhibited by a lower water contact angle.

The results assessing the effects of GI are particularly important. We were able to directly compare control surfaces (i.e., PT or SLA sterilized with GI) with contaminated PT and SLA surfaces that were cleaned with either CP2 or CP3 and then again sterilized with GI. Even though the final step in both cases was sterilization with GI, the cleaning history of the underlying surface played a role in determining the final surface properties of the sterile material. Control surfaces exhibited a higher degree of hydrophobicity than contaminated surfaces that were both secondarily cleaned and sterilized with GI. This

discrepancy validates our initial hypothesis that surface properties are sensitive to the history of the surface treatment.

Interestingly, following sterilization by the AC method, surface roughness of SLA decreased significantly, regardless of the cleaning procedure used, supporting previous observations of Smith et al. in which AC altered the surface structure of Ti alloy and Co-Cr-Mo substrates (91). The mechanism is still not clear. It is likely that autoclaving leaves behind stream-borne surface deposits. In contrast, the SLA-CP(2 or 3)-OP surface roughness increased. This suggests that superficial material removal and sterilization occurs at the same time, contributing to the increased surface roughness. SLA surface roughness increased after UV sterilization. Ponter et al. demonstrated how polymer surface roughness gradually increased after UV sterilization in combination with O_3. It is likely that the terminal groups exposed on SLA surfaces were modified by UV (117). The fact that UV did not alter roughness of the PT surface suggests that chemical groups exposed on the SLA surface were more sensitive to UV.

At least some of the differences in surface morphology were due to specimen handling. Irregular traces on control and secondarily sterilized PT surfaces seen on SEM images were most probably a result of the initial PT preparation process. In addition, these irregular marks may have been due to the cell harvesting process, as contaminated PT and SLA were prepared to add full media with cells and then cells were collected. Additional cracks were observed on SLA surfaces after secondary sterilization. The long sonication time used to clean these surfaces may have contributed to the increased number of cracks on these substrata.

Cell responses were sensitive to different cleaning and sterilization methods. Changes in surface morphology may have accounted for some of this variation, but certainly chemistry played a role as well (4). Alkaline phosphatase specific activity as an early differentiation marker, osteocalcin as a later differentiation marker, and osteoprotegerin, which inhibits osteoclast differentiation, on the SLA-CP(2 or 3)-AC surfaces did not significantly increase as compared to the PT-CP(2 or 3)-AC surfaces, although these outcomes were increased when MG63 cells were grown on unused SLA v. PT (4). These results suggest that MG63 cells are capable of recognizing changes in surface wettability and roughness that are due to the secondary cleaning and sterilization procedures performed on contaminated surfaces. Cell responses observed with the PT-CP2-GI and the SLA-CP2-GI surfaces resembled those obtained with control PT and SLA surfaces. In contrast, the PT or SLA-CP3-GI surfaces supported an opposite cellular response compared to control surfaces. This difference can be induced with different cleaning protocols such as CP2 and CP3. Surface roughness was stable with cleaning and GI sterilization on PT and SLA surface. However, surface wettability was dominantly influenced with cleaning protocols. PT or SLA-CP(2 or 3)-OP, characterized by enhanced wettability and decreased roughenss, showed no differences between PT and SLA and control surfaces, except for osteoprotegerin production levels. While re-sterilization may be sufficient to eliminate viable microorganisms, original implant properties cannot be reproduced.

CONCLUSIONS

In conclusion, bio-contaminated PT and SLA surfaces can be cleaned with CP2 and CP3 without modifying surface roughness. However, the combination of cleaning followed by sterilization can result in altered micrometer scale or submicrometer scale surface morphology, as well as chemistry. AC deposited carbon-rich matter on the surface, increasing hydrophobicity, whereas OP sterilized surfaces showed increased hydrophilicity and roughness due to the concurrent superficial material removal during plasma sterilization. Surface wettability of GI sterilized PT and SLA surfaces was enhanced without changing surface roughness. Modified surface properties regulated osteoblast proliferation and differentiation in a different manner compared to control substrata. Taken together, this study indicates that cleaned and sterilized contaminated titanium disks cannot be considered equivalent to unused status. Furthermore, in vitro study results suggest that different cellular responses were due to the modified surface. Although in vivo and clinical studies need to be performed before making conclusions about performace, the re-use of titanium implants after re-sterilization may not be an option if the same clinical responses as were achieved using unused titanium implants are sought.

CHAPTER 4

ENHANCEMENT OF SURFACE WETTABILITY VIA THE MODIFICATION OF MICROTEXTURED TITANIUM IMPLANT SURFACES WITH POLYELECTROLYTES

INTRODUCTION

The coating of surfaces with polyelectrolytes is a versatile approach to develop a robust and conformal surface through electrostatic forces (76). A polyelectrolyte is a polymer whose repeating units possess an electrolyte group that will dissociate in aqueous solutions, such as water, to form poly-ions. Therefore, polyelectrolytes can consist of either positively-charged groups (poly-cations) or negatively-charged groups (poly-anions) depending on the chemical nature of their repeating units and the pH of the aqueous solution (76, 78, 89). Polyelectrolyte multilayers are formed by electrostatic interactions between the oppositely-charged polyelectrolyte chains (76, 89, 118). The structure of polyelectrolyte multilayers consists of three sections, as shown in Figure 2.3. Section (a) is the first adsorbed layer on the substrate, section (b) is the bulk layer, and section (c) is the top layer, which is the dominant contributor to the chemical properties of the surface (119).

The behavior of polyelectrolyte adsorption on a substrate is dependent upon charge density, polyelectrolyte molecular weight, pH, temperature, and ionic strength (78, 119-122). Consequently, these factors can affect polyelectrolyte diffusion or penetration among interlayers and control multilayer thickness (123). In order to better understand polyelectrolyte multilayers, it is important to know the chemical and physical properties

of the first layer of the adsorbed polyelectrolyte, as shown in Figure 2-4(a), because the first adsorbed layer can directly affect the next adsorbed polyelectrolyte layer conformation and thickness (124, 125).

Polyelectrolyte multilayers may be uniformly coated on substrates having a variety of sizes, shapes, and topographies, with high reproducibility (76). Additionally, a polyelectrolyte coated layer can also protect surfaces from corrosion, due to their pH-buffering properties. For example, coating of biomaterials, such as metal implants, with polyelectrolyte multilayers could increase the robustness and functional durability of such devices (76, 126, 127). Because of these advantageous characteristics, the use of polyelectrolytes has emerged as a promising surface modification method, with potential applicability to the enhancement of the mechanical, chemical and biocompatibility properties of biomedical devices. For example, chitosan (CHI) obtained by deacetylation of chitin has been shown to sustain osteoblast growth and inhibit the growth of fibroblasts (128, 129). Poly(L-glutamic acid) (PGA) and poly(L-lysine) (PLL) are synthetic poly(amino-acid) polyelectrolytes, which exhibit positive and negative charges in solution, respectively. Substrates coated with PGA and PLL films are conducive to cell adhesion, depending on the pH of the medium (88, 130).

Titanium is a well-known biomaterial for orthopaedic and dental implants. It has a high strength and fatigue resistance and a relatively low elastic modulus with low density compared to other metals (131). The titanium surface has a very thin and stable oxide layer (average thickness: 2-6 nm) on the surface that forms upon exposure to air or water, which in turn imparts biocompatibility and corrosion resistance properties to the material (39, 112, 131). The titanium oxide layer consists mainly of TiO_2 (112). The isoelectric

point of TiO_2 is around pH 3.5 – 6.2 (132, 133). It is altered as a function of solution pH, surface impurities, and crystal structure, including amorphous, anatase, and rutile (131, 134-136). TiO_2 has a negative charge in body fluids (pH 7.4), which is higher than the isoelectric point range.

Previous studies have shown that titanium surface properties such as surface roughness, surface energy, and surface chemistry, influence bone formation (4, 30, 32). Surface roughness at the micron scale can enhance osteoblast differentiation *in vitro* (3, 4, 9, 35, 54). Microtextured titanium surfaces that are hydrophilic enhance tissue integration of titanium implants, especially during the early healing stages *in vivo* (4, 9, 54, 73, 137-139). Surface chemistry also plays an important role to regulate the signaling pathways, and downstream cell differentiation (140, 141). In order to reduce healing time and enhance osseointegration in compromised patients, it is important to understand, optimize, and engineer ideal surface properties for dental and orthopaedic implants used in bone applications.

The coating of polyelectrolytes, including CHI, PGA, or PLL, on various materials, such as silicon wafer, quartz, glass coverslips, or TiO_2 particles has been previously reported (78, 142-144). For example, Gao et al. described the coating of poly (L-lysine) and DNA on polished and alkali treated titanium surfaces to build up multilayered films for understanding protein adsorption (145). However, the adsorption of polyelectrolyte on the native oxide layer, which is spontaneously formed on a titanium surface, has seldom been probed. Moreover, micron and submicron-scale rough Ti surfaces have not been directly coated with polyelectrolytes. Hence, in this paper, we developed a deposition process to form a thin polyelectrolyte film on the native titanium

oxide layer on both pretreated (PT) and sand-blasted/acid-etched (SLA) titanium surfaces, similar to those are used in clinical settings. Scheme 2 shows the polyelectrolytes used in this study. X-ray photoelectron spectroscopy (XPS), contact mode profilometry, contact angle measurements, and scanning electron microscopy (SEM), were used to characterize the chemical features of the polyelectrolyte-coated Ti surfaces to determine the surface chemistry, roughness, wettability, and surface coverage.

MATERIALS AND METHODS

Titanium Substrates

Titanium disks were supplied by Institut Straumann AG (Basel, Switzerland) with 1 mm thickness and 15 mm diameter. The disks were manufactured to exhibit two different surface structures: a machined pretreated surface (PT, Ra $\leq$ 0.3 µm) and sandblasted/acid-etched surface (SLA, Ra $\geq$ 3.0 µm) (54). Ti disks were cleaned with a sequential acetone-isopropanol-ethanol protocol, in which disks were rinsed twice for 15 minutes at each step. After cleaning, disks were rinsed with distilled water and sterilized with oxygen plasma followed by steam autoclave.

Preparation of Polyelectrolyte Solutions and Titanium Surface Modification

Chitosan (CHI, Mw = 125,000 - 350,000 g/mol, deacetylation degree 80 - 89%, medical grade) was obtained from NovaMatrix (Drammen, Norway). Poly(L-glutamic acid) (PGA, Mw = 2,000 - 15,000 g/mol) and poly(L-lysine) (PLL, Mw = 150,000 - 300,000 g/mol, medical grade) were purchased from Sigma-Aldrich (St. Louis, MO). Glacial acetic acid, sodium chloride, acetone, isopropanol, and ethanol were obtained from Sigma-Aldrich. PGA and PLL solutions consisted of 0.1 mg/ml in 0.15 M aqueous

NaCl. The CHI solution consisted of 1.5 mg/ml dissolved in 0.1 M acetic acid containing 0.14 M aqueous NaCl (128). All polyelectrolyte solutions were filtered through a sterilized poly(tetrafluoro ethylene) (PTFE) filter (pore size 0.2 μm) before exposure to the surface. The polyelectrolyte layer was prepared on the cleaned and sterilized PT and SLA surfaces by immersing the substrates in 300 μl of the polyelectrolyte solutions at room temperature for 2 hours. Each coating was followed by a 5 minute rinse in either 0.15 M NaCl for PGA and PLL coatings or 0.14 M NaCl for CHI. Surfaces were allowed to dry under UV sterilized hood after the final coating. The filtering and coating processes were performed in a UV sterilized hood. Polyelectrolyte-coated surfaces are denoted as substrate-polyelectrolyte. For example, PT-CHI represents PT surface was coated with chitosan (CHI).

Surface Characterization

X-ray photoelectron spectroscopy (XPS) measurements were performed on an ESCA-SSX 100 (Service Physics, Bend, OR) instrument equipped with a monochromatic Al Kα X-ray source ($h\nu$ = 1486.6 eV). The XPS analysis chamber was evacuated to a pressure of 10^{-8} Torr or lower before collecting XPS spectra. High resolution spectra were obtained using an X-ray spot size of 200 μm and pass energy of 50 eV, with a 0.1 eV increment, at a 55° takeoff angle. Peak fitting was performed using symmetric curves that were 80% Gaussian and 20% Lorentzian. Evaluation of XPS results was carried out using the ESCA 2005G software package provided by Service Physics, Inc.

The surface roughness before and after coating was measured two-dimensionally with a KLA-Tencor P-15 contact mode profilometer (KLA Tencor, CA) equipped with a 2 μm diamond-tracing stylus tip and a 90° point angle. Six random areas were measured

on each sample over a scan length of 500 µm to obtain an average roughness value (Ra, µm).

Contact angle measurement using doubly-distilled water was conducted by using a CAM 100 goniometer (KSV Instruments Ltd., CT) before and after coating. Image analysis was performed by using the KSV CAM 100 software package provided by KSV. Six samples were measured in each group, and two measurements were made from each surface. Polyelectrolyte coated PT and SLA surface morphology as a function of adsorption time was examined by scanning electron microscopy (SEM) using an Ultra 60 field emission (FE) microscope (Carl Zeiss SMT Ltd., Cambridge, UK). Samples were coated with gold, and images were recorded using a 5 kV accelerating voltage.

Statistical Analysis

The data given are the mean ± standard error of six individual surfaces for contact angle and profilometry. Data were first analyzed by analysis of variance (ANOVA). When differences were detected, a Student's *t*-test for multiple comparisons using Bonferroni's modification was used. The $p<0.05$ was considered to be significant.

RESULTS AND DISCUSSION

XPS Chemical Analysis of Polyelectrolyte Layer

To ascertain the adsorption of polyelectrolytes on the PT and SLA surfaces, XPS analysis was conducted before and after polyelectrolyte coating. Figure 4.1 shows the Ti(2p) high resolution XPS spectra of both metallic Ti and TiO_2 on the bare samples and on samples having the adsorbed polyelectrolyte films. Prior to the polyelectrolyte deposition, both species are detectable on the surface. The presence of the Ti($2p_{3/2}$) and

$Ti(2p_{1/2})$ peaks of TiO_2 at 458.20 eV and 464.88 eV, respectively, observed in the spectra of the coated substrates, suggests that the adsorbed polyelectrolytes formed a thin film on the PT or SLA surfaces, having a thickness that was smaller than the penetration depth of the x-ray in the sample (~ 7 nm) (145). Unlike the TiO_2 peaks, the small $Ti^{(0)}$ peak at 454.34 eV is visible only in the PT-CHI and PT-PGA samples (Figure 4.1a), and absent in the PT-PLL and all the coated SLA samples (Figure 4.1b). This suggests that in the PT-CHI and PT-PGA samples there is only partial polyelectrolyte coverage, while in the PT-PLL, SLA-CHI, SLA-PGA, and SLA-PLL samples the coverage is more extensive. This information was further corroborated by the results from SEM images as shown in Figures 4.3 & 4.

Figure 4.2 shows the XPS high resolution analysis of the C(1s), O(1s), and N(1s) core level electrons for the PT control, PT-CHI, PT-PGA, and PT-PLL surfaces. The PT control surface has three elements: titanium (Ti), oxygen (O), and carbon (C). Ti and oxygen originate from the native TiO_2 layer on the surface as shown in Figure 4.1 (112). The carbon is most likely a result of carbon-containing molecules due to exposure to the ambient environment (39). Lausmaa et al. pointed out that the titanium surface always displayed Ti, O, C and N peaks by XPS general survey (112). However, an N signal was not detected on PT surfaces used in this study. The C(1s) XPS spectrum of the PT control surface (Figure 4.2a) shows the aliphatic carbon peak at 284.74 eV and additional peaks at 286.17 eV and 288.0 eV, corresponding to a C-O single bond and C=O double bond, respectively. The amine (C-N) peak was not detected on the PT control surface (Figure 4.2a). However, after adsorption of CHI (Figure 4.2d), PGA (Figure 4.2g), and PLL (Figure 4.2j) to the PT surface, the C(1s) XPS spectra indicated the presence of amine (C-N) bands at 286.45 eV, 285.66 eV, and 286.23 eV, respectively.

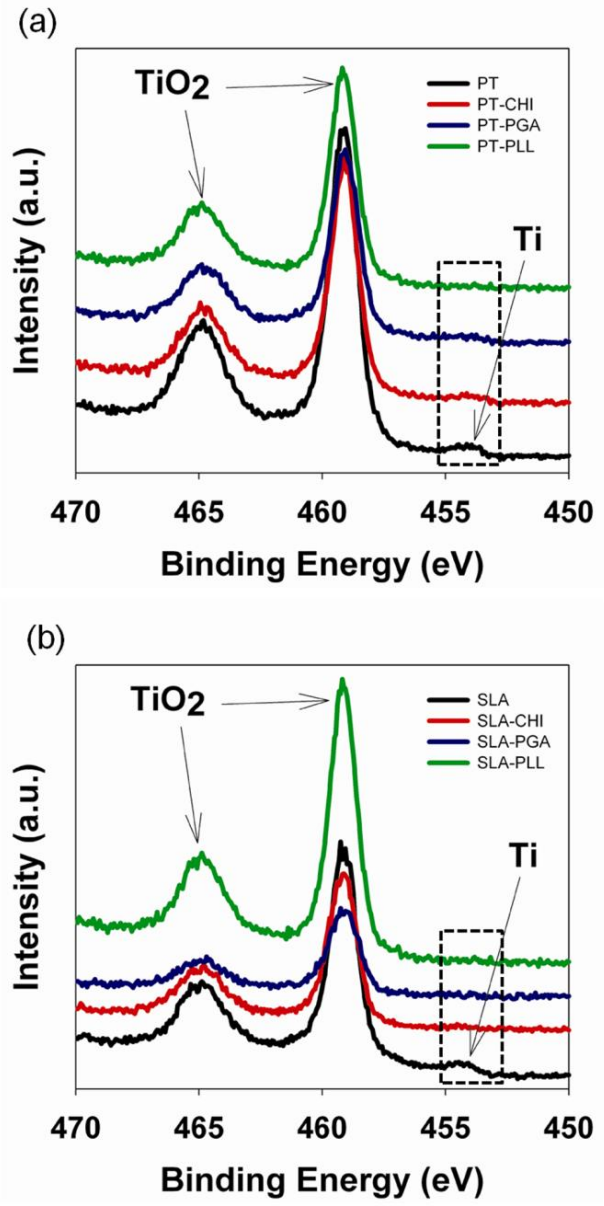

Figure 4.1. X-ray photoelectron spectra (XPS) analysis: evolution of Ti(2p) of Ti surfaces before and after polyelectrolyte coating: (a) PT and PT-polyelectrolyte; (b) SLA and SLA-polyelectrolyte surfaces.

There is a significant carboxylate ($-COO^-$) peak at 288.42 eV on the PT-PGA surface (Figure 4.2g). It is interesting to note that the titanium oxide layer is weakly negatively charged, and PGA has the same charge as the titanium oxide layer. If the electrostatic force is the only source of the interaction between the titanium surface and

PGA, there is a quite limited way to adsorb PGA on titanium surface. However, XPS, considered as one of the most surface sensitive analyses, detected the carboxylate ($-COO^-$) peak on the titanium surface following the adsorption of the PGA, a fact that is commensurate with PGA presence on the surface. Therefore, XPS high resolution analysis data suggest a possible chemical interaction between the oxide layer and PGA, rather than just an electrostatic interaction (130, 143, 146). Also, the negatively charged PGA in solution can be screened due to the repellent force induced by like-charge with the titanium surface. Thus Na^+ ions can have more interaction with a negatively charged Ti surface. Therefore, an electrical double layer may be formed on the titanium surface, causing a limited charge inversion in the double layer, thereby leading to the adsorption of PGA (122, 147, 148).

High resolution XPS spectra of the O(1s) core electrons of the PT control surface (Figure 4.2b) show three components: a titanium oxide peak at 530.10 eV, a carbon-oxygen double bond (C=O) at 531.59 eV, and a hydroxide bond (C-OH) at 532.50 eV. The O(1s) peak shapes are changed after coating with CHI, PGA, and PLL on PT surface corresponding to Figure 4.2e, 2h, and 2k, respectively. The PT-PGA surface (Figure 4.2h) and PT-PLL surface (Figure 4.2k) show similar overall spectral contour in the O(1s) binding energy region because they are both synthetic amino acids as shown in Scheme 2. The peak at 532.09 eV on the PT-PGA surface (Figure 4.2h) belongs to the COO^- group. This carboxylate peak clearly shows that PGA is adsorbed on the PT surface. The different spectral contours of the high resolution peaks among control and modified surfaces can be used as a good index to confirm polyelectrolyte adsorption on the PT

surface. The XPS spectral contour is a result of the population density of the specific chemical species on the surfaces (149).

The N(1s) core bands for the PT control surface (Figure 4.2c) were not detected. However, PT-CHI (Figure 4.2f), PT-PGA (Figure 4.2i), and PT-PLL (Figure 4.2l) surfaces showed N(1s) core bands of the carbon-nitrogen (C-N) group at 399.85 eV, 400.18 eV and 399.98 eV, respectively. The adsorption of CHI, PGA, and PLL on PT surfaces affect the shape of the N(1s) peak. This N(1s) peak results from the amino and amide groups that are present in three polyelectrolytes used in this study as shown in Figure 2.4. In addition, charged nitrogen (NH_3^+) was detected in the N(1s) core spectra at 402.41 eV on PT-CHI surfaces (Figure 2f) and 401.99 eV on PT-PLL surfaces (Figure 4.2l), which is in good agreement with the other reported peaks for charged nitrogen species (150, 151). The high resolution XPS analysis of the control and modified PT surfaces, particularly the presence of the carboxylate group on the PT-PGA surface and the nitrogen-containing functional groups on the PT-CHI surface and the PT-PLL surface, confirm that CHI, PGA, and PLL were adsorbed onto the PT surfaces.

High resolution XPS spectra of C(1s), O(1s), and N(1s) electrons for the SLA control and the polyelectrolyte coated surfaces, as shown in Figure 4.3, were obtained in a similar manner as those described for the PT surfaces. In contrast to the PT control surface (Figure 4.2c), the N(1s) peak was detected on the SLA control surface (Figure 4.3c). PT and SLA surfaces were extensively cleaned and sterilized before coating and therefore, there is a small probability that small molecules could be trapped on the surface. One possible explanation for the observation of the N(1s) peak on the SLA control (Figure 4.3c) is the presence of a small detectable amount of impurity, such as

nitride (TiN) on the oxide surface (112). Also, this discrepancy between PT and SLA surfaces may be due to the difference in surface roughness between the comparatively smooth PT surface and the complex morphology of the rough SLA surface, both at the micron and submicron size scales. Therefore, the N(1s) signal cannot be fully accepted as validation of the adsorption of polyelectrolytes on the SLA surface. Therefore, following the systematic deconvolution of the high-resolution N(1s) spectral contour the percent total area specifically of the C-N peak used to demonstrate the presence of the polyelectrolyte coating on the SLA surfaces. The high-resolution N(1s) spectral contour was different among the various samples, corresponding to the variations in the chemical composition of the polyelectrolytes, leading to different percent total areas for each surface. The percent total area of the C-N peak for SLA-CHI (61%), SLA-PGA (73%), and SLA-PLL (63%) was higher than that for the SLA control (29%) surface. The increase in the intensity of the C-N peak following CHI, PGA, and PLL deposition suggests that the polyelectrolytes were indeed adsorbed on the SLA surface. Moreover, charged nitrogen (NH_3^+) peaks at 402.83 eV and 402.09 eV were observed on the SLA-CHI surface (Figure 4.3f) and the SLA-PLL surface (Figure 4.3l), respectively. The carboxylate ($-COO^-$) peak at 532.05 eV on the SLA-PGA surface (Figure 4.3h) confirmed the presence of the PGA on the modified SLA surface. XPS analysis demonstrated the adsorption of CHI, PGA, and PLL polyelectrolytes on the SLA surface.

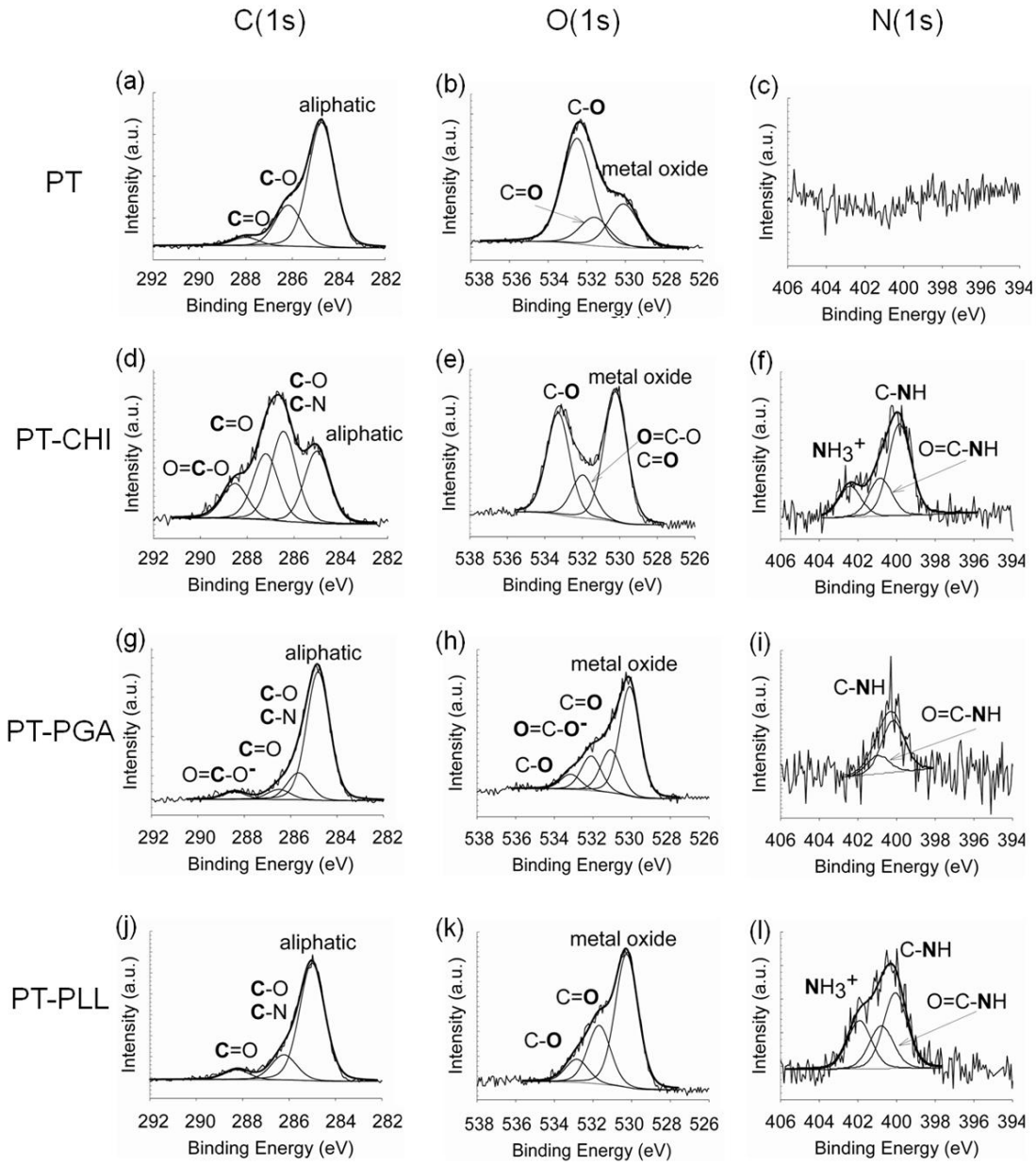

Figure 4.2. High resolution X-ray photoelectron spectra (XPS) of PT surfaces before and after polyelectrolyte coating: (a), (b), and (c) correspond the C(1s), O(1s), and N(1s) core electrons of the control PT, respectively. (d), (e), and (f) correspond the C(1s), O(1s), and N(1s) core electrons of the PT coated with Chitosan (CHI), respectively. (g), (h), and (i) correspond the C(1s), O(1s), and N(1s) core electrons of the PT coated with poly(L-glutamic acid), respectively. (j), (k), and (l) correspond the C(1s), O(1s), and N(1s) core electrons of the PT coated with poly(L-lysine), respectively.

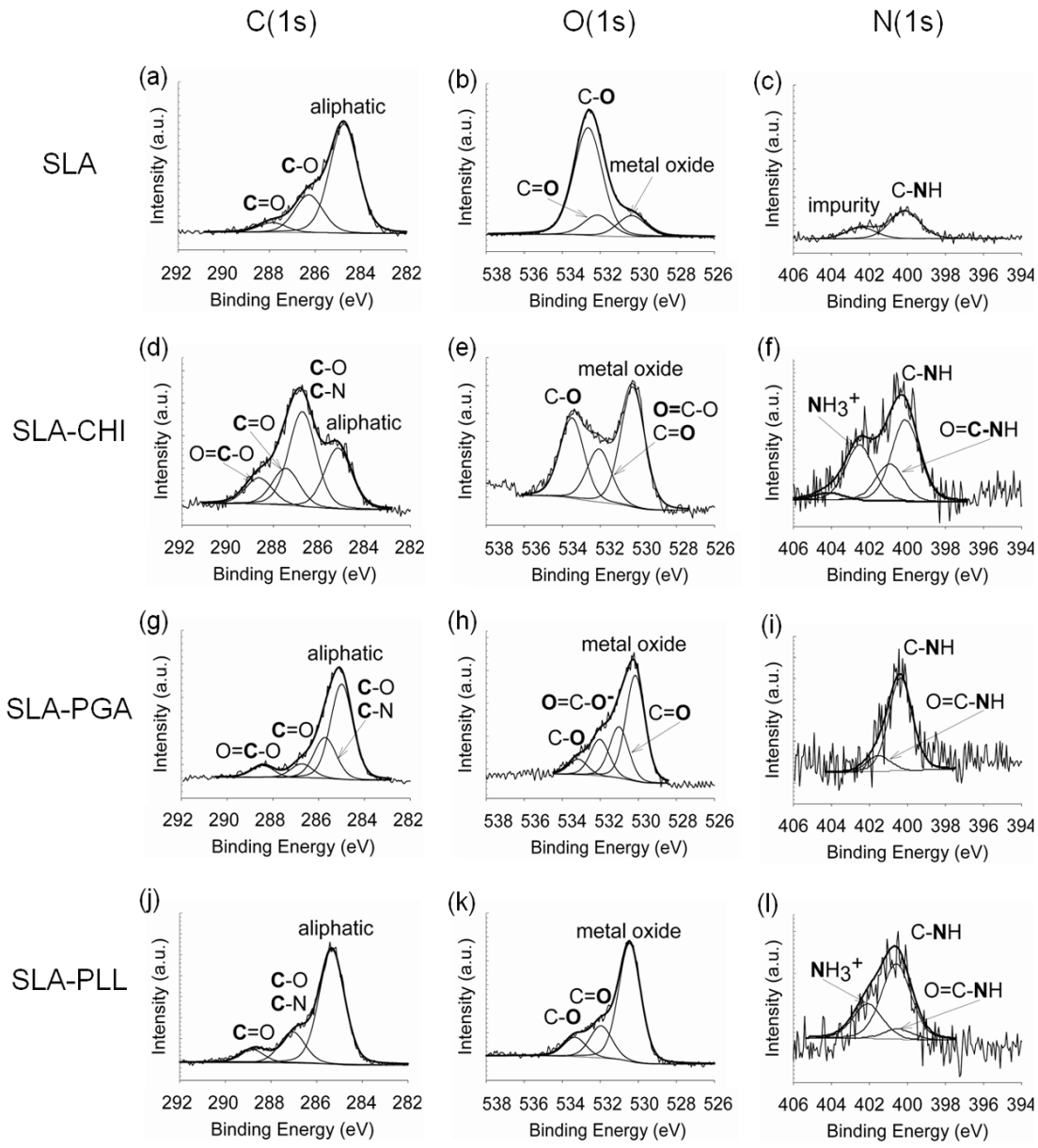

Figure 4.3. High resolution X-ray photoelectron spectra (XPS) of SLA surfaces before and after polyelectrolyte coating: (a), (b), and (c) correspond the C(1s), O(1s), and N(1s) core electrons of the control SLA, respectively. (d), (e), and (f) correspond the C(1s), O(1s), and N(1s) core electrons of the SLA coated with Chitosan (CHI), respectively. (g), (h), and (i) correspond the C(1s), O(1s), and N(1s) core electrons of the SLA coated with poly(L-glutamic acid), respectively. (J), (k), and (l) correspond the C(1s), O(1s), and N(1s) core electrons of the SLA coated with poly(L-lysine), respectively.

Polyelectrolyte Surface Coverage on Titanium Surfaces

The surface coverage defined by the number of adsorbed molecules per unit surface area is important for understanding the interactions between the titanium surface and the polyelectrolytes. Since both the PT and SLA samples have rough surfaces (albeit different degrees of roughness), it is a challenge to measure accurate surface area for the calculation of surface coverage. Therefore, the surface coverage of the polyelectrolytes adsorbed on titanium surfaces was evaluated by examining the pertinent SEM images of the covered surfaces, which are shown in Figures 4.4 & 5, and supported by a quantitative XPS analysis. The PT and SLA surfaces coated with CHI, PGA, and PLL do not exhibit any noteworthy morphological changes when compared to controls under low magnification. However, under high magnification, it appears that the CHI (Figure 4.4d) and PGA (Figure 4.4f) polyelectrolytes coated the titanium substrates evenly, albeit in an incomplete layer.

The flexibility of the polyelectrolyte chain plays an important role in determining the amount of adsorbed polyelectrolyte on substrates (147, 152). Since CHI has abundant hydroxide groups that can form H-bonds between chains, the polymer acts as a rigid and stiff network (153), causing conformational and entropic barriers to adsorption. The PT-PGA system (Figure 4.4f) shows similar surface morphology to that of the PT-CHI system. PGA cannot efficiently adsorb on titanium surfaces due to the repulsive force generated by the same charges found on both materials. However, XPS, contact angle, and SEM images have shown conclusively that PGA has indeed adsorbed on the titanium surface.

Like-charge polyelectrolyte interactions can be explained by the competition among the negatively charged titanium oxide surface, PGA ($-COO^-$) and Na^+ ions, which originate from the 0.15 M NaCl salt solution used in this study. The Na^+ ions in solution are attracted to and interact with the negatively charged titanium oxide surface, thereby reducing the negative character of the surface and allowing the PGA to adsorb.

The PT-PLL (Figure 4.4h) shows uniform coverage on the entire surface. It is difficult to differentiate between the surface morphology of the control and that of the PLL coated surfaces, even under high magnification indicating that PLL is coated on the PT surface without any change in surface morphology. The insert in Figure 4.4h also shows that when a small portion of the PLL overlayer is torn off, the underlying dark PT surface is exposed. This highlights the uniformity of the polyelectrolyte thin layer formed on the surface.

Polyelectrolyte-modified SLA surfaces exhibit different surface morphology than that obtained for PT surfaces, as shown in Figure 4.5. In addition to the adsorbed polyelectrolytes, small salt crystals were also observed on the modified SLA surfaces, most likely generated when rinsing with the NaCl solution. PT and SLA are commercially pure titanium, and the discrepancy between PT and SLA surfaces is their inherent different surface morphology. The SLA surface has micron and sub-micron scale roughness. It is possible that the surface morphology affects on polyelectrolyte adsorption. Nunnery et al. showed that the surface curvature can affect the polymer adsorption behavior and consequently the coverage of the polymer on surfaces (154). Because the SLA surface morphology can be described as concave on the micron scale (hence, at least two orders of magnitude larger than the effective Rg of the polymers),

there is no direct and strong effect on polyelectrolyte chain adsorption. However, the curvature of the SLA surface caused by the higher degree of surface roughness can contribute to an increase the surface area. The adsorption mechanism of polyelectrolytes on surfaces with complex surface morphologies at both the micron- and nano-scale is not clear.

The incomplete coverage of CHI on PT, after the standard 2 h incubation time used for all the samples, was contrary to our expectations, given the positive ionic charge of the polymer. To better assess whether the incomplete coverage was thermodynamically mandated or a result of insufficient adsorption time, we probed the adsorption behavior of the CHI layer on PT and the resulting surface properties as a function of time, as shown in Figure 4.6. The extent of coverage of the adsorbed CHI on PT surfaces was monitored by XPS. The atomic abundance of Ti and N, expressed as atom %, was plotted as a function of the adsorption time (Figure 4.6a). When the angle of incidence of the x-ray beam is fixed, the amount of Ti and N detected depends on the distance of the species from the surface and hence it will change as a function of the polymer layer thickness. The initial decrease of the Ti atom % and the increase of the N atom % are due to the increased polymer coverage. This is coupled with a moderate increase in the coating layer roughness immediately following the onset of adsorption (Figure 4.6b) and a decrease in the coating layer contact angle (Figure 4.6c). After approximately 24 hours of adsorption time, the Ti peak was barely detectable by XPS suggesting that the whole PT surface was covered with CHI. Moreover, after this amount of time, both surface roughness and contact angle reached a constant value, indicating the formation of a complete monolayer.

Surface Roughness

The surface roughness of the polyelectrolyte-modified surface was measured with contact mode profilometry before and after the adsorption of the polyelectrolytes on both the PT and SLA surface. Figure 4.7a shows that surface roughness (Ra, µm) was not significantly altered after coating of the PT and SLA surfaces. Surface roughness has been recognized as one of the most important surface properties in osteoblast differentiation on titanium substrates and in bone-to-implant contact *in vivo* and *in vitro* (88, 139). The modification of the chemical properties of the titanium surfaces while preserving their surface roughness could represent an attractive option for the enhancement of their properties and the cell response.

Surface Wettability

Both surface roughness and surface chemistry can directly influence surface wettability (155, 156). In turn, surface wettability can be ascertained by the measurement of water contact angles (surface hydrophylicity) (54-56). Since both PT and SLA are made of commercially pure titanium, the difference in contact angle between them is due to their different surface treatments that resulted in a rougher surface for SLA. As a result, the SLA control surface is more hydrophobic than the PT control surface, as exhibited by its larger contact angle, shown in Figure 4.7b. The wettabilities of the PT and SLA control surfaces were significantly enhanced when their native oxide layers were coated with CHI, PGA, and PLL, as evidenced by a decrease in the measured contact angles, as shown in Figure 4.7b. There was no statistical difference in contact angles among modified PT and SLA surfaces. While the higher roughness of the uncoated SLA sample implied the availability of a larger surface, and hence, a larger

amount of polyelectrolyte chains that could potentially adsorb, the fact that the surface roughness was not altered indicated that both coated substrates had similar charge densities. Therefore, the changes in surface hydrophylicity, and in particular the drastic change observed for SLA must be due to the nature of the polyelectrolyte coating itself. These results clearly show that we were able to decouple the effects of surface roughness and surface chemistry on surface wettability. Furthermore, we have shown that surface chemistry is the dominant parameter governing surface properties, with the underlying microtexture playing only a secondary role.

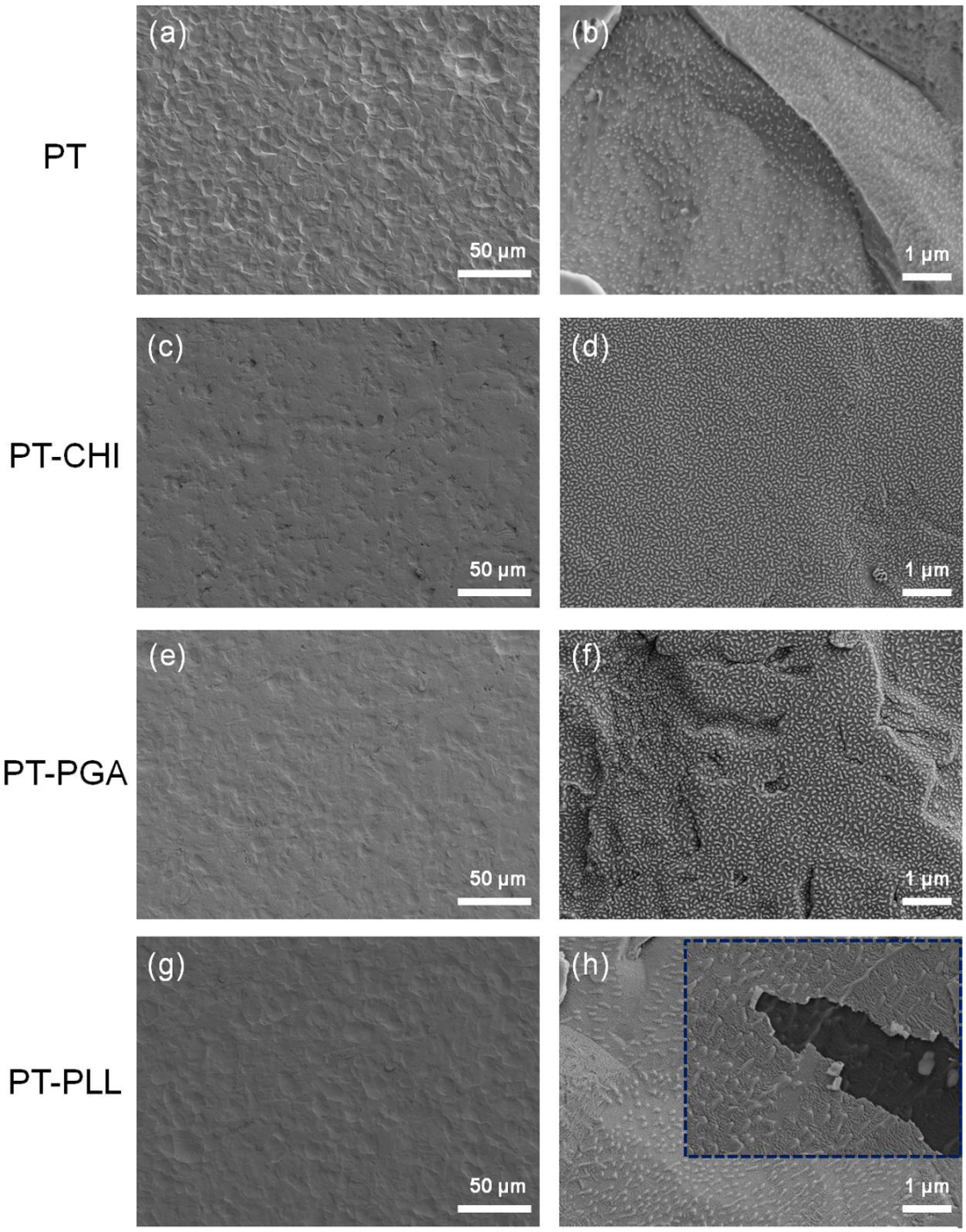

Figure 4.4. SEM surface morphology images of PT surfaces after polyelectrolyte coating: PT control, PT_CHI, PT_PGA, and PT-PLL. The left column (a, c, e, g) of each image shows the surface features in lower magnification and the right column (b, d, f, h) of each image shows the surface features in higher magnification.

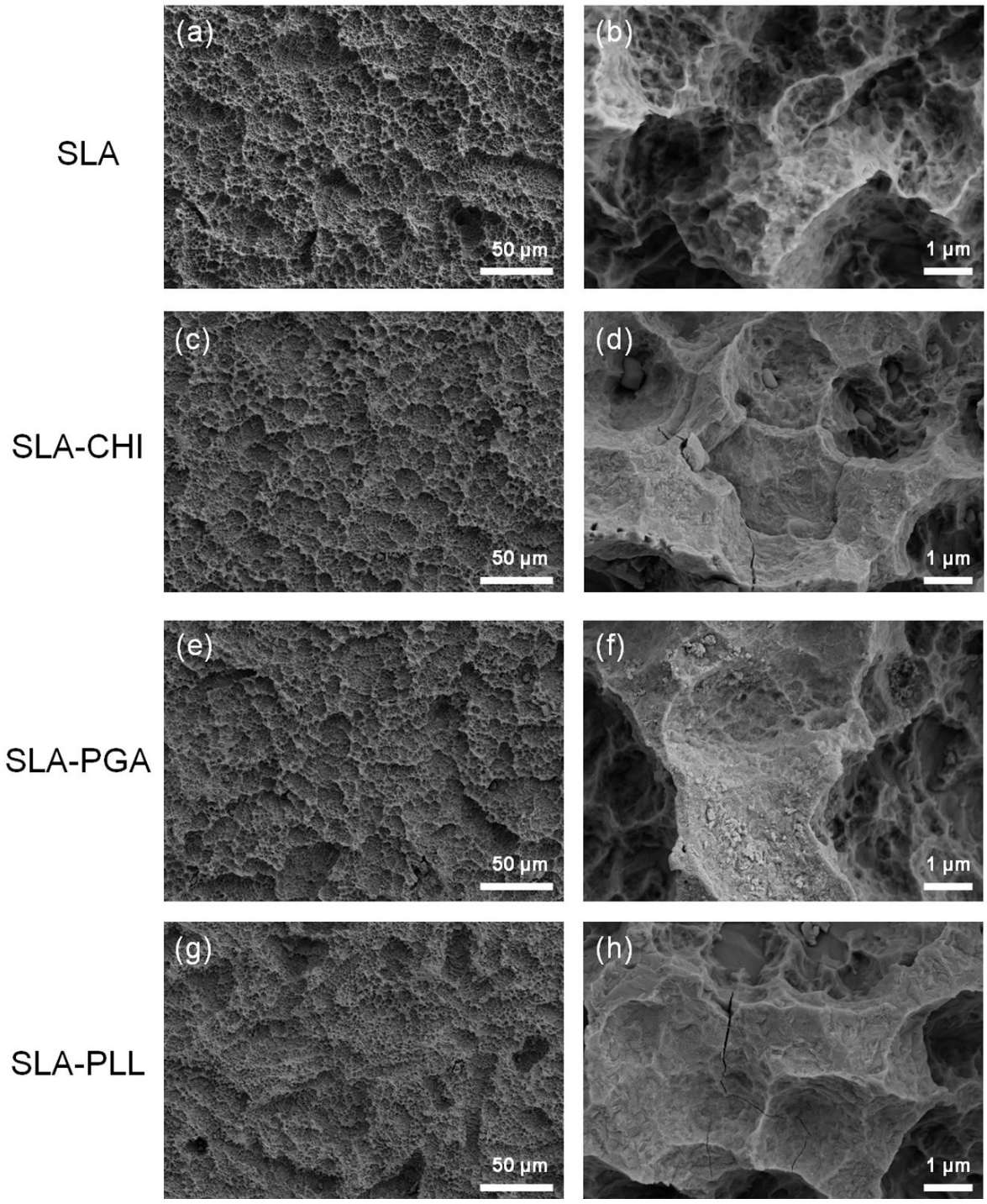

Figure 4.5. SEM surface morphology images of SLA surfaces after polyelectrolyte coating: SLA control, SLA_CHI, SLA_PGA, and SLA-PLL. The left column (a, c, e, g) of each image shows the surface features in lower magnification and the right column (b, d, f, h) of each image shows the surface features in higher magnification.

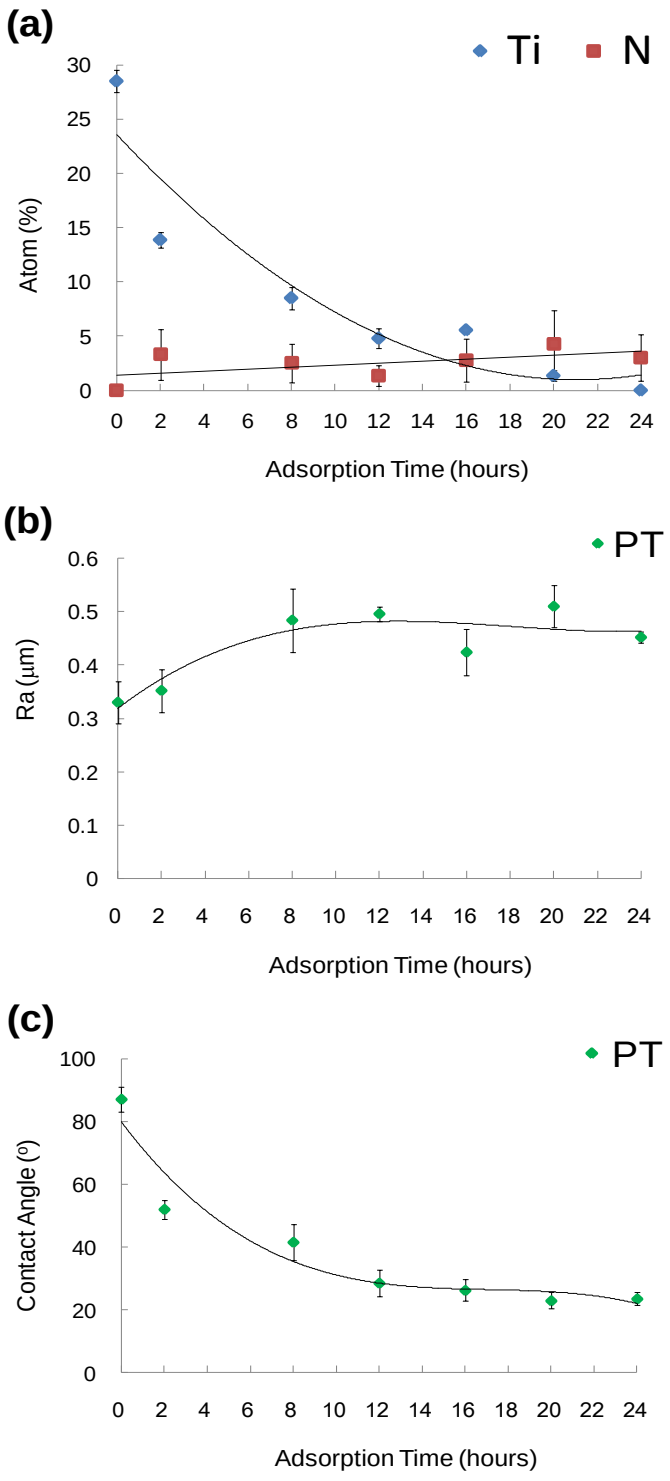

Figure 4.6. Influence of the CHI adsorption time on (a) XPS atom (%) analysis for Ti vs. N, (b) roughness, and (c) contact angle on PT surfaces, respectively.

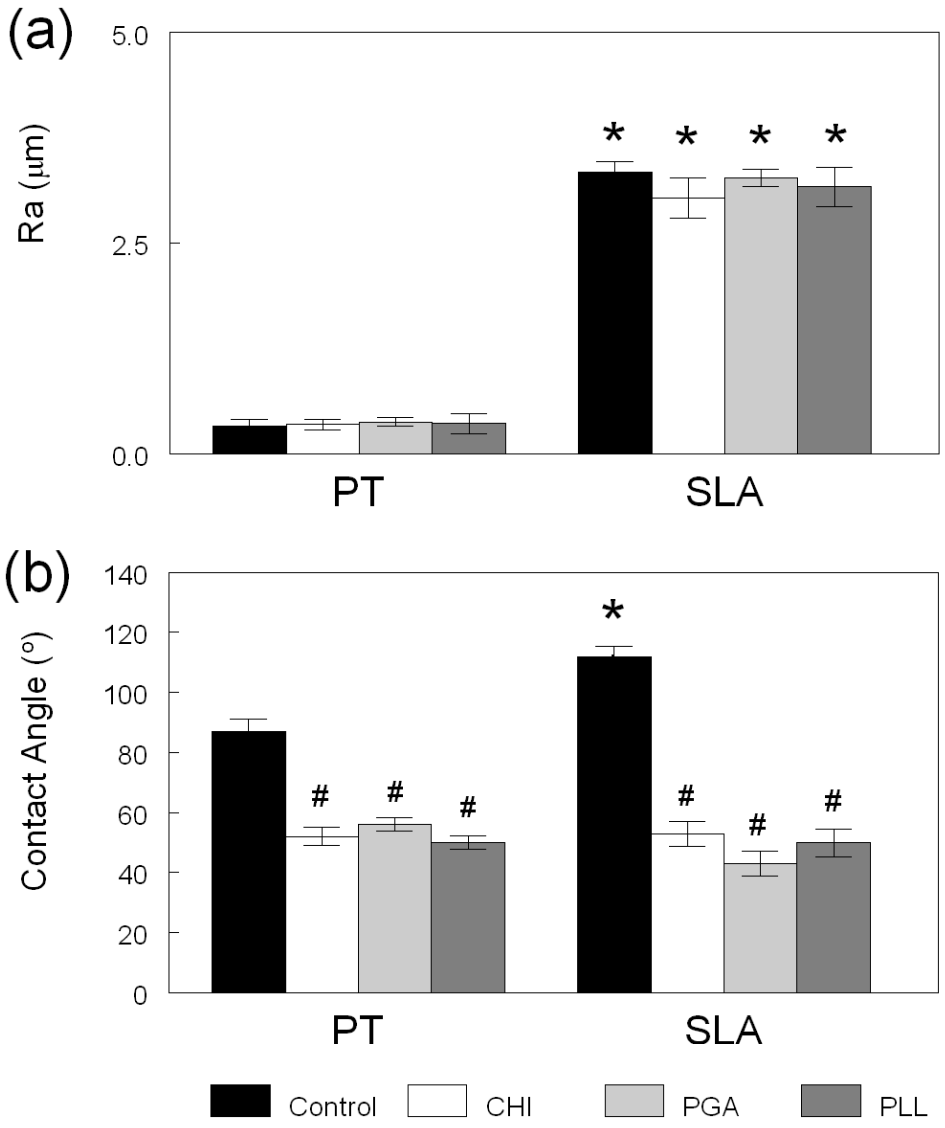

Figure 4.7. Influence of the polyelectrolyte coating on (a) roughness and (b) contact angle on PT and SLA surfaces, respectively. * $p<0.05$, PT vs. SLA surface, # $p<0.05$, polyelectrolyte coated surfaces vs. control surface.

CONCLUSION

We have developed a facile method for the surface modification of Ti surfaces by the adsorption of three different polyelectrolytes: CHI, PGA, and PLL. The coated titanium surfaces were characterized by a variety of methods to ascertain the adsorption of the polyelectrolytes and to evaluate their influence on the surface properties of the titanium surfaces. The results show that the polyelectrolytes used in this study were successfully adsorbed onto PT and SLA surfaces, and enhanced surface wettability without modifying the surface roughness of the substrates. Surprisingly, there was no statistical difference in contact angles among all coated PT and SLA surfaces, with the SLA substrate sustaining a more pronounced decrease than that of PT. The fact that the surface roughness of the substrates was not altered upon polymer adsorption indicated that both coated substrates had similar charge densities. Therefore, the nature of the polyelectrolyte coating itself must have been responsible for the changes in surface hydrophylicity. These results clearly show that we were able to decouple the effects of surface roughness and surface chemistry on surface wettability. Furthermore, we have shown that in these systems, surface chemistry is the dominant parameter governing surface properties, with the underlying microtexture playing only a secondary role.

Because titanium surface roughness and surface wettability are key factors in shortening wound healing time and enhancing osseointegration after device implantation, polyelectrolyte coated PT and SLA surfaces could be used as improved implant materials.

CHAPTER 5

USE OF POLYELECTROLYTE THIN FILMS TO MODULATE OSTEOBLAST RESPONSE TO MICROSTRUCTURED TITANIUM SURFACES

INTRODUCTION

Osseointegration is critical for the success of dental and orthopaedic implants, especially for patients with bone pathology (12). The primary interaction between a biomaterial and the surrounding bone involves the outermost molecular layers of the implant (157). Thus, the surface micro-roughness (3, 31), surface energy, and surface charge of the biomaterial play important roles in influencing cellular response (9, 73).

In order to improve osseointegration, many studies have been devoted to the modification of biomaterial surface properties (158). Titanium surfaces with both micrometer and submicrometer scale roughness have been shown to enhance osteoblast differentiation *in vitro* and bone formation *in vivo* (4). The increased surface area associated with a higher degree of surface roughness provides a larger contact region with the surrounding tissue than that available with a smooth surface, and consequently, provides increased stability for tissue anchoring (43). However, poor surface wettability due to increased surface roughness and adsorption of organic contaminants from the atmosphere can delay the initial interactions with tissue fluids and ultimately impact the rate and extent of new bone formation (40, 159, 160). Enhanced surface wettability on rough titanium implant surfaces shortens wound healing time and increases tissue

integration of titanium implants by forming conditioned protein layers, thereby reducing the gap between tissue and the biomaterial surface (32).

The adsorption of proteins on biomaterial surfaces is controlled to a great extent by surface chemistry and is the key parameter responsible for cell attachment and adhesion, spreading, and proliferation (161). Therefore, in vitro studies using chemically modified surfaces have focused on these parameters (162-164). More recent studies have shown that integrin expression is also sensitive to surface chemistry (140) and that osteoblast differentiation and local factor production are dependent on specific integrin signaling (35). Integrins are heterodimeric transmembrane receptors consisting of α- and β- subunits, which bind to extracellular matrix proteins (34, 165). In addition to surface chemistry, integrin expression is also sensitive to surface wettability and micron-scale roughness (166).

Several studies have shown that integrin signaling modulates different aspects of cellular response to their substrates. When bone marrow cells are cultured on tissue culture polystyrene (TCPS), integrin α5β1 binds to fibronectin, resulting in osteogenic gene expression and mineralization (34). In contrast, overexpression of the αvβ3 integrin stimulates proliferation but down-regulated osteoblastic differentiation (167, 168). Similarly, when osteoblasts are grown on titanium substrates, α5β1 mediates cell attachment and proliferation but inhibits differentiation (35). In contrast to TCPS, osteoblastic differentiation on titanium requires α2β1 signaling and this in further enhanced when osteoblasts are grown on microtextured titanium, particularly when the micro-rough surfaces have been modified to have high surface energy (35).

It is not known whether the dominant property of a titanium surface is its wettability or its microtopography, nor is it known if the method used to achieve enhanced wettability is a critical variable. Surface chemistry and surface wettability are interrelated properties. The effects of varying surface wettability using different chemistries and the resulting influences on cell differentiation, local factor production, and integrin expression have not been well studied, particularly in the context of a complex surface topography.

The objective of this study was to assess the role of chemistry in determining osteoblast responses to microtextured hydrophilic substrates of comparable wettability. A variety of surface modifications have been proposed with the goal of changing surface wettability (169). The thin oxide layer on the surface of titanium exhibits a pH-dependent surface charge (170), making it a useful surface for these kinds of modifications. We previously developed a method for applying polyelectrolyte thin films onto the titanium oxide layer (80), taking advantage of the robust and conformal surface "bottom-up" nanofabrication resulting in a high charge density (76). We used this technology to modify surface wettability by coating polyelectrolyte thin films with different charges directly onto thin titanium oxide layers without altering the microstructure of the titanium surface and examine whether these chemical modifications alter osteoblast maturation, local factor production, and integrin expression.

MATERIAL AND METHODS

Titanium Substrates

Titanium disks (grade 2 commercially pure Ti, Ø 15 mm x 1 mm) were supplied by Institut Straumann AG (Basel, Switzerland). Two different surface topographies were used [32]: a machined surface pretreated using a proprietary method (PT, Sa = 0.38 µm) and a sand blasted/acid-etched surface (SLA, Sa = 2.54 µm). Titanium disks used for the cell study were sterilized with gamma irradiation overnight. The physical and chemical properties of the disks before and after gamma irradiation have been described previously (40).

Preparation of Polyelectrolyte Thin Films

Chitosan (CHI, MW = 125,000 - 350,000 g/mol, deacetylation degree 80 - 89%, medical grade) was obtained from NovaMatrix (Drammen, Norway). Poly(L-glutamic acid) (PGA, MW = 50,000 - 100,000 g/mol) and poly(L-lysine) (PLL, MW = 150,000 - 300,000 g/mol, medical grade) were purchased from Sigma-Aldrich (St. Louis, MO). Polyelectrolyte thin films were directly formed on a thin native oxide layer on PT and SLA surfaces. The titanium oxide layer and the CHI, PGA, and PLL films have different charges at different pH values. Therefore, the electrostatic force induced by different charge interactions is the main driving force for developing the formation of the thin films. To maximize the interaction between the oxide layer and each polyelectrolyte, the isoelectric point of the titanium oxide layer (pH ~ 5.1) was estimated by measuring contact angle as a function of droplet pH (Figure 5.1). The pH of the polyelectrolyte solutions of CHI ($pK_a \approx 6.5$), PGA ($pK_a \approx 4.4$) [23], and PLL ($pK_b \approx 5$) was adjusted to pH 5.8, pH 4.8, and pH 7.0, respectively, as described below.

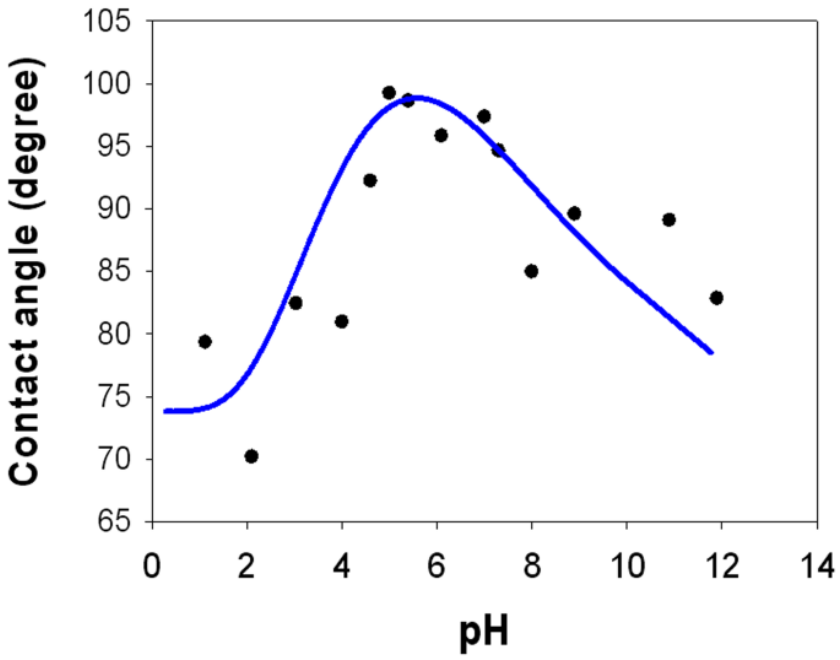

Figure 5.1. The isoelectric point of the titanium oxide layer was estimated using contact angle measurement as a function of different pH of the drop solution. pH was adjusted by using 1N NaOH and 1N HCl.

Glacial acetic acid was obtained from Sigma-Aldrich. PGA (pH 4.8) and PLL (pH 7.0) solutions were prepared by mixing 0.1 mg/ml of the polymer in ultrapure water (18.2 MΩ·cm, Millipore Milli-Q system). The CHI (pH 5.8) solution was prepared by dissolving 1.5 mg/ml in 0.1 M acetic acid. All polyelectrolyte solutions were filtered through a polytetrafluoroethylene (PTFE) filter (pore size 0.2 μm). The polyelectrolyte layer was prepared on the PT or SLA surface by immersing the substrates in 500 μl of the polyelectrolyte solutions at room temperature for 2 hours. Each coating was followed by a 5 minute rinse in ultrapure water. The filtering and coating processes were performed in a UV sterilized hood. Polyelectrolyte-coated surfaces are denoted as substrate-polyelectrolyte. For example, PT-PLL represents a PT surface that was coated with poly(L-lysine). Titanium surfaces without polyelectrolyte coating were used as controls.

Surface Characterization

The surface morphology of polyelectrolyte-coated titanium surfaces was examined by scanning electron microscopy (SEM) using an Ultra 60 field emission (FE) microscope (Carl Zeiss SMT, Ltd., Cambridge, UK) with 5 kV accelerating voltage. For these analyses, the surfaces were sputter-coated with gold.

The stability of polyelectrolyte thin films on PT and SLA substrates was examined by immersion of the coated surfaces into full medium without cells. After 3 days in the cell culture environment (incubation at 37℃), the surfaces were rinsed with abundant ultrapure water and dried at room temperature. Surface morphology and chemical composition were characterized using scanning electron microscopy and X-ray photoelectron microscopy.

The contact angle of polyelectrolyte-coated titanium disks was determined using a Ramé-Hart goniometer (model 250-F1, Mountain Lakes, NJ). Ultrapure water was dropped (2µl), recorded, and analyzed with the DROPimage CA software package (Ramé-Hart Instrument Co.). Three measurements were made on separate surfaces per group. In order to plot a three dimensional (3D) correlation between surface properties and cellular response, the surface water tension was calculated using following equation: $E_s = E_{lv}cos\theta$, where E_{lv} = 72.8 dyne/cm at 20°C for pure water and θ is the contact angle (171).

Surface roughness of titanium disks before and after polyelectrolyte adsorption was measured using a LEXT 3D Material Confocal Laser Microscope (CLM, 100X objective, area scan 128 x 128 µm, Olympus America Inc., PA, USA). Results were evaluated using the LEXT OLS4000 software provided by Olympus. The threshold was

set to 80 μm. PT and polished PT surface roughness also was measured by an atomic force microscopy (AFM, Nano-R^{TM} AFM, Pacific Nanotechnology, CA, USA) in the close contact mode. Data were obtained using silicon probes (Model: P-MAN-SICC-0; tip radius: 10 nm; force: 40 N/m; resonance frequency: 300 kHz; dimensions: 1.14 x 0.25 cm^2). The average surface roughness (S_a, nm) was determined using the NanoRule+ software provided by Pacific Nanotechnology. Three measurements were made on each surface per group.

X-ray photoelectron spectroscopy (XPS) measurements were performed on a Thermo K-Alpha (Thermo Fisher Scientific, Inc., MA, USA). The XPS analysis chamber was evacuated to a pressure of 10^{-9} Torr or lower before collecting XPS spectra. This system was equipped with a monochromatic Al Kα X-ray source (*hv* = 1486.6 eV photons) at a 90^o takeoff angle. XPS results were evaluated using the Thermo Advantage 4.43 software package provided by Thermo Fisher Scientific, Inc.

Cell Response

Cell responses to polyelectrolyte coated PT or SLA surfaces were performed using human osteoblast-like MG63 cells (American Type Culture Collection, Manassas, VA). Cells were plated at a density of 10,000 cells/cm^2 on either tissue culture polystyrene (TCPS) as an internal standard or titanium surfaces and cultured in Dulbecco's modification of Eagle's medium (DMEM, Cellgro®, Mediatech, Inc., Manassas, VA) supplemented with 10% fetal bovine serum (Hyclone, Waltham, MA) and 1% penicillin-streptomycin (Invitrogen, Carlsbad, CA) at 37℃, 5% CO_2, and 100% humidity. Cells were cultured until confluence was achieved on TCPS. Cell number was counted in all cultures 24h after confluence on TCPS. To collect all cells on the rough

titanium surfaces, cells were released by two sequential 10 min incubations in 0.25% trypsin-EDTA. Cells were counted using Z1 Particle Counter (Beckman Coulter, Fullerton, CA). Cellular alkaline phosphatase specific activity was measured by determining *p*-nitrophenol (pNP) release from *p*-nitrophenylphosphate (pNPP) at pH 10.2 in the cell lysate and normalized to total protein content (Macro BCA Protein Assay Kit, Pierce). Osteocalcin (OCN) levels in the conditioned media were determined by radioimmunoassay (Human Osteocalcin RIA Kit, Biomedical Technologies, Stoughton, MA). Osteoprotegerin (OPG) and vascular endothelial growth factor (VEGF) were determined by enzyme-linked immunosorbent assay (ELISA) kit (DuoSet, R&D Systems, Minneapolis, MN). Immunoassay results were normalized to total cell number.

Integrin Expression

MG63 cells were plated and cultured as described above. At confluence on TCPS, all cultures were incubated with fresh medium for 12 hours. RNA was isolated using TriZol (Invitrogen) following the manufacturer's protocol. 250 ng of RNA was reverse transcribed into cDNA (High capacity cDNA Kit, Applied Biosystems, Carlsbad, CA). The resulting cDNA was used in real-time PCR reactions with Power Sybr Green (Applied Biosystems). Levels of mRNA for integrin subunits α1, α2, α5, αv, β1 and β3 were calculated using standard curves generated from known dilutions of MG63 cells and normalized to expression of glyceraldehyde 3-phosphate dehydrogenase (GAPDH). Probes were designed using Beacon Designer Software and synthesized by Eurofins MWG Operon (Huntsville, AL). Table 3 shows primer sequences used for real-time PCR analysis of gene expression.

Statistical Analysis

Data are presented as mean ± SEM for n=6 independent cultures. Data were analyzed using a one-way analysis of variance (ANOVA) for all surfaces. If there was statistical difference, Bonferroni's modification of Student's t-test for multiple comparisons was used. $P < 0.05$ was considered significant. The presented data were one of two repeated experiments, both with comparable results.

Table 3. Primer sequences used for real-time PCR analysis of gene expression.

Gene	**Primer Sequence**		**Accession Number**
GAPDH	R	GCG AGC ACA GGA AGA AGC	NM_002046.3
	F	GCT CTC CAG AAC ATC ATC C	
ITGA1	R	TGC TTC ACC ACC TTC TTG	NM_181501.1
	F	CACTCGTAAATGCCAAGAAAAG	
ITGA2	R	TAGAACCCAACACAAAGATGC	NM_002203
	F	ACT GTT CAA GGA GGA GAC	
ITGA3	R	GTAGTGGTGAGTGAGAAGTGG	NM_002204.2
	F	GGAACAAAGACAGGCAAACG	
ITGA5	R	GGT CAA AGG CTT GTT TAG G	NM_002205
	F	ATC TGT GTG CCT GAC CTG	
ITGAV	R	AAG TTC CCT GGG TGT CTG	NM_002210.2
	F	GTTGCTACTGGCTGTTTTGG	
ITGB1	R	CTGCTCCCTTTCTTGTTCTTC	NM_002211
	F	ATT ACT CAG ATC CAA CCA C	
ITGB3	R	TCC TCC TCA TTT CAT TCA TC	NM_000212
	F	AAT GCC ACC TGC CTC AAC	

RESULTS

Polyelectrolyte Thin Films on Titanium Surfaces

SEM confirmed that polyelectrolyte thin films covered the whole PT and SLA surfaces without forming an incomplete layer (Figure 5.2). The polyelectrolyte film was stable in culture medium. No difference was observed between PT-PGA surfaces that had been immersed in full medium and the original coating surface. PT-CHI and PT-PLL surfaces had a smoother surface morphology after exposure to the full media, but no apparent differences in surface morphology was seen on the SLA-CHI and SLA-PGA surfaces. Submicron scale features of the SLA-PLL surfaces were not observed with SEM imaging.

X-ray photoelectron spectroscopy (XPS) showed that the surfaces reflected the chemical composition of the coating (Figure 5.3A, 3B). A nitrogen (N1s) peak was detected only on the polyelectrolyte-coated PT and SLA surfaces. The high resolution of N1s spectra clearly showed the presence of positively-charged amine groups (NH_3^+) at 402.95 eV, 402.35 eV, 402.49 eV, and 402.27 eV for the PT-CHI, PT-PLL, SLA-CHI, and SLA-PLL surfaces, respectively. The N1s peak detected on the PGA surface originated from the backbone of its chemical structure (Figure 5.3C, 3D). The intensity of Ti2p peak decreased on polyelectrolyte-coated PT surfaces that were immersed in full media. Moreover, Ti2p signals were not observed on polyelectrolyte-coated SLA surfaces (Figure 5.4).

Measurement of contact angles showed that PT and SLA surface wettability was significantly increased after coating with CHI, PGA, and PLL (Figure 5.5A, 5B). The PT-CHI and the PT-PGA surfaces had better wettability than PT or PT-PLL surfaces. SLA

surface wettability was enhanced by polyelectrolyte thin films to a comparable extent on all of the coated SLA surfaces. Surface roughness (Sa, µm) measured by confocal laser microscopy was not significantly altered after coating the PT and SLA surfaces with the polyelectrolytes (Figure 5.5C, 5D). PT surface roughness measured by AFM with 5 µm scan length (Sa, nm), revealed no differences in surface roughness after polyelectrolyte coating (Table 4). Because the scale of SLA roughness is beyond the range of the AFM imaging technique, its roughness could not be validated in this manner.

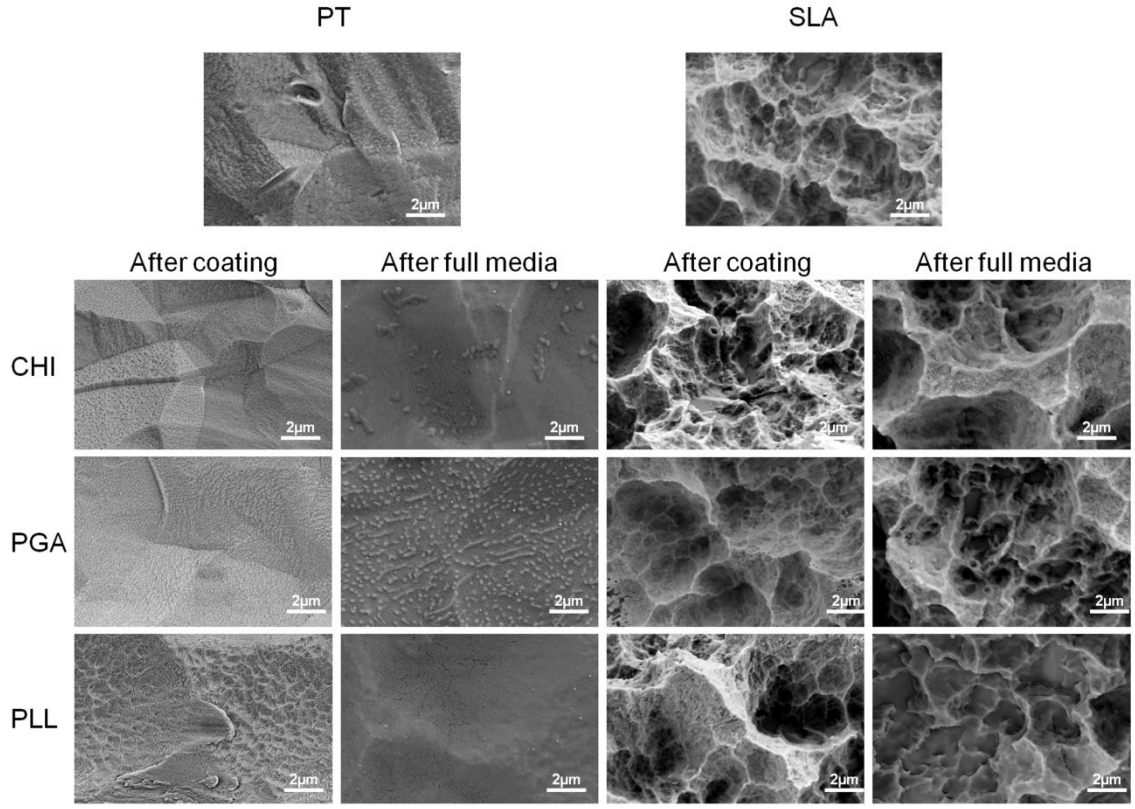

Figure 5.2. Scanning electron microscopy (SEM) images for PT and SLA surfaces before and after coating polyelectrolyte thin films: chitosan (CHI), poly(L-lysine) (PLL), and poly(L-glutamic acid) (PGA). The morphology of polyelectrolyte thin films on PT and SLA surfaces after immersion full media were examined by SEM.

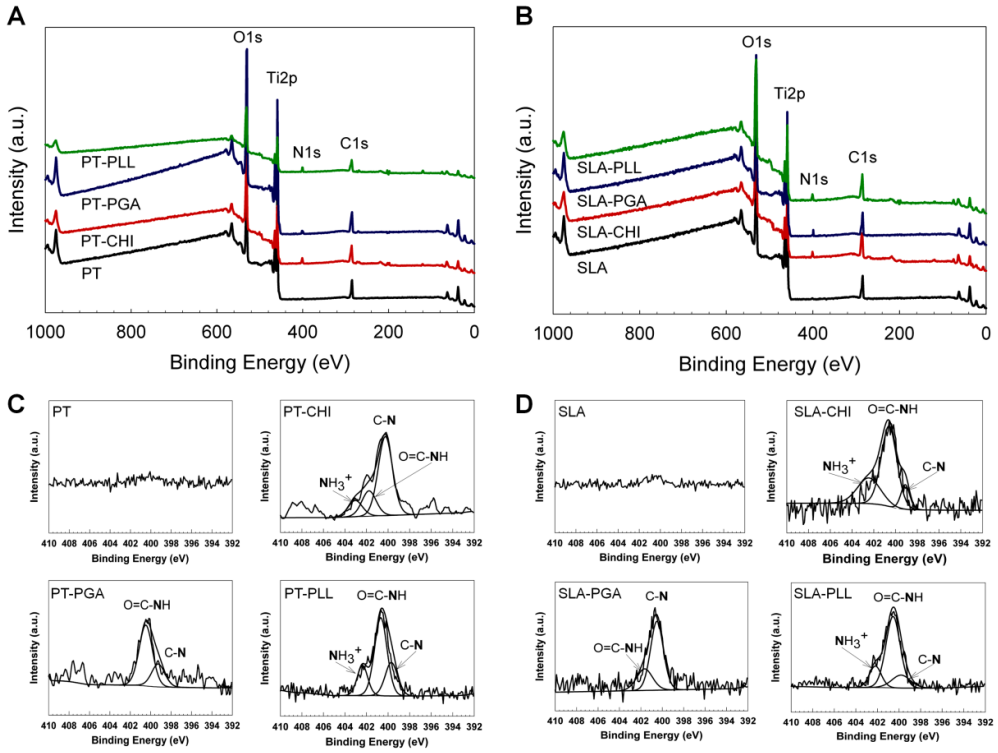

Figure 5.3. Surface chemistry of polyelectrolyte thin films on PT (A) and SLA (B) surfaces was analyzed by x-ray photoelectron spectroscopy (XPS). Nitrogen (N1s) XPS high resolution spectra were obtained from PT (C) and SLA (D) surfaces before and after coating polyelectrolyte thin films.

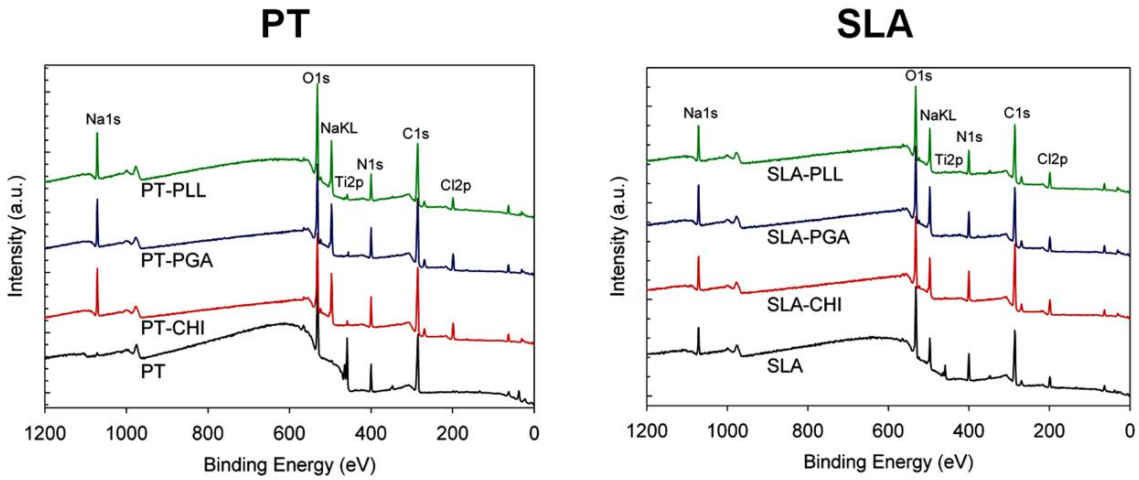

Figure 5.4. The stability of polyelectrolyte thin films coated on PT and SLA surfaces was examined by immersing the coated disks in full medium without cells at 37℃ for 3 days. Surface chemistry was characterized by using XPS.

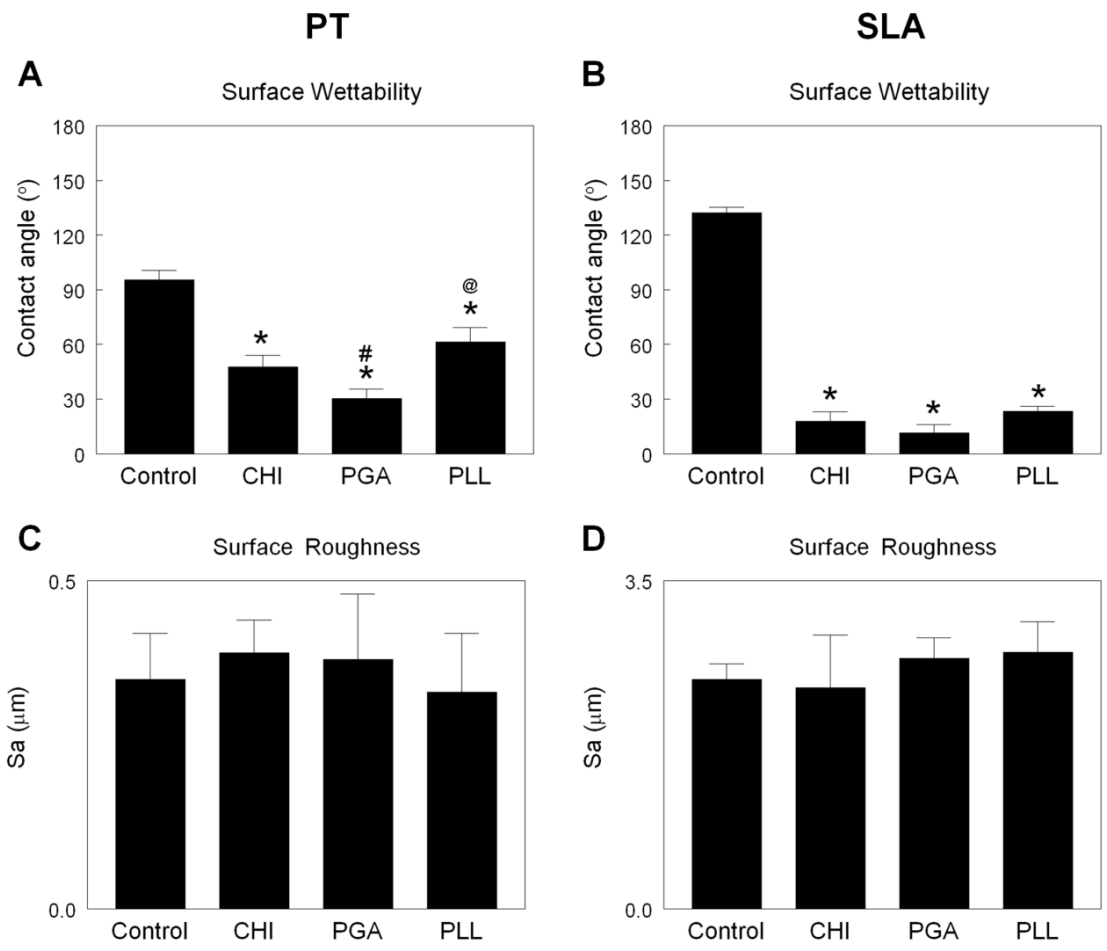

Figure 5.5. Influence polyelectrolyte thin films on surface wettability and roughness. Wettability on PT (A) and SLA (B), roughness on PT (C) and SLA (D). Data were analyzed using ANOVA and statistical significance between groups was determined using 'Bonferroni's modification of student's t-test. * $p < 0.05$ vs. control; # $p < 0.05$ vs. CHI; @ $p < 0.05$ vs. PGA.

Cellular Response of MG63 Cells to Surface Modifications

Osteoblasts were sensitive to surface wettability and roughness. Cell numbers increased on CHI, PGA, or PLL coated PT surfaces compared to the uncoated PT surfaces (Figure 5.6A). SLA-PLL surfaces had more cells than SLA-Control, SLA-CHI, and SLA-PGA surfaces (Figure 5.6B). Alkaline phosphatase specific activity, an early marker of osteogenic differentiation, was not affected by enhanced wettability with different polyelectrolytes on PT surfaces (Figure 5.6C). Cells cultured on SLA-CHI, SLA-PGA, and SLA-PLL surfaces had higher enzyme activity than cells on SLA-Control surfaces (Figure 5.6D). Osteocalcin, a late marker of osteoblast differentiation, decreased on PT surfaces coated with CHI, PGA, or PLL as compared to the PT-Control surfaces (Figure 5.6E). The highest osteocalcin production by MG63 cells was observed in response to the SLA-CHI surface (Figure 5.6F). There was no difference in osteocalcin production on the SLA-PGA and SLA-PLL surfaces compared to the SLA-Control surfaces. Enhanced wettability of the PT surface had no impact on osteoprotegerin (Figure 5.7A) and vascular endothelial growth factor (VEGF) production, except on the PT-PLL surface (Figure 5.7C). Osteoprotegerin was produced in greater amounts on the SLA-CHI and SLA-PGA surfaces compared to SLA-Control surface (Figure 5.7B). There was no difference in VEGF production levels on the SLA-CHI, SLA-PGA, and SLA-PLL as compared to SLA-Control surfaces (Figure 5.7D).

Integrin subunit expression was sensitive to surface chemistry and surface roughness. mRNAs for integrin α1 increased on the PT-CHI surface while decreasing on the PT-PGA surface, and no differences on PT-PLL compared to PT-Control surfaces (Figure 5.8A). α1 expression decreased on the SLA-CHI, SLA-PGA, and SLA-PLL

surfaces compared to SLA-Control surfaces (Figure 5.8A). Changes in mRNAs for integrin α2 on PT surfaces were similar to α1 mRNA. However, α2 expression was less sensitive to enhanced surface wettability on SLA surfaces (Figure 5.8B). Integrin αv mRNAs were higher on PT-CHI and PT-PGA surfaces than on PT-Control or PT-PLL surfaces. αv expression decreased on SLA-PGA or SLA-PLL surfaces compared with SLA-Control and SLA-CHI surfaces (Figure 5.8C). There was no difference in α5 expression on polyelectrolyte-coated PT or SLA surfaces in comparison with control surfaces (Figure 5.8D). Expression of integrin β1 and β3 was not affected surface wettability induced with polyelectrolyte thin films on PT surfaces (Figure 5.8E, 8F), but β3 expression was reduced with enhanced wettability and roughness (Figure 5.8F).

The correlation between surface properties of the polyelectrolyte thin films on structured titanium and cell response is shown in Figure 5.9. Surface contact angle data were converted to surface tension (Table 4), the PT or SLA-Control surfaces had negative surface tension values while polyelectrolyte-coated PT and SLA surface had positive values. Three dimensional plots of surface tension, roughness, and cell response showed a higher number of cells present on smooth surfaces with higher surface tension than on rough surfaces (Figure 5.9A). Similar relationships were observed for the early-stage differentiation of MG63 cells, i.e. alkaline phosphatase specific activity (Figure 5.9B). Osteocalcin (Figure 5.9C), osteoprotegerin (Figure 5.9D), and VEGF (Figure 5.9E) levels were highly regulated on surfaces with positive surface tension and rougher topography. In particular, osteocalcin production levels were enhanced on the SLA-CHI surface (blue dot).

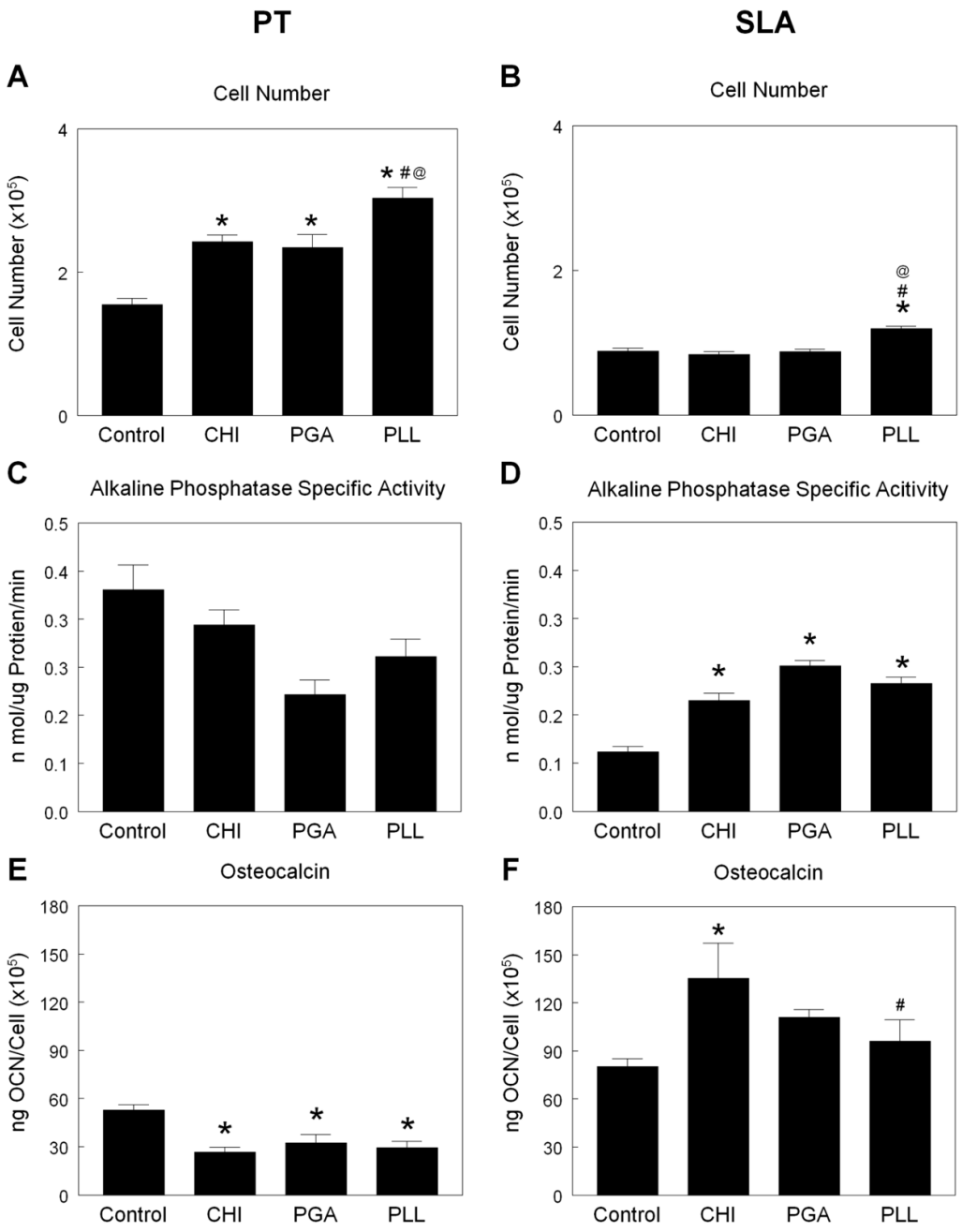

Figure 5.6. Response of MG63 cells cultured on polyelectrolyte thin films coated PT and SLA surfaces: cell number on PT (A) and SLA (B), alkaline phosphatase specific activity on PT (C) and SLA (D), and osteocalcin levels in the conditioned medium on PT (E) and SLA (F). Cell number and proteins were determined in all cultures 24 hours after confluence on tissue culture polystyrene (TCPS). The data presented are from one of two separate experiments, both with compared results. Data were analyzed using ANOVA and statistical significance between groups was determined using 'Bonferroni's modification of Student's t-test. * $p < 0.05$ vs. control; # $p < 0.05$ vs. CHI; @ $p < 0.05$ vs. PGA.

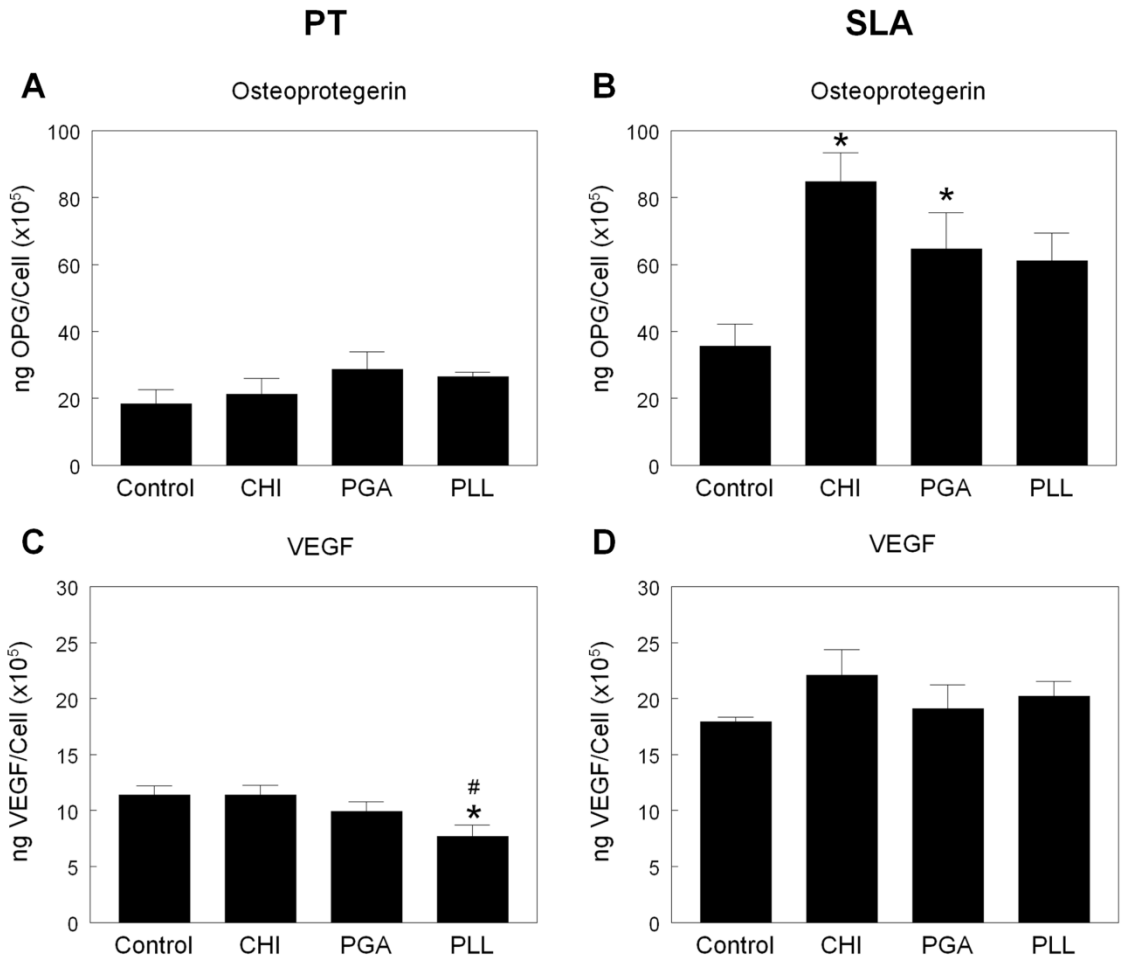

Figure 5.7. Response of MG63 cells cultured on polyelectrolyte thin films coated PT and SLA surfaces: osteoprotegerin levels on PT (A) and SLA (B) and VEGF levels on PT (C) and SLA (D) in the conditioned medium. Proteins were determined in all cultures 24 hours after confluence on tissue culture polystyrene (TCPS). Data were analyzed using ANOVA and statistical significance between groups was determined using Bonferroni's modification of Student's t-test. * $p < 0.05$ vs. control; # $p < 0.05$ vs. CHI.

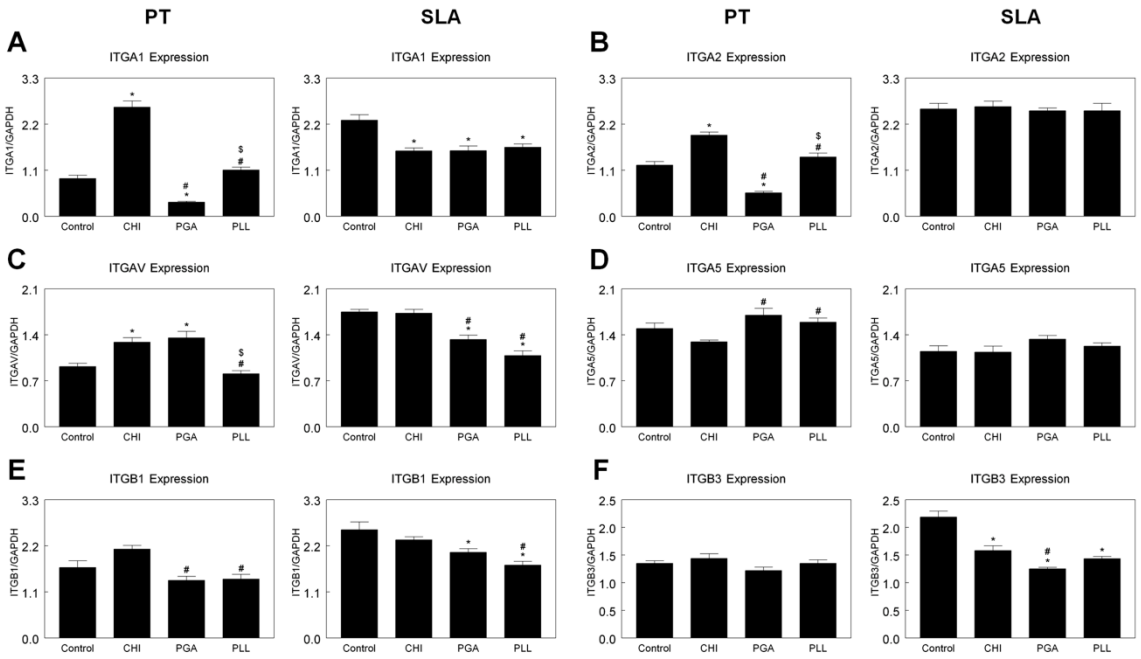

Figure 5.8. Effect of surface chemistry and roughness on integrin mRNA expression in MG63 cells were evaluated 12 hours after confluence on tissue culture polystyrene (TCPS). Cells were cultured on control PT and SLA surfaces (Cont) that were not coated with polyelectrolyte and PT and SLA surfaces that were coated with chitosan (CHI), poly(L-glutamic acid) (PGA), and poly(L-lysine) (PLL). (A) α1; (B) α2; (C) αV; (D) α5; (E) β1; and (F) β3. *, $p < 0.05$, vs. control; # $p < 0.05$ vs. CHI; $ $p < 0.05$ vs. PGA.

Table 4. Summary of surface contact angle, surface tension, and roughness on PT and SLA surfaces before and after polyelectrolyte coating. Surface tension was calculated based on the equation $E_s = E_{lv}cos\theta$, where E_{lv} = 72.8 dyne/cm at 20℃ for pure water and θ is a contact angle (171). Roughness was determined by using confocal laser microscope (CLS) and atomic force microscope (AFM) (n=6).

	Contact angle (°)	Surface tension (dyne/cm)	Roughness	
			CLM, Sa (μm)	AFM, Sa (nm)
PT-Control	95.6 ± 5.0	-7.1	0.35 ± 0.07	176.5 ± 48.0
PT-CHI*	47.7 ± 6.3	49.0	0.33 ± 0.05	169.8 ± 26.3
PT-PGA**	30.3 ± 5.2	62.9	0.39 ± 0.10	146.4 ± 16.3
PT-PLL***	61.5 ± 7.9	34.7	0.36 ± 0.09	141.0 ± 10.5
SLA-Control	132 ± 3.0	-49.0	2.45 ± 0.16	-
SLA-CHI*	17.8 ± 5.2	69.3	2.74 ± 0.56	-
SLA-PGA*	11.5 ± 4.4	71.3	2.36 ± 0.22	-
SLA-PLL*	23.3 ± 2.7	66.9	2.33 ± 0.32	-

* $p < 0.05$, vs. Ti-Control; ** $p < 0.05$, vs. Ti-CHI; *** $p < 0.05$, vs. Ti-PGA. - AFM tip detection limitation was not able to measure SLA surfaces.

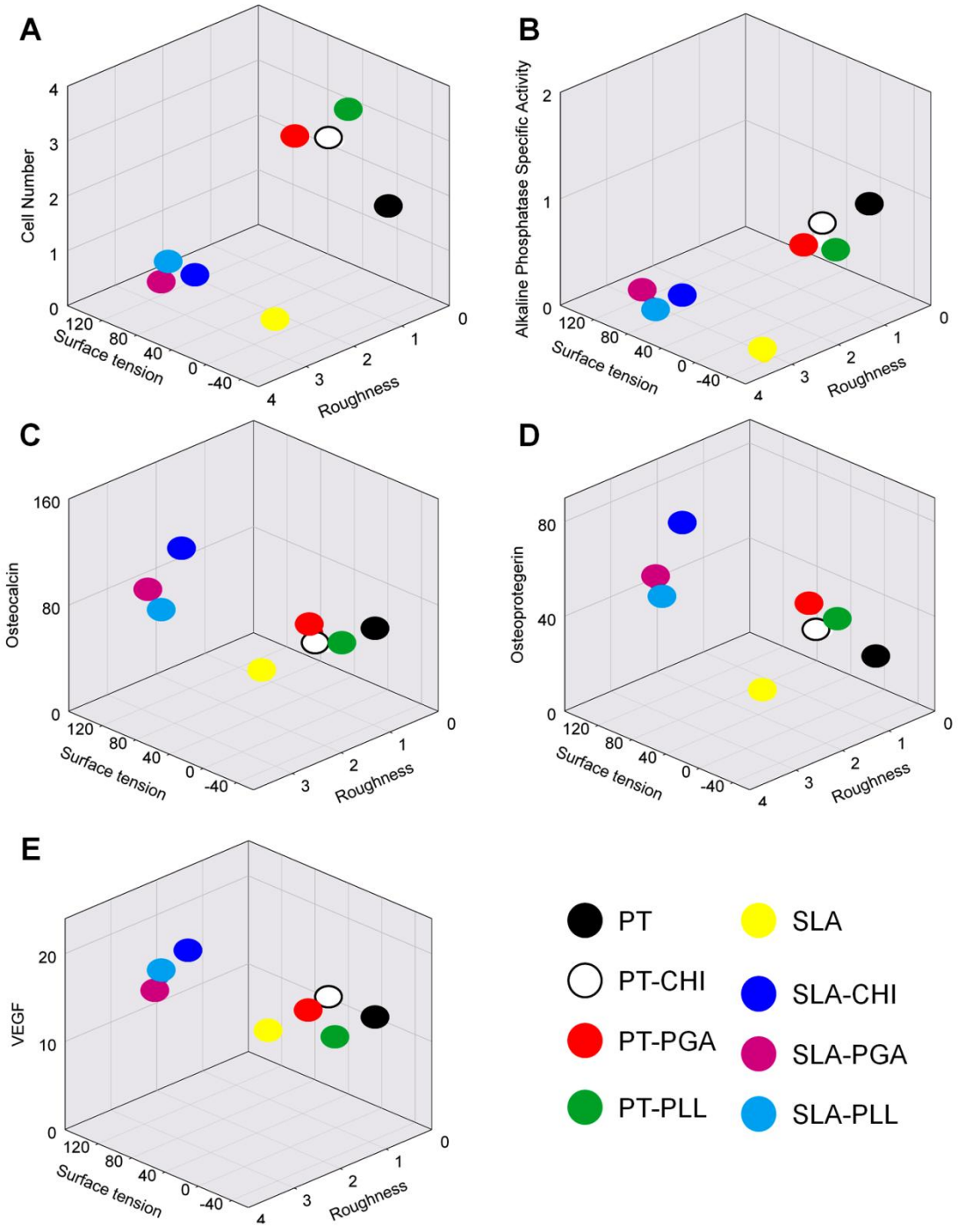

Figure 5.9. Correlation among surface properties including surface tension and roughness and cellular responses.

DISCCUSSION

Enhanced initial surface wettability plays an important role in the improvement of the early bone healing at the interface between bone and biomaterials, increasing protein adsorption, stimulating cell attachment, adhesion, and spreading (159, 163). Osteoblast maturation on surfaces with enhanced wettability having different chemistries is an important factor in engineering implant surfaces for osseointegration, but has been less studied. Our results demonstrate that surface wettability induced with different surface chemistry can regulate MG63 cell response, including early and later differentiation, local factor production levels, and integrin expression.

Surface wettability was modified by coating polyelectrolyte thin films on microstructured titanium surfaces. A number of factors influence polyelectrolyte adsorption, including concentration, ionic strength, and pH (80, 172). In this study, the adsorption conditions of polyelectrolyte chains on the substrate were optimized by adjusting pH of polyelectrolyte solutions and salt concentration. Previously we showed that PT surfaces were not fully covered with CHI and PGA with salt addition in polyelectrolyte solutions (80). However, in salt-free conditions used here, PT and SLA surfaces were completely covered with CHI, PGA, and PLL. Optimized polyelectrolyte adsorption conditions enhance PT and SLA surface wettability compared with polyelectrolyte thin films prepared with salt addition. Enhanced wettability of PT and SLA surfaces after polyelectrolyte adsorption was mainly controlled by the different surface chemistry since all polyelectrolyte-coated PT and SLA surfaces had the comparable surface roughness. Importantly, the micron-scale roughness of the surfaces was not altered by the films.

The stability of polyelectrolyte thin films is critical because delaminated film from metallic surfaces can release metal ions due to electrochemical reactions in the exposed environment (173), and may lead to implant failure. We demonstrated that the polyelectrolyte thin films were stable on the native titanium oxide layer when exposed to the cell culture environment. SEM and XPS analysis data confirmed that the integrity of the thin films was not compromised. There were changes in surface topography, however, that were polyelectrolyte specific. The smoother morphology of the PT-PLL and SLA-PLL surface after immersion in full medium may be due to swelling of the thin films in the presence of salt and ions in the culture medium (174). The intensity of the Ti2p peak detected on the polyelectrolyte-coated PT and SLA surfaces decreased with increasing Cl2p and Na1s peak intensity, possibly due to proteins that were adsorbed on the outermost polyelectrolyte-coated layers.

These results indicate that the polyelectrolyte thin films on microstructured titanium surfaces are stable and robust. Fabricating metal surfaces using polyelectrolyte thin films can provide a pH-buffering effect, thereby preventing metal ion release due to electrochemical reactions in the physiological environment, which has been hypothesized to negatively impact osteoblast differentiation and function (126, 175, 176). Furthermore, it is possible that corrosion of metal implants can be minimized with polyelectrolyte thin films.

Although surface wettability achieved with different chemistry was comparable, differences in composition and charge species of the polyelectrolyte thin films may have contributed to the differences in cell responses that were observed, since microtopography of the PT and SLA surfaces was not changed. Cell number increased on

positively charged (NH_3^+) PT-PLL and SLA-PLL rather than on negatively charged SLA-PGA. Although CHI has positively charged (NH_3^+) groups, the cell number increased only on PT. Surface wettability with different chemistry and charges on rough SLA surfaces modulated alkaline phosphatase activity, whereas the same chemistry had no effect on smooth surfaces. Osteocalcin production was decreased on more wettable smooth surfaces compared to the control PT surface, but on the rough surfaces, CHI with positive charge (NH_3^+) surface dominantly induced a greater osteocalcin and osteoprotegerin production than PGA (COO^-) and PLL (NH_3^+). Although PLL had the same charge in a CHI, the cellular response was different in a surface roughness dependent manner. Since the wettability was comparable among SLA-CHI, SLA-PGA, and SLA-PLL surfaces, it suggests that surface chemical composition of CHI, PGA, and PLL plays a role in modulating osteoblast differentiation based on osteocalcin production.

Others have shown that surface chemistry exhibiting hydroxyl (-OH) and amine (-NH_2) groups increased osteoblast differentiation markers compared with carboxyl (-COOH) and methyl (-CH_3) groups (140). These earlier observations used coated tissue culture surfaces, which differ from the titanium substrates used in the present study. Here we show that VEGF production was dominantly modulated by surface roughness. In addition, the differences in cell response between PT and SLA surfaces suggest that surface roughness is a critical factor influencing cell response as well as surface wettability and chemistry. Integrin expression is also sensitive to surface wettability as well as surface roughness. The integrin expression on smooth PT surface is regulated by

surface chemistry. In contrast, the roughness on SLA surfaces is a more critical factor to induce integrin expression.

Our results indicate that surface wettability, chemistry, and roughness are essential parameters for understanding the correlation between surface properties and cell response in order to design ideal biomaterials. By correlating surface tension, roughness, and cell responses, our findings suggest that surface roughness is the primary and surface tension is the secondary regulator of osteoblast differentiation.

CONCLUSION

In this work, we have shown enhanced wettability achieved using different surface chemistries without modifying microtopography can modulate integrin expression, cell proliferation, differentiation, and production of local factors. Wettability on smooth surfaces is important for regulating cell number while surface roughness with a specific chemistry dominantly impacts osteoblast differentiation and local factor production. Integrin expression on smooth PT surfaces is controlled by surface chemistry but on rough SLA surfaces is regulated by surface roughness. Overall, surface wettability, chemistry, charge, and roughness are connected to each other and contribute to the overall cell response.

CHPATER 6

SURFACE WETTABILITY INDUCED BY CHITOSAN NANOFILM ON MICROSTRUCTURED TITANIUM SURFACE AND UNIQUE BIOLOGY RESPONSE

INTRODUCTION

Many studies have shown that titanium surface roughness, chemistry, energy, and wettability play an important role to regulate osteoblast response through interaction between the outermost implant surfaces and bone (42, 55, 177). Osteoblasts show more differentiated phenotype on complicated micron-/submicronscale rough surfaces than on smooth titanium surfaces (8, 42). Materials with different chemistry including tissue culture polystyrene (TCPS), pure titanium, titanium alloy with oxide layer, and hydroxylapatite-coated titanium surfaces yield differential cellular responses through variations in protein adsorption and integrin expression (178-180).

Surface wettability has been recognized as an important factor to control the dynamic interaction at interfaces between an implanted surface and serums or blood in the physiological system *in vitro* and *in vivo*. (63, 181). For examples, hydrophobic surfaces support protein adsorption than hydrophilic surfaces (182). Blood plasma coagulation is slowly processed on hydrophobic surfaces whereas blood can quickly contact with hydrophilic surfaces and efficiently activate blood plasma coagulation cascade (63). Titanium surfaces with both excellent wettability and micron-/submicronscale complex roughness can synergistically enhance osseointegration through fast blood clot stabilization and shortened wound healing time (9).

Osteoblasts cannot directly interact with material surfaces, but instead interact with adsorbed extracellular matrix on materials from culture medium *in vitro* or physiological fluids *in vivo* (30). Integrins, heterodimeric transmembrane receptors with non-covalently bounded α- and β- subunits, are sensitive to the adsorbed matrix proteins, and cell surface receptors bind between extracellular matrix (ECM) and actin cytoskeleton (30, 34, 35, 183). The connection between ECM-integrin-cytoskeleton/signal protein kianses can be able to transmit the signal both inside-out and outside-in direction. So, two pathways of signal transduction can mediate cell behavior (184). Previous studies have shown that integrin expression can be regulated by surface chemistry (35) and osteoblast maturation and local factor production are dependent on specific integrin signaling (34). The straightforward conclusions about how surface wettability can regulate the interaction at the interface and modulate cellular response are still not fully addressed.

Surface wettability has been modified with several different methods including building self-assembled monolayer with different functional groups, conjugating reactive chemical species, coating polyelectrolytes, changing morphology and so on (80, 185). We previously demonstrated that enhanced surface wettability can be induced by coating different polyelectrolytes on sandblasted/acid-etched (SLA) surfaces. Chitosan coated SLA surfaces showed increased osteocalcin, a later osteoblast differentiation marker, and osteoprotegerin, a local factor produced by osteoblasts that inhibits osteoclasts differentiation (186), production levels compared to SLA surfaces with/without coating either poly(L-glutamic acid) or poly(L-lysine).

Different surface chemistry and wettability impacted on cell response at the same time. Therefore, it was not clear which properties dominantly regulate to different cell response in terms of proliferation and differentiation. Hence, this study was designed to investigate the role of surface wettability on osteoblast response. In order to achieve our object, we developed the novel method to prepare the surface wettability gradient with chitosan nanofilm due to osteocalcin production levels. Osteocalcin is the most abundant non-collagenous protein in the organic matrix of bone and dentin (26, 27) and synthesized by osteoblasts and mainly accumulated in the extracellular matrix of bone (27). Furthermore, effect of surface wettability gradient on integrin expression was examined.

MATERIALS AND METHODS

Titanium Substrate

Commercially pure titanium disks with grade 2 (Ø 15 mm x 1 mm, Institut Straumann AG, Basel, Switzerland) were used in this study. Titanium disks were treated with sandblasted/acid- etched surface (SLA, Sa = 3.1 μm). Chitosan (MW = 125,000 - 350,000 g/mol, deacetylation degree 80 - 89%, medical grade) obtained from NovaMatrix (Drammen, Norway) solution was prepared with 1.5 mg/ml dissolved in 0.1 M acetic acid (reagent grade, Sigma-Aldrich, Milwaukee, WI, USA) and filtered through a sterilized polytetrafluoroethylene (PTFE) filter (pore size 0.2 μm, Nalgene®, Rochester, NY).

Surface Preparation

In order to build the wettability gradient, SLA surfaces were treated oxygen plasma (PDC-32G, Harrick Plasma, NY, USA) for 3 minutes followed by aging in a

closed container for 0, 2, 10, or 24 hours. Chitosan nanofilms were coated on oxygen plasma treated and aged SLA surfaces by adding 500 µl of chitosan solution at room temperature for 30 minutes. After immersion, surfaces were rinsed 3 times for 10 minutes in ultrapure water. All surface preparation was performed in a sterilize hood using asceptic techniques. Unprocessed SLA surfaces were used as a control. For simplicity, modified SLA surfaces is denoted as SLA/different aged hours since this is the distinguishing factor in surface preparation steps (i.e., SLA10 represents that SLA surfaces treated by oxygen plasma and aged for 10 hours before chitosan coating). Surface preparation is depicted in Figure 6.1.

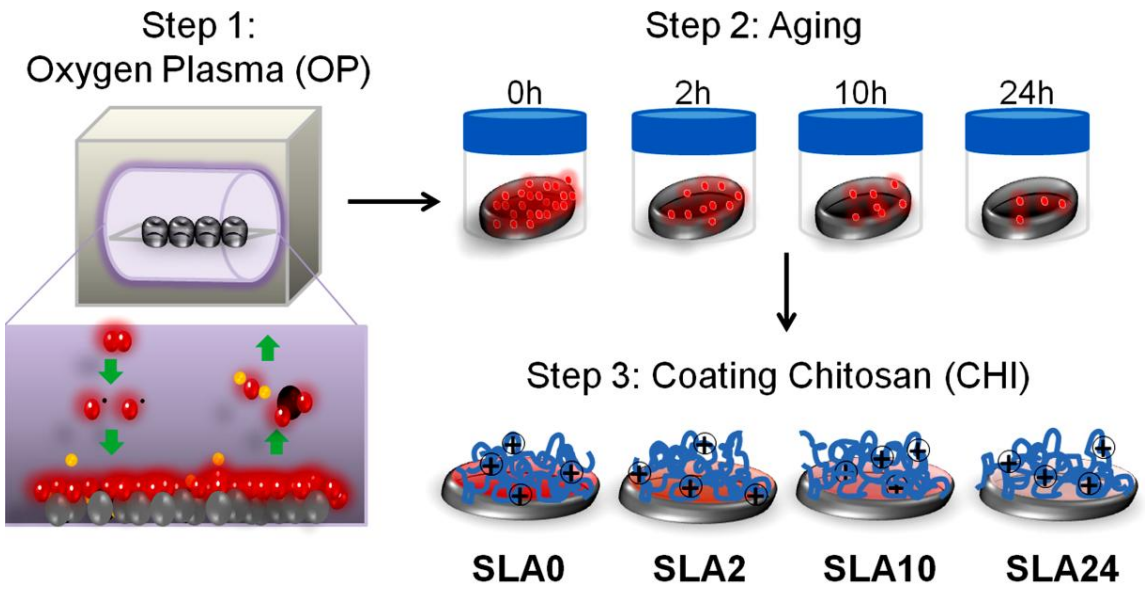

Figure 6.1. Illustration of surface modification process. Step 1: SLA surfaces were treated with oxygen plasma for 3 minutes per each side. Step 2: oxygen plasma treated SLA surfaces and stored closed container for 0, 2, 10, and 24 hours. Step 3: coating chitosan on surfaces for 30 minutes and rinse.

Surface Characterization

Wettability of modified SLA surfaces was determined by measuring contact angle with a Ramé-Hart goniometer (model 250-F1, Mountain Lakes, NJ). Consistent volumes (2 µl) of ultrapure water (18.2 MΩ·cm, Millipore Milli-Q system) were used as a droplet. Dropped liquid images were recorded and analyzed with the DROPimage CA software package (Ramé-Hart Instrument Co.). Surface roughness was measured by using a LEXT 3D Material Confocal Laser Microscope (CLM, 50X objective, Olympus America Inc., PA, USA) with threshold 100 µm. Roughness results were analyzed with the LEXT OLS4000 software provided by Olympus. The surface morphology was obtained by using an Ultra 60 field emission (FE) scanning electron microscopy (SEM, Carl Zeiss SMT Ltd., Cambridge, UK) with accelerating voltage (5kV) and gold coating with Hummer 5 Gold Sputterer (thickness ≈ 10 nm). The amount of adsorbed chitosan solution on titanium substrates was estimated by UV-Vis spectrophotometer (λnm = 230). The absorbance was normalized by 0.1 M acetic acid. Surface chemistry was analyzed by using Thermo K-Alpha X-ray photoelectron spectroscopy (XPS, Thermo Fisher Scientific Inc., MA, USA) equipped ultra high vacuum (10^{-9} Torr or lower) and with a monochromatic Al Kα X-ray source ($h\nu$ = 1486.6 eV photons) at a 90^{o} takeoff angle. The Thermo Advantage 4.43 software package (Thermo Fisher Scientific, Inc) was used to evaluate XPS spectrum results. Three random spots per three different specimens were used to characterize contact angle, CLM, and XPS.

Cell Response

Cell responses on wettability gradient surfaces were performed using human osteoblast-like MG63 cells (American Type Culture Collection, Manassas, VA). Cells

were plated either tissue culture polystyrene (TCPS) or OP treated SLA followed by coating CHI thin film surfaces at a density of 10,000 cells/cm^2. TCPS surfaces were used as an internal standard. Dulbecco's Modification of Eagle's Medium (Cellgro®, Mediatech Inc., Manassas, VA) supplemented with 10% fetal bovine serum (Hyclone, Waltham, MA) and 1% penicillin-streptomycin (Invitrogen, Carlsbad, CA) at 37℃, 5% CO_2, and 100% humidity. Cells were grown until cultures reached confluence achieved on TCPS. Cell number was counted in all cultures 24 hours after confluence on TCPS. To collect all cells on the rough titanium surfaces, cells were released by two sequential 10 min incubations in 0.25% trypsin-EDTA. Cells were counted using Z1 Particle Counter (Beckman Coulter, Fullerton, CA) and cell number used to normalized immunoassay results. Cellular alkaline phosphatase specific activity measured by determining *p*-nitrophenol (pNP) release from *p*-nitrophenylphosphate (pNPP) at pH 10.2 in the cell lysate and normalized to total protein content (Macro BCA Protein Assay Kit, Pierce). Osteocalcin levels in the conditioned media were determined by radioimmunoassay (Human Osteocalcin RIA Kit, Biomedical Technologies, Stoughton, MA). Osteoprotegerin and vascular endothelial growth factor (VEGF) were determined by enzyme-linked immunosorbent assay (ELISA) kit (DuoSet, R&D System, Minneapolis, MN).

Integrin Expression

MG63 cells were plated on TCPS, SLA, or chitosan-modified SLA surfaces and cultured as described above. At confluence, cultures were incubated with fresh media for 12 hours. RNA was isolated using TriZol (Invitrogen) following manufacturer's protocol. 500 ng of RNA was reverse transcribed into cDNA (High Capacity cDNA Kit, Applied

Biosystems, Carlsbad, CA). The resulting cDNA was used in real-time PCR reactions with Power Sybr Creen (Applied Biosystems). Starting mRNA quantities of integrin subunits α1, α2, α5, α3, β1 and β3 were calculated using standard curves generated from known dilutions of MG63 cells and normalized to expression of glyceraldehyde 3-phosphate dehydrogenase (GAPDH). Gene specific primers (Table 3) were designed using Beacon Designer Software and synthesized by Eurofins MWG Operon (Huntsville, AL).

Statistical Analysis

Presented cellular response data in this study was from one of two replicated experiments with 6 individual cultures per variable. Data were analyzed using a one-way analysis of variance (ANOVA) for all surfaces. If there was statistical difference, Student's t-test for multiple comparisons using Bonferroni's modification was used. $P < 0.05$ was considered significant. One of repeated experiments was presented.

RESULTS

Surface Wettability Gradient Characterization

Contact angle was gradually increased on oxygen plasma treated SLA surface, an effect dependent on aging time (Table 5). Oxygen plasma treated SLA surface followed 24 hours aging exhibits less water wettable among other surfaces. Shifted surface wettability gradient was obtained after chitosan coating (Table 5 & Figure 6.2A). SLA24 surfaces showed the most water wettable surface after coating chitosan nanofilms. The micron-scale surface roughness (Sa, μm) measured by CLM was not modified by coating (Figure 6.2B). The morphology of chitosan nanofilm foamed on SLA surfaces including

SLA0, SLA2, SLA10, and SLA24 was confirmed by SEM images (Figure 2C). The surfaces were fully covered without adding micron scale features.

Titanium (Ti), oxygen (O), and carbon (C) were primarily detected on all surfaces by XPS (Table 5). O and C concentration on oxygen plasma treated and aged SLA surfaces were sensitive to the aged hours (Table 5). Detected nitrogen (N) peak on chitosan nanofilm coated SLA surfaces confirmed the adsorption of chitosan (Table 5). The high resolution of N spectra showed a gradient of positively-charged amine groups (NH_3^+) on SLA0, SLA2, SLA10, and SLA24, respectively (Figure 6.2D). To quantify the adsorbed chitosan on SLA surfaces, the chitosan solution was collected after coating, and measured UV absorbance at λ_{max} = 230 nm (Table 5). The intensity of UV absorbance decreased on SLA0, SLA2, SLA10, and SLA24, respectively. The thickness of chitosan nanofilms was measured by obtaining N concentration as a depth dependence manner by sputtering Ar^+ ions (etching rate 0.017 nm/s) (Figure 6.2F). SLA0 (7.14 nm) surfaces showed thicker coatings than SLA2 (6.12 nm), SLA10 (5.10 nm), and SLA24 (6.46 nm) surfaces (Figure 6.2F).

Table 5. Surface chemical composition (%) of SLA, oxygen plasma treated SLA surfaces, and chitosan nanofilm coated on oxygen plasma treated SLA surfaces was obtained by XPS. Contact angle were measured with ultrapure water, and the amount of adsorbed chitosan on oxygen plasma treated SLA surfaces was calculated by using UV absorbance.

	Chemical Composition (%)				Contact Angle (degree)	Chitosan Adsorption (%)***
	Ti2p	O1s	C1s	N1s	Ultrapure water	
SLA	20.1 ± 0.1	52.9 ± 0.4	27.1 ± 0.5		130 ± 3.3	0
*SLA/OP/0h	24.3 ± 0.2	65.9 ± 0.4	9.8 ± 0.5		24.0 ± 2.3	n/a
*SLA/OP/2h	23.9 ± 0.1	63.8 ± 0.3	12.3 ± 0.3		35.0 ± 1.1	n/a
*SLA/OP/10h	21.5 ± 0.1	60.1 ± 0.4	18.4 ± 0.4		49.0 ± 1.2	n/a
*SLA/OP/24h	20.6 ± 0.4	58.8 ± 0.2	20.6 ± 0.5		59.0 ± 0.5	n/a
**SLA0	10.2 ± 4.4	52.5 ± 1.1	32.7 ± 3.1	4.9 ± 1.1	81.0 ± 8.3	25 ± 0.6
**SLA2	9.4 ± 1.5	43.9 ± 0.9	42.0 ± 2.0	4.7 ± 0.5	65.0 ± 7.4	20 ± 0.7
**SLA10	11.4 ± 1.1	43.8 ± 2.4	40.8 ± 3.6	4.1 ± 0.7	27.0 ± 2.8	18 ± 0.7
**SLA24	12.3 ± 5.4	47.5 ± 5.3	35.5 ± 2.4	4.2 ± 1.1	15.0 ± 1.1	19 ± 0.7

(mean ± sem, n=2)

*SLA/OP/2h: SLA surfaces was treated with oxygen plasma and aged for 2 hours.

**SLA2: SLA surfaces was treated with oxygen plasma and aged for 2 hours followed by coating chitosan

***UV adsorbance (λnm = 230) was measured for collected chitosan solution after coating on SLA surfaces.

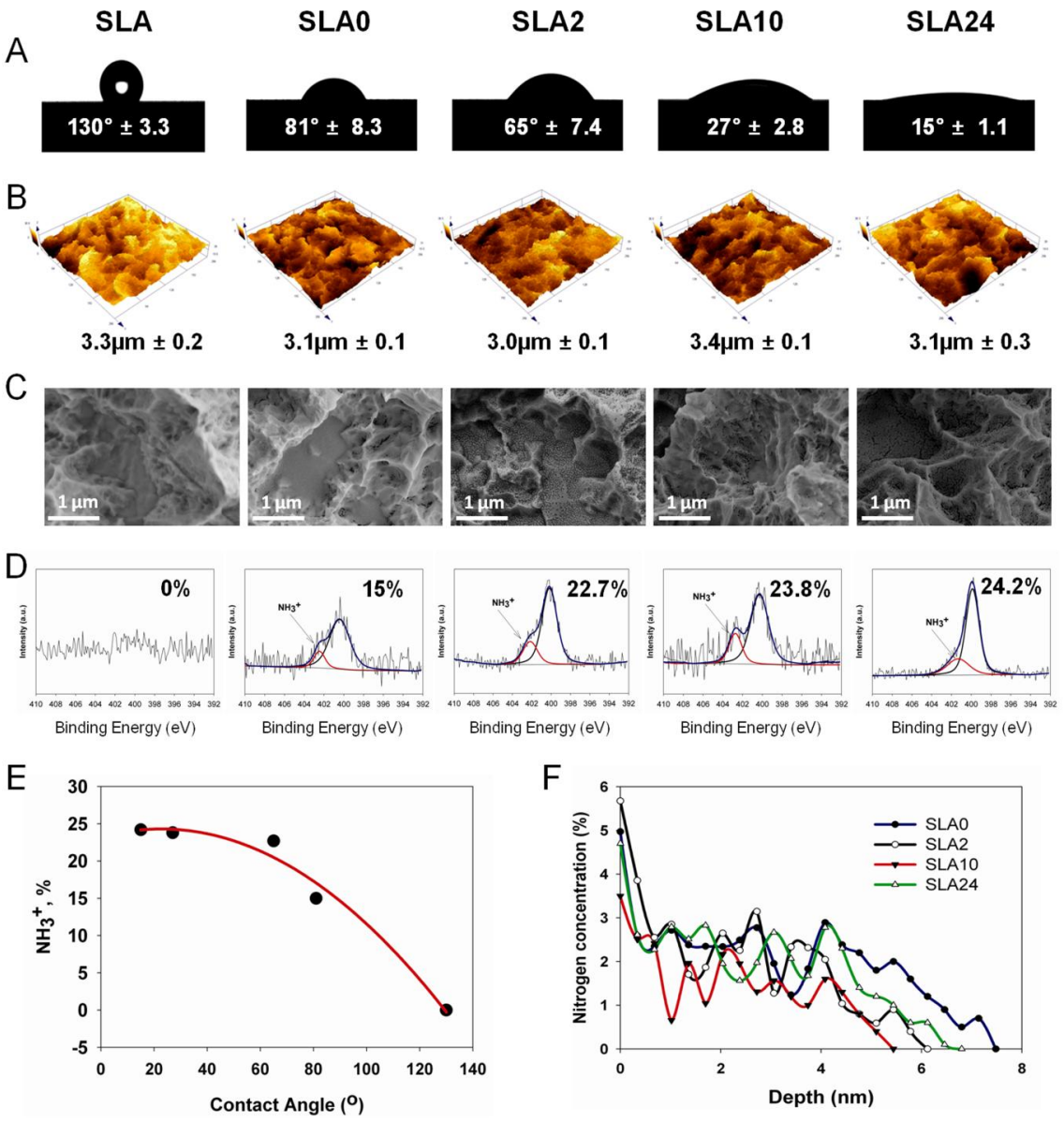

Figure 6.2. Surface wettability measured by contact angel (A), roughness determined with confocal laser microscopy (B), surface morphology SEM images (C), and high-resolution X-ray photoelectron spectra (XPS) of nitrogen (N1s) spectra (D) on surfaces before and after coating chitosan nanofilm on oxygen plasma treated SLA surfaces. The co-relation between changing contact angle and charge density variation on SLA surfaces treated with oxygen plasma and then coated chitosan polyelectrolyte (E). The depth profile of chitosan thin film was characterized by XPS (F).

Cell Response

Osteoblast response was sensitive to surface wettability gradient. Cell number decreased on SLA0, SLA2, SLA10, and SLA24 surfaces compared to SLA surfaces (Figure 6.3A). SLA0, SLA2, and SLA10 showed decreased cell numbers as surface wettability dependent manner. The most wettable surface, SLA24, had more cells than SLA and SLA10 (Figure 6.3A). Cells cultured on SLA0, SLA2, SLA10 and SLA24 surfaces had no significant difference in alkaline phosphatase specific activity, an early marker of osteogenic differentiation, compared to SLA surfaces (Figure 6.3B). Enzyme activity was not affected by gradient wettability with a specific chemistry on SLA surfaces. Osteocalcin, a late marker of osteoblast differentiation, gradually increased on SLA0, SLA2, and SLA10 surfaces as compared to SLA surfaces. The highest osteocalcin production by osteoblasts was observed in response to the SLA10 surfaces (Figure 6.3C). There was no difference in osteocalcin level on SLA24 surfaces compared to the SLA surfaces. Osteocalcin levels were lower on the most water wettable surface, SLA24, than SLA2 and SLA10 surfaces. SLA surface wettability gradient showed impact on osteoprotegerin production levels (Figure 6.3D). Osteoprotegerin was produced in higher amount on SLA0, SLA2, and SLA10 as increased wettability except SLA24 surfaces compared to SLA surfaces. The production of VEGF was not affected by different surface wettability.

Integrin expression was also sensitive to surface wettability gradient. mRNAs for integrin α1 and α2 decreased on wettability gradient dependent manner (Figure 6.4A, 4B). However, α3 expression was not changed on SLA and modified SLA surfaces (Figure 6.4C). mRNAs for integrin α5 increased on SLA0, SLA2, SLA10, and SLA24,

respectively (Figure 6.4E). The expression of integrin β1 in cells decreased on modified SLA surfaces in comparison with SLA surfaces (Figure 4E). While cells on all substrates had similar expression of integrin β3 on modified SLA surfaces (Figure 6.4F).

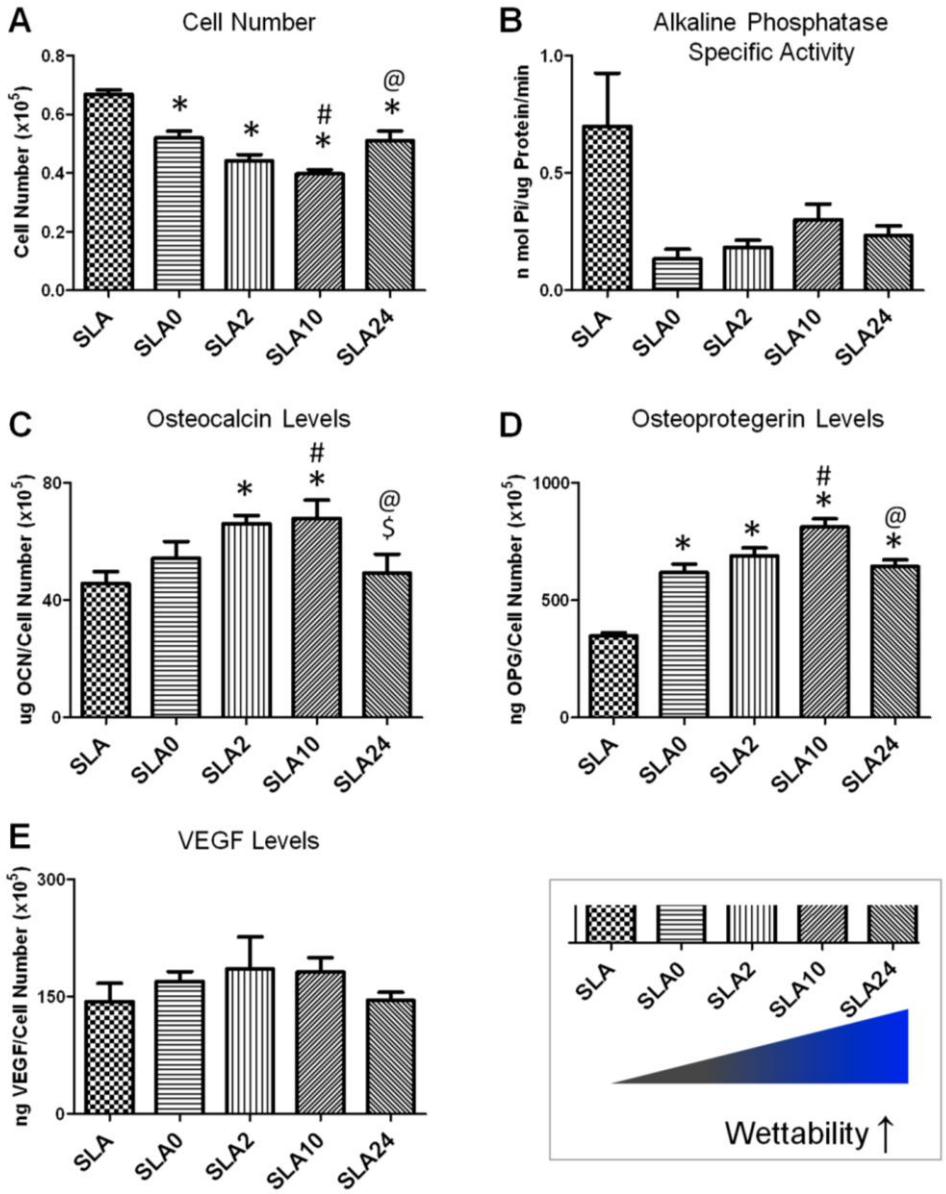

Figure 6.3 Effect of the surface wettability gradient on MG63 cell response. MG63 cells were cultured on tissue culture polystyrene (TCPS), modified SLA surfaces and grown to confluence. Cell number and proteins were determined in all cultures 24 hours after confluence on TCPS, cell number (A), alkaline phosphatase specific activity (B), osteocalcin production levels (C), osteoprotegerin production levels (D), and VEGF (E) were determined. *, $p<0.05$ vs. SLA; #, $p<0.05$ vs. SLA0; $, $p<0.05$, vs. SLA2; @, $p<0.05$, vs. SLA10.

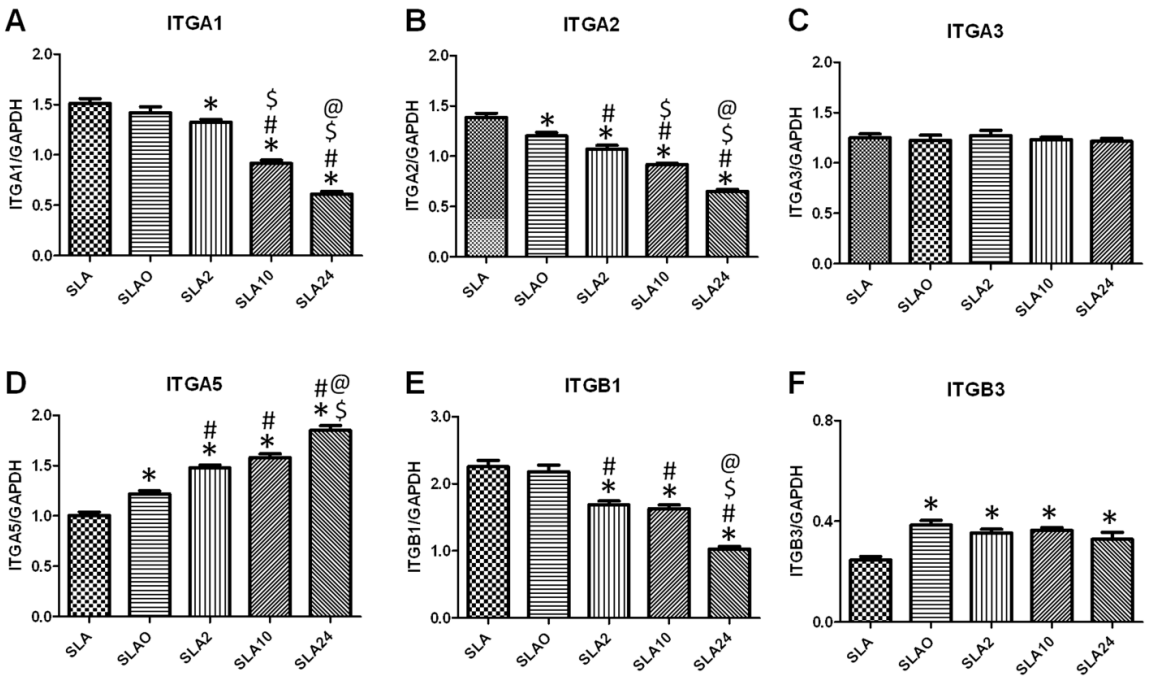

Figure 6.4. Effect of the surface wettability gradient on integrin mRNA expression in MG63 cells were evaluated 12 hours after confluence on tissue culture polystyrene (TCPS), modified SLA surfaces. (A) α1. (B) α2. (C) α3. (D) α5. (E) β1. (F) β3. *, $p < 0.05$ vs. SLA; # $p < 0.05$ vs. SLA0; $ $p < 0.05$ vs. SLA2; @ $p < 0.05$ vs. SLA10.

DISCUSSION

Surface wettability plays an important role in the improvement of the early bone healing through protein adsorption, blood clot, cell attachment, and adhesion (9, 63). There is evidence to support that surface wettability can impact to osteoblast cellular response, but the mechanism is still not clear (187). The major contribution of wettability is at the initial interaction level, which happens within a few seconds. Therefore, the analysis resolution is quite limited. Moreover, the preparation of different wettability under controlled surface chemistry is technical challenge (80, 188, 189). The model designed in this study may contribute to clarify how surface wettability can regulate not only osteoblast response but also integrin expression.

The developed novel surface modification successfully controlled surface wettability without altering micronscale roughness. Surface preparation consists of three steps: treating oxygen plasma on SLA surfaces followed by aging, and coating chitosan nanofilm. Oxygen plasma treatment has been widely used to clean, sterilize, and modify surface energy (40, 190). In this study, oxygen plasma was used for impregnating reactive oxygen on SLA surfaces with removing carbon from surfaces. Highly reactive oxygen species generated by oxygen plasma are not stable, in order to lower the energy levels, reactive oxygen can easily bind to other molecules (40, 190, 191). Induced oxygen density gradient after ageing can explain that freely dangled unstable oxygen on the outer most surface layer dissipates or binds other molecules from atmosphere which confirmed by XPS and contact angle measurement: decreasing oxygen with increasing carbon concentration as time dependent manner. After coating chitosan nanofilm on SLA surface with oxygen density gradient, the wettability was oppositely shifted. Shifted wettability

before and after coating can be explained with adsorbed chitosan chain conformations on surfaces. Chitosan, polysaccharides, consisted with both β-1,4-glucosamine (positive charge) and N-acetyl glucosamine and the degree of deacetylation 80 ~ 89 % was used in this study (80). In solutions, linear polysaccharides can typically have random coil conformation characterized by disordered conformation with continued fluctuations of local conformation (192). Adsorbed polymer chain on surfaces can have loop, tail, and train confirmations depending on the mode of adsorption, complex architectures of polymer chain, substrate topography, and the difference entropy between polymer chains and surfaces (193-196). In that sense, positively charged chitosan chains can absorb on surfaces in a different way with oxygen density gradient. Oxygen charge density decreased with increasing aged hours, SLA0, SLA2, SLA10, and SLA24, respectively. For SLA0 surfaces characterized as the highest oxygen density on surfaces, positively charged chitosan chains can be adsorbed non-specifically followed by increasing anchoring points, and then foaming densely packed conformation. Less oxygen density can induce charged chitosan chains can be more selectively anchored on SLA2, SLA10, and SLA24 than on SLA0 surfaces. It impacts the mobility of chitosan chains. The electrostatic force is the main driving source between positively charged chitosan chains and reactive oxygen species (79). When the charge density of either chitosan or active surfaces is low, the electrostatic forces are reduced. Therefore, positively charged chitosan chains adsorb with a high number of loops and tails (194, 197). The thickness of chitosan nanofilm was less than 10 nm (around 5 ~ 7 nm), and medium molecular weight of chitosan used in this study is long enough to have the number of segments (193, 194). Consequently, the adsorbed chitosan chains can have loop or tail confirmations. In

addition, the relationship between the charge density from XPS high resolution data and contact angle on surfaces suggested that N-acetyl glucosamine and β-1,4-glucosamine may have different distribution on the surfaces. Later this difference can contribute to induce different surface wettability.

MG63 cell response was sensitive to surface wettability. Cell number decreased while osteocalcin levels and osteoprotegerin as a inhibiting the differentiation of osteoclast increased with increasing surface wettability. Previous studies have shown that osteoblasts are more differentiated on microstructured implant surfaces modified to have excellent wettability than on same roughness with poor wettability (4). Interestingly, osteoblast cell number, differentiation, and local factor production were not impacted on the most water wettable surface (SLA24). Different cellular response can be explained with nanoscale loops or tails induced by chitsoan chain confirmation and imbalanced forces generated by charge density distribution. Imposed nanoscale features can influence the protein adsorption and affect integrin expression, followed by different cellular response. In addition, the differently arranged positively chitosan chains may cause to generate the different degree of interacting water molecules (63). The reason is not clear why osteoblasts response on the most water wettable surface (SLA24) shows differently instead of following wettability gradient dependent manner like integrin expression. It can be explained that cells recognize SLA10 surface conditions as optimized for fully differentiable and thus readily producing key functional proteins characteristic of mature osteoblasts.

Integrin expression is sensitive to surface wettability gradient on rough surfaces. The results of this study show that mRNA levels for integrin subunits α1, α2, and β1

decreased while increasing expression of integrin α5 with positively correlated increased wettability comparing to SLA surfaces. In contrast, there was no effect on integrin expression of α3 and β3 on SLA, SLA0, SLA2, SLA10, and SLA24 surfaces. It has been demonstrated that primary human osteoblasts can exhibit differential integrin expression profiles depending on substrates grown cells. For example, integrin expression of α3, α5, and β1 subunits are major receptors on extracellular matrix-coated TCPS compared to titanium and cobalt-chrome surfaces (198). Interestingly, previous studies showed that expression of integrin α2 and β1 increases when osteoblasts are grown on microstructured surfaces (199). Since micronscale surface roughness was not modified after coating chitosan nanofilms, the results indicate that surface wettability regulates integrin expression in a differential integrin expression profiles.

CONCLUSIONS

This study has shown that surface wettability gradient was successfully developed with identical chemistry without altering microstructure of SLA surfaces. Osteoblast differentiation is mediated by the surface wettability dependent manner which decreased cell number with increased osteocalcin and osteoprotegerin on SLA0, SLA2, and SLA10 surfaces. However, the most water wettable surface, SLA24, contributes to cell response in a different way comparing to less water wettable surfaces. Gradually increased wettability directly impacts to integrin expression as well as surface roughness.

CHAPTER 7

CONCLUSIONS AND FUTURE WORK

The presented results in this thesis show the important role that biomaterial properties have in regulating the osteoblast response *in vitro*. Specifically, the thesis presented herein demonstrates that titanium surface wettability and topography can affect not only osteoblastic differentiation of cells but also integrin expression. Further, this study has demonstrated that by controlling surface wettability with a specific chemistry without changing surface roughness, osteoblast maturation is sensitive to a certain range of surface wettability. Although these studies have provided insight into the role that biomaterial chemistry may have in regulating osteoblast differentiation, there are still several questions to be answered regarding the mechanism by which this process occurs. We must achieve a greater understanding of how biomaterial surface properties modulate host cellular and tissue response to allow for implant design that can enhance osseointegration, extend implant lifetimes, and increase implant success rates.

Role of Cleaning and Sterilization

The results presented in Chapter 3 of this thesis show that both cleaning and sterilization for used titanium implants directly impacts the surface properties and mediate osteoblast proliferation, differentiation, and local factor production differently compared to unused new surfaces. Surface roughness is stable with the cleaning process. However, the combination of cleaning followed by sterilization can result in altered roughness, as well as chemistry. Autoclave sterilization deposited carbon-rich matter on the surface, increasing hydrophobicity, whereas oxygen plasma sterilized surfaces

showed increased hydrophilicity and roughness due to the concurrent superficial material removal during plasma sterilization. Observed different cellular response indicates that MG63 cells, a line derived from an osteosarcoma, are capable of recognizing changes in surface wettability and roughness that are due to the secondary cleaning and sterilization procedures performed on contaminated surfaces. Among the several sterilization methods used in this study, gamma irradiation is quite effective in terms of relative consistence of surface roughness and wettability, followed by cellular response.

This study investigated development of cleaning procedures and sterilization methods, including autoclave, oxygen plasma, ultraviolet, and gamma irradiation. These cleaning and sterilization methods can minimize the risk for infection associated with invasive and noninvasive medical devices with proper use. However, original implant properties cannot be reproduced. Therefore, this study indicates that cleaned and sterilized contaminated titanium disks cannot be considered equivalent to unused status. Because *in vivo* and clinical studies need to be performed before making conclusions about performance, the re-use of titanium implants after re-sterilization may not be an option if the same clinical responses are achieved using unused titanium implants.

Role of Surface Chemistry and Wettability

Surface chemistry is the most sensitive property to influence other properties. Many studies have demonstrated the role of surface chemistry on the adsorption of proteins and cell attachment and adhesion. A well-known key factor to modulate osteoblast differentiation is surface roughness. However, the effect of surface wettability, and not just roughness, governed by surface chemistry on osteoblast maturation and

integrin expression has been less studied. Therefore, we developed a model to study the role of surface wettability on osteoblast response.

In order to modify surface wettability of PT and SLA surfaces, the substrates were coated with three polyelectrolytes including: chitosan (positively charged, CHI), poly(L-lysine) (positively charged, PLL), and poly(L-glutamic acid) (negatively charged, PGA). In both air and aqueous environments, titanium has oxide layers formed on top of the titanium surface and has different charges based on pH. For that reason, coating polyelectrolytes on differently charged titanium oxide layers is a practical way to modify surface wettability. In addition, charged polymer chains can absorb on surfaces with less geometrical restriction. Enhanced surface wettability without modifying the surface roughness of the substrates was confirmed by intensive surface characterization. The results show that this model successfully decouples the effects of roughness and chemistry from surface wettability. Therefore, surface chemistry is the dominant parameter governing surface properties, with the underlying microtexture playing only a secondary role in terms of modifying surface wettability. Interestingly, surface wettability achieved with different chemistry was comparable although the SLA substrate sustaining a more pronounced enhanced wettability than PT surfaces. Differences in composition and charge of the polyelectrolyte thin films may have contributed to the differences in cell responses that were observed.

Surface wettability with different chemistry and charges on rough SLA surfaces modulated alkaline phosphatase activity, osteocalcin, osteoprotegerin, and VEGF; whereas, the same chemistry had no effect on smooth surfaces. Although PLL had the same charge as CHI, the cellular response was observed to be different in a surface

roughness dependent manner. The wettability was comparable among SLA-CHI, SLA-PGA, and SLA-PLL surfaces, which suggests that surface chemical composition of CHI, PGA, and PLL plays a role in modulating osteoblast differentiation when it comes to osteocalcin production.

Cellular proliferation and differentiation are controlled by a cascade of intercellular signaling pathways mediated by integrin receptor complexes. The results show that integrin expression is sensitive to surface wettability as well as surface roughness. The integrin expression on smooth PT surface is regulated by surface chemistry. In contrast, the roughness on SLA surfaces is a more critical factor to induce specific integrin expression.

Since surface chemistry and wettability impacted cellular response at the same time, it is not clear which property can dominantly regulate different cell responses in terms of proliferation and differentiation. Hence, a novel method was developed for preparation of the surface wettability gradient with positively charged CHI on microstructured titanium surface. Surface characterization results indicate that complicated micronscale surface had a wettability gradient with identical chemistry without altering roughness. Detailed procedures can be found in Chapter 6. The results demonstrate that cellular response is modulated by surface wettability in a gradient dependent manner. Surprisingly, osteoblast cell number, differentiation, and local factor production were not impacted on the most water wettable surface. Previous studies have shown that more bone formation is found around modSLA characterized with microtextured implant surfaces modified to have high surface energy than around SLA implants with the same topography but with a more hydrophobic surface. In addition,

osteoblasts are more differentiated when grown on modSLA than on SLA exhibiting increases in prostaglandin E_2, TGF-β1, and osteoprotegerin content of the conditioned media (35, 62). The reason is not clear why osteoblasts response on the most water wettable surface (SLA24) does not follow a wettability gradient dependent manner like integrin expression does. Integrin α1, α2, and β1 expression decreased while increasing expression of integrin α5 was positively correlated increased with wettability. In contrast, there was no effect on integrin expression of α3 and β3 on SLA, SLA0, SLA2, SLA10, and SLA24 surfaces. The results indicate that cells may recognize SLA10 surface conditions as optimized for fully differentiable; thus, readily producing key functional proteins characteristic of mature osteoblasts through binding of different integrin expression profiles depending on substrates used to grow cells.

Future Work

In this dissertation, we demonstrated that surface chemical composition, charge, and wettability regulated osteoblast maturation. On wettability gradient surfaces, osteoblasts secrete more differentiation markers and produce an osteogenic microenvironment. However, similar results were not obtained on the most wettable surfaces. Definitely, more studies should be performed to further understand the mechanism.

Osteoblasts are not the first and only cells when the implants are introduced in physiological systems. Hematomas form around the surface of implants and inflammatory cells are recruited to the insertion site. Consequently, stem cells and osteoprogenitor cells are attracted to the surfaces and differentiate into osteoblasts. Therefore, further studies of the effects of surface wettability on stem cell differentiation

will allow us to gain a better understanding and help correlate *in vitro* and *in vivo* bone responses. In order to better understand how surface properties can directly or indirectly regulate cellular response, an *in vivo* study has to be followed by an *in vitro* study.

Integrins play an important role in transferring the surface structure signal to cell response through binding of these cell membrane receptors to extracellular matrix proteins. Previous studies in our lab have shown that integrin α2 and β1 modulate osteoblast differentiation on rough surfaces, and inhibition of either integrin α2 or β1 expression can block cell responses to surface topography. The results in this dissertation show that α1, α2, and β1 decreased with increasing surface wettability while α5 increased with a surface wettability dependent manner on rough surfaces. To confirm the role of surface wettability on integrin α2 and β1 expression, more studies are being performed to examine the protein expression of either α2 or β1 silenced cells.

REFERENCES

1. Mavrogenis AF, Dimitriou R, Parvizi J, Babis GC. Biology of implant osseointegration. Journal of Musculoskeletal & Neuronal Interactions. 2009;9(2):61-71.

2. Declercq H, Van den Vreken N, De Maeyer E, Verbeeck R, Schacht E, De Ridder L, et al. Isolation, proliferation and differentiation of osteoblastic cells to study cell/biomaterial interactions: comparison of different isolation techniques and source. Biomaterials. 2004;25(5):757-68.

3. Kieswetter K, Schwartz Z, Hummert TW, Cochran DL, Simpson J, Dean DD, et al. Surface roughness modulates the local production of growth factors and cytokines by osteoblast-like MG-63 cells. Journal of Biomedical Materials Research. 1996;32(1):55-63.

4. Zhao G, Raines AL, Wieland M, Schwartz Z, Boyan BD. Requirement for both micron- and submicron scale structure for synergistic responses of osteoblasts to substrate surface energy and topography. Biomaterials. 2007;28(18):2821-9.

5. Bowers KT, Keller JC, Randolph BA, Wick DG, Michaels CM. Optimization of surface micromorphology for enhanced osteoblast responses in vitro. Int J Oral Maxillofac Implants. 1992;7(3):302-10.

6. Keller JC, Schneider GB, Stanford CM, Kellogg B. Effects of implant microtopography on osteoblast cell attachment. Implant Dent. 2003;12(2):175-81.

7. Boyan BD, Lossdoerfer S, Wang L, Zhao G, Lohmann CH, Cochran DL, et al. Osteoblasts generate an osteogenic microenvironment when grown on surfaces with rough microtopographies. European Cells & Materials. 2003;6(July-December Cited October 24, 2003):22-7.

8. Lossdorfer S, Schwartz Z, Wang L, Lohmann CH, Turner JD, Wieland M, et al. Microrough implant surface topographies increase osteogenesis by reducing osteoclast formation and activity. Journal of Biomedical Materials Research Part A. 2004;70A(3):361-9.

9. Schwarz F, Wieland M, Schwartz Z, Zhao G, Rupp F, Geis-Gerstorfer J, et al. Potential of Chemically Modified Hydrophilic Surface Characteristics to Support Tissue Integration of Titanium Dental Implants. Journal of Biomedical Materials Research Part B-Applied Biomaterials. 2009;88B(2):544-57.

10. Klein MO, Bijelic A, Toyoshima T, Gotz H, von Koppenfels RL, Al-Nawas B, et al. Long-term response of osteogenic cells on micron and submicron-scale-structured hydrophilic titanium surfaces: sequence of cell proliferation and cell differentiation. Clinical Oral Implants Research. 2010;21(6):642-9.

11. Eriksson C, Nygren H, Ohlson K. Implantation of hydrophilic and hydrophobic titanium discs in rat tibia: cellular reactions on the surfaces during the first 3 weeks in bone. Biomaterials. 2004;25(19):4759-66.

12. Vandamme K, Holy X, Bensidhoum M, Logeart-Avramoglou D, Naert IE, Duyck JA, et al. In vivo molecular evidence of delayed titanium implant osseointegration in compromised bone. Biomaterials. 2011;32(14):3547-54.

13. Marco F, Milena F, Gianluca G, Vittoria O. Peri-implant osteogenesis in health and osteoporosis. Micron. 2005;36(7-8):630-44.

14. Zhang H, Lewis CG, Aronow MS, Gronowicz GA. The effects of patient age on human osteoblasts' response to Ti-6Al-4V implants in vitro. Journal of Orthopaedic Research. 2004;22(1):30-8.

15. Olivares-Navarrete R, Hyzy SL, Park JH, Dunn GR, Haithcock DA, Wasilewski CE, et al. Mediation of osteogenic differentiation of human mesenchymal stem cells on titanium surfaces by a Wnt-integrin feedback loop. Biomaterials. 2011;32(27):6399-411.

16. Linder L, Obrant K, Boivin G. Osseointegration of metallic implants.2. transmission electron-microscopy in the rabbit. Acta Orthopaedica Scandinavica. 1989;60(2):135-9.

17. Stanford CM, Keller JC, Solursh M. Bone cell expression on titanium surfaces is altered by sterilization treatments. Journal of Dental Research. 1994;73(5):1061-71.

18. Michaels CM, Keller JC, Stanford CM. In-vitro periodontal ligament fibroblast attachment to plasma-cleaned titanium surfaces. Journal of Oral Implantology. 1991;17(2):132-9.

19. Rigo ECS, Boschi AO, Yoshimoto M, Allegrini S, Konig B, Carbonari MJ. Evaluation in vitro and in vivo of biomimetic hydroxyapatite coated on titanium dental implants. Materials Science & Engineering C-Biomimetic and Supramolecular Systems. 2004;24(5):647-51.

20. Proff P, Roemer P. The molecular mechanism behind bone remodelling: a review. Clinical Oral Investigations. 2009;13(4):355-62.

21. Olszta MJ, Cheng X, Jee SS, Kumar R, Kim Y-Y, Kaufman MJ, et al. Bone structure and formation: A new perspective. Materials Science & Engineering R-Reports. 2007;58(3-5):77-116.

22. Rho JY, Kuhn-Spearing L, Zioupos P. Mechanical properties and the hierarchical structure of bone. Medical Engineering & Physics. 1998;20(2):92-102.

23. Choi K, Kuhn JL, Ciarelli MJ, Goldstein SA. The elastic-moduli of human subchondral, trabecular, and cortical bone tissue and the size-dependency of cortical bone modulus. Journal of Biomechanics. 1990;23(11):1103-13.

24. Goldstein SA. The mechanical-properties of trabecular bone-dependence on anatomic location and function. Journal of Biomechanics. 1987;20(11-12):1055-61.

25. Riggs BL, Parfitt AM. Drugs used to treat osteoporosis: The critical need for a uniform nomenclature based on their action on bone remodeling. J Bone Miner Res. 2005;20(2):177-84.

26. Gundberg CM. Biology, physiology, and clinical chemistry of osteocalcin. J Clin Ligand Assay. 1998;21(2):128-38.

27. Polak-Jonkisz D, Zwolinska D. Osteocalcin as a biochemical marker of bone turnover. Nephrology. 1998;4(5-6):339-46.

28. Lian JB, Gundberg CM. Osteocalcin-biochemical considerations and clinical-applications. Clinical Orthopaedics and Related Research. 1988(226):267-91.

29. Boskey AL, Gadaleta S, Gundberg C, Doty SB, Ducy P, Karsenty G. Fourier transform infrared microspectroscopic analysis of bones of osteocalcin-deficient mice provides insight into the function of osteocalcin. Bone. 1998;23(3):187-96.

30. Schwartz Z, Boyan BD. Underlying mechanisms at the bone-biomaterial interface. Journal of Cellular Biochemistry. 1994;56(3):340-7.

31. Raines AL, Olivares-Navarrete R, Wieland M, Cochran DL, Schwartz Z, Boyan BD. Regulation of angiogenesis during osseointegration by titanium surface microstructure and energy. Biomaterials. 2010;31(18):4909-17.

32. Boyan BD, Hummert TW, Dean DD, Schwartz Z. Role of material surfaces in regulating bone and cartilage cell response. Biomaterials. 1996;17(2):137-46.

33. Maheshwari G, Brown G, Lauffenburger DA, Wells A, Griffith LG. Cell adhesion and motility depend on nanoscale RGD clustering. Journal of Cell Science. 2000;113(10):1677-86.

34. Siebers MC, ter Brugge PJ, Walboomers XF, Jansen JA. Integrins as linker proteins between osteoblasts and bone replacing materials. A critical review. Biomaterials. 2005;26(2):137-46.

35. Olivares-Navarrete R, Raz P, Zhao G, Chen J, Wieland M, Cochran DL, et al. Integrin alpha 2 beta 1 plays a critical role in osteoblast response to micron-scale surface structure and surface energy of titanium substrates. Proceedings of the National Academy of Sciences of the United States of America. 2008;105(41):15767-72.

36. Protivinsky J, Appleford M, Strnad J, Helebrant A, Ong JL. Effect of chemically modified titanium surfaces on protein adsorption and osteoblast precursor cell Behavior. International Journal of Oral & Maxillofacial Implants. 2007;22(4):542-50.

37. Hao L, Lawrence J. Wettability modification and the subsequent manipulation of protein adsorption on a Ti6Al4V alloy by means of CO2 laser surface treatment. Journal of Materials Science-Materials in Medicine. 2007;18(5):807-17.

38. Cai KY, Bossert J, Jandt KD. Does the nanometre scale topography of titanium influence protein adsorption and cell proliferation? Colloids and Surfaces B-Biointerfaces. 2006;49(2):136-44.

39. Lausmaa J. Surface spectroscopic characterization of titanium implant materials. Journal of Electron Spectroscopy and Related Phenomena. 1996;81(3):343-61.

40. Park JH, Olivares-Navarrete R, Baier RE, Meyer AE, Tannenbaum R, Boyan BD, et al. Effect of cleaning and sterilization on titanium implant surface properties and cellular response. Acta Biomaterialia. 2012;8(5):1966-75.

41. Diebold U. The surface science of titanium dioxide. Surface Science Reports. 2003;48(5-8):53-229.

42. Gittens RA, McLachlan T, Olivares-Navarrete R, Cai Y, Berner S, Tannenbaum R, et al. The effects of combined micron-/submicron-scale surface roughness and nanoscale features on cell proliferation and differentiation. Biomaterials. 2011;32(13):3395-403.

43. Hansson S. The implant neck: smooth or provided with retention elements - A biomechanical approach. Clinical Oral Implants Research. 1999;10(5):394-405.

44. Hayes JS, Khan IM, Archer CW, Richards RG. The role of surface microtopography in the modulation of osteoblast differentiation. European Cells & Materials. 2010;20:98-108.

45. Le Guehennec L, Soueidan A, Layrolle P, Amouriq Y. Surface treatments of titanium dental implants for rapid osseointegration. Dental Materials. 2007;23(7):844-54.

46. Buser D, Schenk RK, Steinemann S, Fiorellini JP, Fox CH, Stich H. Influence of characteristics on bone integration of titanium implants - a histomorphometric study in miniature pigs. Journal of Biomedical Materials Research. 1991;25(7):889-902.

47. Zhao G, Zinger O, Schwartz Z, Wieland M, Landolt D, Boyan BD. Osteoblast-like cells are sensitive to submicron-scale surface structure. Clinical Oral Implants Research. 2006;17(3):258-64.

48. Sul YT, Johansson C, Wennerberg P, Cho LR, Chang BS, Albrektsson P. Optimum surface properties of oxidized implants for reinforcement of osseointegration: Surface chemistry, oxide thickness, porosity, roughness, and crystal structure. International Journal of Oral & Maxillofacial Implants. 2005;20(3):349-59.

49. Le Guehennec L, Lopez-Heredia MA, Enkel B, Weiss P, Amouriq Y, Layrolle P. Osteoblastic cell behaviour on different titanium implant surfaces. Acta Biomaterialia. 2008;4(3):535-43.

50. Curtis A, Wilkinson C. Nantotechniques and approaches in biotechnology. Trends in Biotechnology. 2001;19(3):97-101.

51. Dalby MJ, McCloy D, Robertson M, Wilkinson CDW, Oreffo ROC. Osteoprogenitor response to defined topographies with nanoscale depths. Biomaterials. 2006;27(8):1306-15.

52. Dalby MJ, Gadegaard N, Tare R, Andar A, Riehle MO, Herzyk P, et al. The control of human mesenchymal cell differentiation using nanoscale symmetry and disorder. Nat Mater. 2007;6(12):997-1003.

53. Webster TJ, Ergun C, Doremus RH, Siegel RW, Bizios R. Enhanced functions of osteoblasts on nanophase ceramics. Biomaterials. 2000;21(17):1803-10.

54. Rupp F, Scheideler L, Olshanska N, de Wild M, Wieland M, Geis-Gerstorfer J. Enhancing surface free energy and hydrophilicity through chemical modification of microstructured titanium implant surfaces. Journal of Biomedical Materials Research Part A. 2006;76A(2):323-34.

55. Olivares-Navarrete R, Hyzy SL, Hutton DL, Erdman CP, Wieland M, Boyan BD, et al. Direct and indirect effects of microstructured titanium substrates on the induction of mesenchymal stem cell differentiation towards the osteoblast lineage. Biomaterials. 2010;31(10):2728-35.

56. Rausch-fan XH, Qu Z, Wieland M, Matejka M, Schedle A. Differentiation and cytokine synthesis of human alveolar osteoblasts compared to osteoblast-like cells (MG63) in response to titanium surfaces. Dental Materials. 2008;24(1):102-10.

57. Hori N, Iwasa F, Ueno T, Takeuchi K, Tsukimura N, Yamada M, et al. Selective cell affinity of biomimetic micro-nano-hybrid structured TiO(2) overcomes the biological dilemma of osteoblasts. Dental Materials. 2010;26(4):275-87.

58. Boyan BD, Lohmann CH, Dean DD, Sylvia VL, Cochran DL, Schwartz Z. Mechanisms involved in osteoblast response to implant surface morphology. Annual Review of Materials Research. 2001;31:357-71.

59. Teitelbaum SL. Bone resorption by osteoclasts. Science. 2000;289(5484):1504-8.

60. Harada S, Rodan GA. Control of osteoblast function and regulation of bone mass. Nature. 2003;423(6937):349-55.

61. Confavreux CB. Bone: from a reservoir of minerals to a regulator of energy metabolism. Kidney International. 2011;79:S14-S9.

62. Buser D, Broggini N, Wieland M, Schenk RK, Denzer AJ, Cochran DL, et al. Enhanced bone apposition to a chemically modified SLA titanium surface. Journal of Dental Research. 2004;83(7):529-33.

63. Vogler EA. Structure and reactivity of water at biomaterial surfaces. Advances in Colloid and Interface Science. 1998;74:69-117.

64. Healy KE, Thomas CH, Rezania A, Kim JE, McKeown PJ, Lom B, et al. Kinetics of bone cell organization and mineralization on materials with patterned surface chemistry. Biomaterials. 1996;17(2):195-208.

65. Davies JE, Causton B, Bovell Y, Davy K, Sturt CS. The migration of osteoblasts over substrata of discrete surface-charge. Biomaterials. 1986;7(3):231-3.

66. Rebl H, Finke B, Ihrke R, Rothe H, Rychly J, Schroeder K, et al. Positively Charged Material Surfaces Generated by Plasma Polymerized Allylamine Enhance Vinculin Mobility in Vital Human Osteoblasts. Advanced Engineering Materials. 2010;12(8):B356-B64.

67. Cobos JA, Yang JP, Zhang RW, Krukowski M, Simmons DJ. Positively charged dextran resin inhibits trabecular bone repair in the rabbit tibial physis. Journal of Biomedical Materials Research. 1998;39(3):458-61.

68. Krukowski M, Snyders RV, Eppley BL, Simmons DJ. Negatively charged resins stimulate bone-formation in subperiosteal sites in rats - the effect of age. Clinical Orthopaedics and Related Research. 1994(298):266-71.

69. Schwartz Z, Raz P, Zhao G, Barak Y, Tauber M, Yao H, et al. Effect of Micrometer-Scale Roughness of the Surface of Ti6Al4V Pedicle Screws in Vitro and in Vivo. Journal of Bone and Joint Surgery-American Volume. 2008;90A(11):2485-98.

70. Steinemann SG. Titanium - the material of choice? Periodontology 2000. 1998;17:7-21.

71. Lincks J, Boyan BD, Blanchard CR, Lohmann CH, Liu Y, Cochran DL, et al. Response of MG63 osteoblast-like cells to titanium and titanium alloy is dependent on surface roughness and composition. Biomaterials. 1998;19(23):2219-32.

72. Delange GL, Donath K. Interface between bone tissue and implants of solid hydroxyapatite or hydroxyapatite-coated titanium implants. Biomaterials. 1989;10(2):121-5.

73. Zhao G, Schwartz Z, Wieland M, Rupp F, Geis-Gerstorfer J, Cochran DL, et al. High surface energy enhances cell response to titanium substrate microstructure. Journal of Biomedical Materials Research Part A. 2005;74A(1):49-58.

74. Cochran DL, Buser D, ten Bruggenkate CM, Weingart D, Taylor TM, Bernard JP, et al. The use of reduced healing times on ITI (R) implants with a sandblasted and acid-etched (SLA) surface: Early results from clinical trials on ITI (R) SLA implants. Clinical Oral Implants Research. 2002;13(2):144-53.

75. Nanci A, Wuest JD, Peru L, Brunet P, Sharma V, Zalzal S, et al. Chemical modification of titanium surfaces for covalent attachment of biological molecules. Journal of Biomedical Materials Research. 1998;40(2):324-35.

76. Decher G. Fuzzy nanoassemblies: Toward layered polymeric multicomposites. Science. 1997;277(5330):1232-7.

77. Dautzenberg H, Karibyants N. Polyelectrolyte complex formation in highly aggregating systems. Effect of salt: response to subsequent addition of NaCl. Macromolecular Chemistry and Physics. 1999;200(1):118-25.

78. Yoo D, Shiratori SS, Rubner MF. Controlling bilayer composition and surface wettability of sequentially adsorbed multilayers of weak polyelectrolytes. Macromolecules. 1998;31(13):4309-18.

79. Lyklema J, Deschenes L. The first step in layer-by-layer deposition: Electrostatics and/or non-electrostatics? Advances in Colloid and Interface Science. 2011;168(1-2):135-48.

80. Park JH, Schwartz Z, Olivares-Navarrete R, Boyan BD, Tannenbaum R. Enhancement of Surface Wettability via the Modification of Microtextured Titanium Implant Surfaces with Polyelectrolytes. Langmuir. 2011;27(10):5976-85.

81. Thunemann AF, Muller M, Dautzenberg H, Joanny JFO, Lowen H. Polyelectrolyte complexes. Polyelectrolytes with Defined Molecular Architecture Ii. 2004;166:113-71.

82. Scranton AB, Rangarajan B, Klier J. Biomedical applications of polyelectrolytes. Biopolymers Ii. 1995;122:1-54.

83. Angele P, Johnstone B, Kujat R, Zellner J, Nerlich M, Goldberg V, et al. Stem cell based tissue engineering for meniscus repair. Journal of Biomedical Materials Research Part A. 2008;85A(2):445-55.

84. Gravel M, Gross T, Vago R, Tabrizian M. Responses of mesenchymal stem cell to chitosan-coralline composites microstructured using coralline as gas forming agent. Biomaterials. 2006;27(9):1899-906.

85. Franzesi GT, Ni B, Ling Y, Khademhosseini A. A controlled-release strategy for the generation of cross-linked hydrogel microstructures. Journal of the American Chemical Society. 2006;128(47):15064-5.

86. Strand BL, Ryan L, Veld PI, Kulseng B, Rokstad AM, Skjak-Braek G, et al. Poly-L-lysine induces fibrosis on alginate microcapsules via the induction of cytokines. Cell Transplantation. 2001;10(3):263-75.

87. Orive G, Tam SK, Pedraz JL, Halle JP. Biocompatibility of alginate-poly-L-lysine microcapsules for cell therapy. Biomaterials. 2006;27(20):3691-700.

88. Richert L, Arntz Y, Schaaf P, Voegel JC, Picart C. pH dependent growth of poly(L-lysine)/poly(L-glutamic) acid multilayer films and their cell adhesion properties. Surface Science. 2004;570(1-2):13-29.

89. Hammond PT. Form and function in multilayer assembly: New applications at the nanoscale. Advanced Materials. 2004;16(15):1271-93.

90. Costerton JW, Stewart PS, Greenberg EP. Bacterial biofilms: A common cause of persistent infections. Science. 1999;284(5418):1318-22.

91. Smith DC, Pilliar RM, Chernecky R. Dental implant materials. I. Some effects of preparative procedures on surface topography. J Biomed Mater Res. 1991;25(9):1045-68. Epub 1991/09/01.

92. Zahraoui C, Sharrock P. Influence of sterilization on injectable bone biomaterials. Bone. 1999;25(2):63S-5S.

93. Keller JC, Draughn RA, Wightman JP, Dougherty WJ, Meletiou SD. Characterization of sterilized cp titanium implant surfaces. International Journal of Oral and Maxillofacial Implants. 1990;5(4):360-8.

94. Smith DC, Pilliar RM, Metson JB, McIntyre NS. Dental implant materials. 2. preparative procedures and surface spectroscopic studies. Journal of Biomedical Materials Research. 1991;25(9):1069-84.

95. Kasemo B, Lausmaa J. Biomaterial and implant surfaces - on the role of cleanliness, contamination, and preparation procedures. Journal of Biomedical Materials Research-Applied Biomaterials. 1988;22(A2):145-58.

96. Baier RE, Meyer AE, Akers CK, Natiella JR, Meenaghan M, Carter JM. Degradative effects of conventional steam sterilizaiton on biomaterial surfaces. Biomaterials. 1982;3(4):241-5.

97. Martin JY, Dean DD, Cochran DL, Simpson J, Boyan BD, Schwartz Z. Proliferation, differentiation, and protein synthesis of human osteoblast-like cells (MG63) cultured on previously used titanium surfaces. Clinical Oral Implants Research. 1996;7(1):27-37.

98. Kilpadi DV, Weimer JJ, Lemons JE. Effect of passivation and dry heat-sterilization on surface energy and topography of unalloyed titanium implants. Colloids and Surfaces A: Physicochemical and Engineering Aspects. 1998;135(1-3):89-101.

99. Doundoulakis JH. Surface-analysis of titanium after sterilizaiton - role in implant-tissue interface and bioadhesion. Journal of Prosthetic Dentistry. 1987;58(4):471-8.

100. Roth S, Feichtinger J, Hertel C. Characterization of Bacillus subtilis spore inactivation in low-pressure, low-temperature gas plasma sterilization processes. Journal of Applied Microbiology. 2010;108(2):521-31.

101. Rossi F, Kylian O, Rauscher H, Hasiwa M, Gilliland D. Low pressure plasma discharges for the sterilization and decontamination of surfaces. New Journal of Physics. 2009;11.

102. Yang LQ, Chen JR, Gao JL, Guo YF. Plasma sterilization using the RF glow discharge. Applied Surface Science. 2009;255(22):8960-4.

103. Singh S, Schaaf NG. Dynamic sterilization of titanium implants with ultraviolet light. Int J Oral Maxillofac Implants. 1989;4(2):139-46.

104. Premnath V, Harris WH, Jasty M, Merrill EW. Gamma sterilization of UHMWPE articular implants: an analysis of the oxidation problem. Biomaterials. 1996;17(18):1741-53.

105. Lausmaa J, Kasemo B, Hansson S. Accelerated oxide growth on titanium implants during autoclaving caused by fluorine contamination. Biomaterials. 1985;6(1):23-7.

106. Holyoak GR, Wang S, Liu Y. Toxic effects of ethylene oxide residues on in vitro production of bovine embryos. Theriogenology. 1995;43(1):237.

107. Qiu QQ, Connor J. Effects of gamma-irradiation, storage and hydration on osteoinductivity of DBM and DBM/AM composite. Journal of Biomedical Materials Research Part A. 2008;87A(2):373-9.

108. Serro AP, Saramago B. Influence of sterilization on the mineralization of titanium implants induced by incubation in various biological model fluids. Biomaterials. 2003;24(26):4749-60.

109. Fleith S, Ponche A, Bareille R, Amedee J, Nardin M. Effect of several sterilisation techniques on homogeneous self assembled monolayers. Colloids and Surfaces B-Biointerfaces. 2005;44(1):15-24.

110. Pandiyaraj KN, Selvarajan V, Pavese M, Falaras P, Tsoukleris D. Investigation on surface properties of TiO2 films modified by DC glow discharge plasma. Current Applied Physics. 2009;9(5):1032-7.

111. Pegueroles M, Gil FJ, Planell JA, Aparicio C. The influence of blasting and sterilization on static and time-related wettability and surface-energy properties of titanium surfaces. Surface & Coatings Technology. 2008;202(15):3470-9.

112. Lausmaa J, Kasemo B, Mattsson H. Surface spectrocopic characterization of titanium implant materials. Applied Surface Science. 1990;44(2):133-46.

113. Esposito M, Lausmaa J, Hirsch JM, Thomsen P. Surface analysis of failed oval titanium implants. Journal of Biomedical Materials Research. 1999;48(4):559-68.

114. Gengenbach TR, Vasic ZR, Chatelier RC, Griesser HJ. A Multitechnique study of the spontaneous oxidation of n-hexane plasma polymers. Journal of Polymer Science Part a-Polymer Chemistry. 1994;32(8):1399-414.

115. Suzuki T, Hori N, Att W, Kubo K, Iwasa F, Ueno T, et al. Ultraviolet Treatment Overcomes Time-Related Degrading Bioactivity of Titanium. Tissue Engineering Part A. 2009;15(12):3679-88.

116. Machnee CH, Wagner WC, Jaarda MJ, Lang BR. Identification of oxide layers of commercially pure titanium in response to cleaning procedures. Int J Oral Maxillofac Implants. 1993;8(5):529-33.

117. Ponter AB, Jinna KR, Asapu M, Jones WR. Surface energy and surface roughness changes produced by irradiating polymers with ultraviolet-ozone. Contact Angle, Wettability and Adhesion, Vol 2. 2002:331-44.

118. Tang ZY, Wang Y, Podsiadlo P, Kotov NA. Biomedical applications of layer-by-layer assembly: From biomimetics to tissue engineering. Advanced Materials. 2006;18(24):3203-24.

119. Ladam G, Schaad P, Voegel JC, Schaaf P, Decher G, Cuisinier F. In situ determination of the structural properties of initially deposited polyelectrolyte multilayers. Langmuir. 2000;16(3):1249-55.

120. Clark SL, Montague MF, Hammond PT. Ionic effects of sodium chloride on the templated deposition of polyelectrolytes using layer-by-layer ionic assembly. Macromolecules. 1997;30(23):7237-44.

121. McAloney RA, Sinyor M, Dudnik V, Goh MC. Atomic force microscopy studies of salt effects on polyelectrolyte multilayer film morphology. Langmuir. 2001;17(21):6655-63.

122. Dan N. Charge inversion and layer-by-layer deposition of non-polymeric macroions. Nano Letters. 2003;3(6):823-7.

123. Halthur TJ, Elofsson UM. Multilayers of charged polypeptides as studied by in situ ellipsometry and quartz crystal microbalance with dissipation. Langmuir. 2004;20(5):1739-45.

124. de Gennes PG. Polymers at an interface; a simplified view. Advances in Colloid and Interface Science. 1987;27(3-4):189-209.

125. Castelnovo M, Joanny JF. Formation of polyelectrolyte multilayers. Langmuir. 2000;16(19):7524-32.

126. Andreeva DV, Fix D, Mohwald H, Shchukin DG. Buffering polyelectrolyte multilayers for active corrosion protection. Journal of Materials Chemistry. 2008;18(15):1738-40.

127. Laurent D, Schlenoff JB. Multilayer assemblies of redox polyelectrolytes. Langmuir. 1997;13(6):1552-7.

128. Chua PH, Neoh KG, Kang ET, Wang W. Surface functionalization of titanium with hyaluronic acid/chitosan polyelectrolyte multilayers and RGD for promoting osteoblast functions and inhibiting bacterial adhesion. Biomaterials. 2008;29(10):1412-21.

129. Lahiji A, Sohrabi A, Hungerford DS, Frondoza CG. Chitosan supports the expression of extracellular matrix proteins in human osteoblasts and chondrocytes. Journal of Biomedical Materials Research. 2000;51(4):586-95.

130. Schmidt M. X-ray photoelectron spectroscopy studies on adsorption of amino acids from aqueous solutions onto oxidised titanium surfaces. Archives of Orthopaedic and Trauma Surgery. 2001;121(7):403-10.

131. Tengvall P, Lundstrom I. Physico-chemical considerations of titanium as biomaterial. Clinical Materials. 1992;9(2):115-34.

132. Roessler S, Zimmermann R, Scharnweber D, Werner C, Worch H. Characterization of oxide layers on Ti6Al4V and titanium by streaming potential and

streaming current measurements. Colloids and Surfaces B-Biointerfaces. 2002;26(4):387-95.

133. Parks GA. Isoelectric points of solid oxides solid hydroxides and aqueous hydroxo complex systems. Chemical Reviews. 1965;65(2):177-&.

134. Foissy A, Mpandou A, Lamarche JM, Jaffrezicrenault N. Surface and diffuse-layer charge at the TiO2-electrolyte interface. Colloids and Surfaces. 1982;5(4):363-8.

135. Kosmulski M, Gustafsson J, Rosenholm JB. Ion specificity and viscosity of rutile dispersions. Colloid and Polymer Science. 1999;277(6):550-6.

136. Sugita M, Tsuji M, Abe M. Synthetic inorganic ion-exchange materials. 54. the amphoteric behavior of hydrous titanium-dioxide ion-exchanges in different preparations. Bulletin of the Chemical Society of Japan. 1990;63(2):559-64.

137. Molenberg A, Schwarz F, Herten M, Berner S, de Wild M, Wieland M. Improved osseointegration of a novel, hydrophilic Ti surface - a review. Materialwissenschaft Und Werkstofftechnik. 2009;40(1-2):31-5.

138. Elias CN, Oshida Y, Lima JHC, Muller CA. Relationship between surface properties (roughness, wettability and morphology) of titanium and dental implant removal torque. Journal of the Mechanical Behavior of Biomedical Materials. 2008;1(3):234-42.

139. Yahyapour N, Eriksson C, Malmberg P, Nygren H. Thrombin, kallikrein and complement C5b-9 adsorption on hydrophilic and hydrophobic titanium and glass after short time exposure to whole blood. Biomaterials. 2004;25(16):3171-6.

140. Keselowsky BG, Collard DM, Garcia AJ. Integrin binding specificity regulates biomaterial surface chemistry effects on cell differentiation. Proceedings of the National Academy of Sciences of the United States of America. 2005;102(17):5953-7.

141. Zreiqat H, Valenzuela SM, Ben Nissan B, Roest R, Knabe C, Radlanski RJ, et al. The effect of surface chemistry modification of titanium alloy on signalling pathways in human osteoblasts. Biomaterials. 2005;26(36):7579-86.

142. Dierich A, Le Guen E, Messaddeq N, Stoltz JF, Netter P, Schaaf P, et al. Bone formation mediated by synergy-acting growth factors embedded in a polyelectrolyte multilayer film. Advanced Materials. 2007;19(5):693-7.

143. Markarian MZ, Moussallem MD, Jomaa HW, Schlenoff JB. Hydrogen bonding versus ion pairing in polyelectrolyte multilayers with homopolynucleotides. Biomacromolecules. 2007;8(1):59-64.

144. Tentorio A, Canova L. Adsorption of alpha-amino-acids on spherical TiO2 particles. Colloids and Surfaces. 1989;39(4):311-9.

145. Gao WL, Feng B, Ni YX, Yang YL, Lu XO, Weng J. Protein adsorption and biomimetic mineralization behaviors of PLL-DNA multilayered films assembled onto titanium. Applied Surface Science. 2010;257(2):538-46.

146. Roiter Y, Minko S. Adsorption of polyelectrolyte versus surface charge: in situ single-molecule atomic force microscopy experiments on similarly, oppositely, and heterogeneously charged surfaces. Journal of Physical Chemistry B. 2007;111(29):8597-604.

147. Messina R. Electrostatics in soft matter. Journal of Physics-Condensed Matter. 2009;21(11).

148. Messina R, Holm C, Kremer K. Like-charge colloid-polyelectrolyte complexation. Journal of Chemical Physics. 2002;117(6):2947-60.

149. Jedlicka SS, Rickus JL, Zemyanov DY. Surface analysis by x-ray photoelectron spectroscopy of sol-gel silica modified with covalently bound peptides. Journal of Physical Chemistry B. 2007;111:11850-7.

150. Rojas OJ, Ernstsson M, Neumann RD, Claesson PM. X-ray photoelectron spectroscopy in the study of polyelectrolyte adsorption on mica and cellulose. Journal of Physical Chemistry B. 2000;104(43):10032-42.

151. Martin HJ, Schulz KH, Bumgardner JD, Walters KB. XPS study on the use of 3-aminopropyltriethoxysilane to bond chitosan to a titanium surface. Langmuir. 2007;23(12):6645-51.

152. Wallin T, Linse P. Monte Carlo simulations of polyelectrolytes at charged micelles .1. Effects of chain flexibility. Langmuir. 1996;12(2):305-14.

153. Brugnerotto J, Desbrieres J, Roberts G, Rinaudo M. Characterization of chitosan by steric exclusion chromatography. Polymer. 2001;42(25):9921-7.

154. Nunnery G, Hershkovits E, Tannenbaum A, Tannenbaum R. Adsorption of poly(methyl methacrylate) on concave Al2O3 surfaces in nanoporous membranes. Langmuir. 2009;25(16):9157-63.

155. Koch K, Barthlott W. Superhydrophobic and superhydrophilic plant surfaces: an inspiration for biomimetic materials. Philosophical Transactions of the Royal Society a-Mathematical Physical and Engineering Sciences. 2009;367(1893):1487-509.

156. Gao LC, McCarthy TJ. How Wenzel and Cassie were wrong. Langmuir. 2007;23(7):3762-5.

157. Kasemo B, Lausmaa J. Material-tissue interfaces-the role of surface-properties and processes. Environmental Health Perspectives. 1994;102:41-5.

158. Lasprilla AJR, Martinez GAR, Lunelli BH, Jardini AL, Filho RM. Biomaterials for application in bone tissue engineering. Journal of Biotechnology. 2010;150, Supplement(0):455.

159. Ponsonnet L, Reybier K, Jaffrezic N, Comte V, Lagneau C, Lissac M, et al. Relationship between surface properties (roughness, wettability) of titanium and titanium alloys and cell behaviour. Materials Science & Engineering C-Biomimetic and Supramolecular Systems. 2003;23(4):551-60.

160. Lim YJ, Oshida Y, Andres CJ, Barco MT. Surface characterizations of variously treated titanium materials. International Journal of Oral & Maxillofacial Implants. 2001;16(3):333-42.

161. Park JW, Kim YJ, Park CH, Lee DH, Ko YG, Jang JH, et al. Enhanced osteoblast response to an equal channel angular pressing-processed pure titanium substrate with microrough surface topography. Acta Biomaterialia. 2009;5(8):3272-80.

162. Liu HA, Webster TJ. Nanomedicine for implants: A review of studies and necessary experimental tools. Biomaterials. 2007;28(2):354-69.

163. Hallab NJ, Bundy KJ, O'Connor K, Moses RL, Jacobs JJ. Evaluation of metallic and polymeric biomaterial surface energy and surface roughness characteristics for directed cell adhesion. Tissue Engineering. 2001;7(1):55-71.

164. Ruardy TG, Schakenraad JM, van der Mei HC, Busscher HJ. Adhesion and spreading of human skin fibroblasts on physicochemically characterized gradient surfaces. Journal of Biomedical Materials Research. 1995;29(11):1415-23.

165. Otani Y, Tabata Y, Ikada Y. Rapidly curable biological glue composed of gelatin and poly(-glutamic acid). Biomaterials. 1996;17(14):1387-91.

166. Lim YW, Kwon SY, Sun DH, Kim HE, Kim YS. Enhanced Cell Integration to Titanium Alloy by Surface Treatment with Microarc Oxidation: A Pilot Study. Clinical Orthopaedics and Related Research. 2009;467(9):2251-8.

167. Moursi AM, Globus RK, Damsky CH. Interactions between integrin receptors and fibronectin are required for calvarial osteoblast differentiation in vitro. Journal of Cell Science. 1997;110:2187-96.

168. Cheng SL, Lai CF, Blystone SD, Avioli LV. Bone mineralization and osteoblast differentiation are negatively modulated by integrin alpha v beta 3. J Bone Miner Res. 2001;16(2):277-88.

169. Khang D, Lu J, Yao C, Haberstroh KM, Webster TJ. The role of nanometer and sub-micron surface features on vascular and bone cell adhesion on titanium. Biomaterials. 2008;29(8):970-83.

170. Bullard JW, Cima MJ. Orientation dependence of the isoelectric point of TiO2 (rutile) surfaces. Langmuir. 2006;22(24):10264-71.

171. Lim JY, Liu XM, Vogler EA, Donahue HJ. Systematic variation in osteoblast adhesion and phenotype with substratum surface characteristics. Journal of Biomedical Materials Research Part A. 2004;68A(3):504-12.

172. Dubas ST, Schlenoff JB. Factors controlling the growth of polyelectrolyte multilayers. Macromolecules. 1999;32(24):8153-60.

173. Aparicio C, Gil FJ, Fonseca C, Barbosa M, Planell JA. Corrosion behaviour of commercially pure titanium shot blasted with different materials and sizes of shot particles for dental implant applications. Biomaterials. 2003;24(2):263-73.

174. Dubas ST, Schlenoff JB. Swelling and smoothing of polyelectrolyte multilayers by salt. Langmuir. 2001;17(25):7725-7.

175. Thompson GJ, Puleo DA. Effects of sublethal metal-ion concentrations on osteogenic cells derived from bone-marrow stromal cells. Journal of Applied Biomaterials. 1995;6(4):249-58.

176. Nichols KG, Puleo DA. Effect of metal ions on the formation and function of osteoclastic cells in vitro. Journal of Biomedical Materials Research. 1997;35(2):265-71.

177. Schwartz Z, Olivares-Navarrete R, Wieland M, Cochran DL, Boyan BD. Mechanisms regulating increased production of osteoprotegerin by osteoblasts cultured on microstructured titanium surfaces. Biomaterials. 2009;30(20):3390-6.

178. Lavenus S, Pilet P, Guicheux J, Weiss P, Louarn G, Layrolle P. Behaviour of mesenchymal stem cells, fibroblasts and osteoblasts on smooth surfaces. Acta Biomaterialia. 2011;7(4):1525-34.

179. Webster TJ, Ergun C, Doremus RH, Bizios R. Hydroxylapatite with substituted magnesium, zinc, cadmium, and yttrium. II. Mechanisms of osteoblast adhesion. Journal of Biomedical Materials Research. 2002;59(2):312-7.

180. Dulgar-Tulloch AJ, Bizios R, Siegel RW. Human mesenchymal stem cell adhesion and proliferation in response to ceramic chemistry and nanoscale topography. Journal of Biomedical Materials Research Part A. 2009;90A(2):586-94.

181. Uedayukoshi T, Matsuda T. Cellular-responses on a wettability gradient surface with continuous variations in surface compositions of carbonate and hydroxyl-groups. Langmuir. 1995;11(10):4135-40.

182. Vieira EP, Rocha S, Pereira MC, Moehwald H, Coelho MAN. Adsorption and Diffusion of Plasma Proteins on Hydrophilic and Hydrophobic Surfaces: Effect of Trifluoroethanol on Protein Structure. Langmuir. 2009;25(17):9879-86.

183. Ballester-Beltran J, Rico P, Moratal D, Song W, Mano JF, Salmeron-Sanchez M. Role of superhydrophobicity in the biological activity of fibronectin at the cell-material interface. Soft Matter. 2011;7(22):10803-11.

184. Berman AE, Kozova NI, Morozevich GE. Integrins: Structure and signaling. Biochemistry-Moscow. 2003;68(12):1284-99.

185. Genzer J, Bhat RR. Surface-bound soft matter gradients. Langmuir. 2008;24(6):2294-317.

186. Lacey DL, Timms E, Tan HL, Kelley MJ, Dunstan CR, Burgess T, et al. Osteoprotegerin ligand is a cytokine that regulates osteoclast differentiation and activation. Cell. 1998;93(2):165-76.

187. Altankov G, Grinnell F, Groth T. Studies on the biocompatibility of materials: Fibroblast reorganization of substratum-bound fibronectin on surfaces varying in wettability. Journal of Biomedical Materials Research. 1996;30(3):385-91.

188. Miranda Coelho N, Gonzalez-Garcia C, Salmeron-Sanchez M, Altankov G. Arrangement of Type IV Collagen on NH(2) and COOH Functionalized Surfaces. Biotechnology and Bioengineering. 2011;108(12):3009-18.

189. Arifvianto B, Suyitno, Mahardika M, Dewo P, Iswanto PT, Salim UA. Effect of surface mechanical attrition treatment (SMAT) on microhardness, surface roughness and wettability of AISI 316L. Materials Chemistry and Physics. 2011;125(3):418-26.

190. Greene G, Yao G, Tannenbaum R. Wetting characteristics of plasma-modified porous polyethylene. Langmuir. 2003;19(14):5869-74.

191. Greene G, Tannenbaum R. Adsorbtion of polyelectrolyte multilayers on plasma-modified porous polyethylene. Applied Surface Science. 2004;238(1-4):101-7.

192. Morris ER, Rees DA, Thom D, Welsh EJ. Conformation and intermolecular interactions of carbohydrate chains. Journal of Supramolecular Structure. 1977;6(2):259-74.

193. Hershkovits E, Tannenbaum A, Tannenbaum R. Polymer adsorption on curved surfaces: A geometric approach. Journal of Physical Chemistry C. 2007;111(33):12369-75.

194. O'Shaughnessy B, Vavylonis D. Non-equilibrium in adsorbed polymer layers. Journal of Physics-Condensed Matter. 2005;17(2):R63-R99.

195. Granick S, Kumar SK, Amis EJ, Antonietti M, Balazs AC, Chakraborty AK, et al. Macromolecules at surfaces: Research challenges and opportunities from tribology to biology. Journal of Polymer Science Part B-Polymer Physics. 2003;41(22):2755-93.

196. Fleer GJ, Scheutjens J. Interaction between adsorbed layers of macromoleuces. Journal of Colloid and Interface Science. 1986;111(2):504-15.

197. Panja D, Barkema GT, Kolomeisky AB. Non-equilibrium dynamics of single polymer adsorption to solid surfaces. Journal of Physics-Condensed Matter. 2009;21(24).

198. Sinha RK, Tuan RS. Regulation of human osteoblast integrin expression by orthopedic implant materials. Bone. 1996;18(5):451-7.

199. Raz P, Lohmann CH, Turner J, Wang L, Poythress N, Blanchard C, et al. 1 alpha,25(OH)(2)D-3 Regulation of integrin expression is substrate dependent. Journal of Biomedical Materials Research Part A. 2004;71A(2):217-25.